UNIVERSIDAD POLITÉCNICA DE MADRID

Escuela Técnica Superior de Ingenieros Industriales

Contributions to forecasting problems in the electric power market

DOCTORAL THESIS

Submitted for the degree of Doctor by:

Shadi Nouhi Tehrani

MSc. Industrial Engineering

Madrid, 2024

UNIVERSIDAD POLITÉCNICA DE MADRID
Escuela Técnica Superior de Ingenieros Industriales

Doctoral Degree in Management Engineering

Contributions to forecasting problems in the electric power market

DOCTORAL THESIS

Submitted for the degree of Doctor by:

Shadi Nouhi Tehrani
MSc. Industrial Engineering

Under the supervision of:
Eduardo Caro Huertas
Doctor Ingeniero por la Universidad de Castilla-La Mancha

Jesús Juan Ruiz
Doctor Ingeniero por la Universidad Politécnica de Madrid

Madrid, 2024

Title: Contributions to forecasting problems in the electric power market

Author: Shadi Nouhi Tehrani

Doctoral Programme: Management Engineering

Thesis Supervision:

Dr. Eduardo Caro Huertas - Doctor Ingeniero por la Univ. de Castilla-La Mancha

Dr. Jesús Juan Ruiz - Doctor Ingeniero por la Universidad Politécnica de Madrid

External Reviewers:

Thesis Defense Committee:

Thesis Defense Date:

Acknowledgement

I express my deepest gratitude to my supervisors, Prof. Jesus Juan and Eduardo Caro, for their invaluable guidance and support. Their expertise and encouragement have been instrumental in the completion of this thesis.

I am grateful Department of Management Engineering, Business Administration and Statistics the necessary resources and support.

Heartfelt thanks to my parents and sister for their constant support. And I extend my appreciation to my colleagues and friends for their encouragement and stimulating discussions.

This thesis is dedicated to my parents, whose love and sacrifice have been my foundation, and to my mentors and friends, whose guidance and encouragement have been invaluable.

Abstract

The electric power market is a vital component of modern economies, as it provides the energy needed to power homes, businesses, and industries. This market is uniquely complex due to the limited capacity for energy storage and the unpredictability of various power sources. Forecasting the demand or price of electricity, as well as energy generation from renewable sources, is a complex and challenging task. In recent years, significant contributions have been made to the field of electric power market forecasting through the use of advanced statistical and machine learning methods. The purpose of this thesis is to investigate and analyse the current state of the art in forecasting problems concerning the electric power market and to provide a set of contributions in the field, with a focus on demand forecasting, supply forecasting from renewable sources, and price forecasting. The research presented in this thesis will provide a comprehensive understanding of the current state of the art in forecasting problems in the electric power market and will identify opportunities for future research to improve forecast accuracy and reliability in the electric power market.

Specifically, this thesis includes three contributions. The contribution regarding electricity demand forecasts: a methodology is developed to improve the quality of forecasts by means of an optimal selection of meteorological variables. Contributions regarding renewable energy generation: an algorithm is developed to combine a set of probabilistic predictions, by means of the optimal combination of predictions based on the "Bernstein Online Aggregation" technique, a variance-covariance matrix calculation using the EWMA method, and finally using the Johnson SU distribution to improve the accuracy of probabilistic predictions. Finally, the third contribution refers to electricity prices: The time series of the main European electricity markets are analysed, and different alternatives for the prediction of future values are proposed.

Resumen

El mercado de la energía eléctrica es un componente vital de las economías modernas, ya que proporciona la energía necesaria para alimentar hogares, empresas e industrias. Este mercado posee complejidades específicas debido a la dificultad de almacenar energía eléctrica y a la enorme incertidumbre asociada a ciertas fuentes de energía. Prever la demanda o el precio de la electricidad, así como la generación de energía a partir de fuentes renovables, es una tarea compleja y difícil. En los últimos años, se han realizado importantes contribuciones al campo de la previsión del mercado de la energía eléctrica mediante el uso de métodos estadísticos avanzados y de aprendizaje automático. El objetivo de esta tesis es investigar y analizar el estado actual de los problemas de previsión relativos al mercado de la energía eléctrica y proporcionar varias contribuciones en este campo, centrándose en la previsión de la demanda, la previsión de la oferta a partir de fuentes renovables y la previsión de precios. La investigación presentada en esta tesis proporcionará una comprensión global del estado actual de los problemas de previsión en el mercado de la energía eléctrica e identificará oportunidades de investigación futura para mejorar la precisión de las previsiones y la fiabilidad del mercado de la energía eléctrica.

En concreto, esta tesis incluye tres contribuciones. La contribución en referencia a las predicciones de demanda eléctrica: se desarrolla una metodología para mejorar la calidad de las predicciones mediante una selección óptima de variables meteorológicas. La contribución en referencia a la generación de energía renovable: se desarrolla un algoritmo para combinar un conjunto de predicciones probabilísticas, mediante la combinación óptima de predicciones basada en la técnica "Bernstein Online Aggregation", un cálculo de la matriz de varianza-covarianza utilizando el método EWMA, y finalmente utilizando la distribución Johnson SU para mejorar la precisión de las predicciones probabilísticas. Por último, la tercera contribución se refiere a los precios de la electricidad: se analizan las series temporales de los principales mercados eléctricos europeos y se proponen distintas alternativas para la predicción de valores futuros.

Table of contents

Acknowledgement ..... **iii**

Abstract ..... **v**

Resumen ..... **vii**

List of Figures ..... **xiii**

List of Tables ..... **xvii**

Abbreviations and acronyms ..... **xviii**

1. INTRODUCTION **1**

1.1. Methodological approach: 2

1.2. Motivation and research objectives: 3

1.2.1. Research objectives *4*

1.3. Research structure 4

2. UNDERSTANDING THE SIGNIFICANCE OF FORECASTING IN THE ELECTRIC POWER MARKET **5**

2.1. Overview of the electric power market: importance and complexity 5

2.2. The European electricity market 6

2.2.1. The origin of electricity markets *6*

2.2.2. The European electricity market today *7*

2.3. The Spanish electricity system 11

2.3.1. The Spanish electricity market *13*

2.4. Day-ahead market 15

2.4.1. Market matching process *15*

2.4.2. Intraday markets *16*

2.5. Marketing 17

2.6. Forecasting problems 18

3. BASIC MODEL **21**

3.1. Introduction 21

3.1.1. Motivation and literature review *21*

3.1.2. Structure *25*

3.1.3. Inputs variables *25*

3.1.4. Weather forecast for AEMET *25*

3.1.5. ECMWF weather forecast *26*
3.1.6. Observed meteorological data *33*
3.1.7. Observed demand *34*
3.2. Mathematical model 35
3.2.1. Periodic Reg-ARIMA model *35*
3.2.2. Modeling the influence of temperature *36*
3.2.3. Modeling the influence of special days *38*
3.2.4. Hourly correction *40*
3.3. Conclusion 41

4. OPTIMAL SELECTION OF WEATHER STATIONS FOR ELECTRIC LOAD FORECASTING AND ITS APPLICATION TO THE SPANISH SYSTEM 43

4.1. Introduction 43
4.1.1. Contribution *45*
4.1.2. Structure *45*
4.2. Optimal selection of weather stations 45
4.2.1. Method 1: exhaustive analysis *48*
4.2.2. Computational effort and feasibility *48*
4.2.3. Modified demand time series without the holidays effect *49*
4.2.4. Method 2: Incremental search *51*
4.2.5. Method 3: Decremental search *53*
4.3. Case study 54
4.3.1. First case study: analysis of 2018 ..... *55*
4.3.1.1. Case A: Exhaustive analysis 55
4.3.1.2. Case B: Incremental search and decremental search 58
4.3.2. Second case study: analysis of 2019 ..... *58*
4.3.3. Third case study: ECMWF database *60*
4.4. Conclusion 62

5. CONTRIBUTIONS TO RENEWABLE ENERGIES FORECASTING: THE AGGREGATION PROBLEM 63

5.1. Computation of prediction intervals of wind energy 63
5.1.1. Motivation *63*
5.1.2. Literature review *64*
5.1.3. Contribution *66*
5.1.4. Structure *66*
5.2. Proposed methodology: computation of prediction intervals 67

5.2.1. Forecast: punctual and probabilistic ... *67*
5.2.1.1. Punctual forecasts ... 67
5.2.1.2. Probabilistic forecasts ... 68
5.2.2. Scheme of the proposed algorithm ... *69*
5.2.3. Combination of predictors ... *70*
5.2.3.1. Uniform weights ... 70
5.2.3.2. Bernstein online aggregation (BOA) ... 71
5.2.4. Interval width of aggregation ... *71*
5.2.4.1. Johnson S_U distribution ... 72
5.2.5. Exponentially weighted moving average technique ... *73*
5.2.6. Estimating the variance matrix including uncertainty ... *74*
5.3. Case study ... 75
5.3.1. Descriptive statistics ... *76*
5.3.2. Analysis of individual predictions ... *77*
5.3.2.1. Analysis of punctual individual forecasts ... 77
5.3.2.2. Probabilistic individual forecasts ... 80
5.3.2.3. Prediction interval width: standard deviations ... 82
5.3.2.4. Coverage analysis ... 84
5.3.3. Application of the proposed procedure ... *86*
5.3.3.1. Berstein online aggregation: case study ... 86
5.3.3.2. EWMA method: case study ... 88
5.3.3.3. Johnson distribution: case study ... 88
5.3.3.4. Coverage analysis: case study ... 89
5.3.3.5. Interval width analysis: case study ... 90
5.3.4. Case study: varying the prediction horizon ... *91*
5.4. Conclusions ... 94

6. CONTRIBUTIONS TO PRICE FORECASTING: DIFFERENCE AMONG EUROPEAN COUNTRIES ... 97

6.1. Introduction ... 97
6.1.1. Motivation and literature review ... *97*
6.1.2. Contribution ... *100*
6.1.3. Structure ... *101*
6.2. Electricity prices dataset ... 101
6.2.1. Characteristics ... *101*
6.2.2. Single-day-ahead coupling ... *102*
6.2.3. Dataset ... *103*
6.3. ARIMA models and outliers ... 107
6.3.1. Detection of outliers ... *107*

6.3.2. ARIMA model estimation 109
6.4. GARCH models 112
6.4.1. Introduction GARCH models 112
6.4.2. sGARCH models 115
6.4.3. Comparison of GARCH models 117
6.5. Asymmetry 119
6.6. Out-of-sample forecasts 121
6.7. Discussion 125
6.8. Conclusions 128
7. CONCLUSIONS AND FURTHER RESEARCH 131
7.1. Conclusions 131
7.1.1. Contributions referred to forecasting electricity demand 131
7.1.2. Contributions referred to renewable energy forecasting 132
7.1.3. Contributions referred to electricity price forecasting 133
7.2. Contributions to the technical literature 135
7.2.1. Journal articles published 135
7.2.2. International Conferences 136
7.3. Future work 137
References 139

List of Figures

Figure 2-1: Europe's Energy History....9

Figure 2-2: The physical flow of the electricity distribution. 13

Figure 2-3: Aggregate supply and demand curves MIBEL for hour 1 of 10.01.2024 [7]....15

Figure 2-4: Time sequence of the daily and intraday market in MIBEL [8]....17

Figure 3-1: Real-time demand prediction by the ETSII-UPM forecaster. 24

Figure 3-2: AEMET weather forecast consultation on its official website....25

Figure 3-3: Predicted maximum temperature file. 26

Figure 3-4: ECMWF model temperature forecast. 27

Figure 3-5: Prediction of meteorological variables: temperature. 29

Figure 3-6: Prediction of meteorological variables: radiation. 30

Figure 3-7: Prediction of meteorological variables: cloudiness. 31

Figure 3-8: Prediction of meteorological variables: wind modulus. 32

Figure 3-9: Observed weather information from the AEMET website. 33

Figure 3-10: Observed weather file. 34

Figure 3-11: Observed demand from REE's website. 34

Figure 3-12: Observed demand obtained by file. 35

Figure 3-13: Matrix of correlation coefficients between the errors of each daily series. 40

Figure 4-1: Scatterplot denoting the non-linear relationship between demand of working days (Y axis, in GWh) and temperature (X axis, in ºC)....46

Figure 4-2: Thermal effect on Spanish electricity consumption (Z-axis), as a function of maximum temperature (X-axis) and time (Y-axis)....47

Figure 4-3: Observed demand for December 3rd-9th, 2018 and demand after removing the holidays effect. 50

Figure 4-4: Number of evaluations for methods 1 and 2, and the reduction of computational cost..... 53

Figure 4-5: Flowchart of the proposed algorithm..... 54

Figure 4-6: Exhaustive analysis: (left plot) boxplot of RMSPE errors, as a function of the number of weather stations considered; (right plot) hourly RMSPE. Color code: number of weather stations considered. 56

Figure 4-7: Hourly errors for the reference and optimal-location models. Prediction period: from Jan. 2019 to Dec. 2019. 59

Figure 4-8: Incremental search algorithm (method 2): iterations employing the ECMWF database. 61

Figure 4-9: ECMWF: hourly errors for the ref. model (orange), just one loc. (blue) and optimized-locations model (green). 62

Figure 5-1: Flowchart of the proposed methodology. 69

Figure 5-2. Hourly production of wind energy in the Spanish peninsula system..... 76

Figure 5-3. Histogram of hourly wind energy generated. 76

Figure 5-4. Hourly wind generation (black) and predictions (E1: red, E2: blue, E3: green)..... 77

Figure 5-5. Scatter plots of prediction errors. 79

Figure 5-6. Monthly evolution of MAEs for the three models..... 79

Figure 5-7. The normal PDF curve and the quantiles provided in the predictions.... 80

Figure 5-8. The time series of actual wind production (black), its point predictions (red), and the 90% prediction intervals (blue and green dashed lines) for the three models..... 81

Figure 5-9. Estimation of st by least squares for the three models at a specific instant. 82

Figure 5-110. Average hourly standard deviations (GWh) of 24-hour horizon predictions by month. 83

Figure 5-11. Weights assigned to each of the three methods in the BOA. 86

Figure 5-12. Monthly evolution of the MAEs for the three predictors and the aggregators UNIF and BOA. 87

Figure 5-13. Histogram of BOA standardized prediction errors. Blue line: Gaussian distribution. Red line: Johnson distribution 89

Figure 5-14. Bar chart of the coverage rates for the considered models. 89

Figure 5-15. Monthly evolutions of the amplitudes of the prediction intervals for the three predictors and two aggregators: the UNIF and BOA. 91

Figure 5-16. Bias, MAE, MAPE, and RMSE for prediction horizons ranging from 1 to 48 hours 92

Figure 5-17. Coverage and width of prediction intervals for horizons ranging from 1 to 48 h. 93

Figure 6-1: Flow diagram of the analysis performed. 101

Figure 6-2: The median prices for each of the 24-hourly series for each country (left plot) and the robust estimate of the standard deviation (right plot) 105

Figure 6-3: The daily average price (€) series with the mean values and the standard deviation. 106

Figure 6-4: Total number of outliers in each country (total in gray, downward in blue, upward in red). 109

Figure 6-5: Summary of the analysis performed using the ARIMA time series models 110

Figure 6-6: σ and θ estimates for ARIMA and GARCH models. 112

Figure 6-7: The values of the estimates of the two parameters of the sGARCH equation. 116

Figure 6-8: The ordinate at the origin of the eGARCH equation (left plot), and the estimate persistence (right plot). 117

Figure 6-9: The changes in the parameter estimate according to the different models for each country. 119

Figure 6-10: The γ estimates for the gjrGARCH and apARCH models and the α parameter (with sign changed) for the eGARCH model. 121

Figure 6-11: MWE of IMA(1,1) and sGARCH for each country (grey and red, respectively). 123

Figure 6-12: behavior of the method to predict two-week (Monday through Friday) of March 2019 prices in the six market. 125

List of Tables

Table 4-1: The reference configuration and the twenty configurations with lower forecasting errors. 57

Table 4-2: Methods 2 and 3: results for the period from Jan. 2018 until Dec. 2018... 58

Table 4-3: Hourly and monthly errors for the reference and optimal-location models. Prediction period: Jan.-Dec. 2019. 60

Table 4-4: Incremental search algorithm (method 2): iterations employing the ECMWF database. 61

Table 5-1: Performance metrics for punctual forecasts 68

Table 5-2: Basic descriptions of the prediction errors of the three models. 78

Table 5-3. Average standard deviation of intervals for the three models. 82

Table 5-4. Percentage of times the actual value falls in each of the eight classes generated by prediction intervals. 84

Table 5-5. The coverage of the prediction intervals at 70%, 80%, or 90%. 85

Table 5-6. Global MSE for each method 87

Table 5-7. Estimated variance matrix using the EWMA procedure for a specific instant. 88

Table 5-8. Amplitudes of the predictors and the UNIF and BOA aggregators. 91

Table 6-1: The correlation matrix of the differenced series 107

Table 6-2: The MSEs of the six models for all countries 117

Table 6-3: MWE for original observations of 2019, without removing outliers. 122

Table 6-4: MWE for a situation that is unrealistic but provides information on the sensitivity of the models (2019). 124

Abbreviations and acronyms

AEMET	Agencia Estatal de Meteorología (State Meteorological Agency)
AO	Additive Outliers
apARCH	Asymmetric Power ARCH
ARCH	Autoregressive Conditional Heterogeneity
ARIMA	Auto-Regressive Integrated Moving Average
ARMA	Autoregressive Moving Average
ARMAX	Autoregressive moving average with exogenous variables
BOA	Bernstein Online Aggregation
cGARCH	Component GARCH
ECM	Enterprise content management
ECMWF	European Centre for Medium-Range Weather Forecasts
ECSC	European Coal and Steel Community
EEC	European Economic Community
eGARCH	Exponential GARCH
EUPHEMIA	Pan-European Hybrid Electricity Market Integration Algorithm
Euratom	The European Atomic Energy Community
EWMA	Exponentially Weighted Moving Average
GARCH	Generalised Autoregressive Conditional Heteroskedasticity
gjrGARCH	Glosten-Jagannathan-Runkle GARCH
GRIB	General Regularly distributed Information in Binary form
iGARCH	Integrated GARCH
IMA	Integrated Moving Average
ISOs	Independent System Operators
ITOs	Independent Transmission Operators
KDE	Kernel Density Estimation
LS	Level shifts
LSSVM	Least Squares Support Vector Machine
MAE	Mean Absolute Error

MAPE	Mean Absolute Percentual Error
MIBEL	Iberian Electricity Market
MSE	Mean Squared Error
MWE	Mean Week Error
NEMO	Nominated Electricity Market Operator
NS	North-South
OMIE	Operador del Mercado Ibérico de Energía
PVPC	Voluntary Price for Small Consumers
REE	Red Eléctrica de España
RMSE	Root Mean Squared Error
RMSPE	Root Mean Squared Percentual Error
SD	Standard Deviation
SDAC	Single-Day-Ahead Coupling
sGARCH	Standard GARCH
SLS	Seasonal-level shifts
TC	Temporary Changes
TSO	Transmission System Operator
UPM	Universidad Politécnica de Madrid
VMD	Variational Mode Decomposition
WE	West-East

1. INTRODUCTION

The electric power market is a critical component of modern economies, providing essential energy to households, businesses, and industries. This market is uniquely complex due to the limited capacity for energy storage and the randomness of various power sources. Accurately forecasting electricity demand, prices, and renewable energy generation poses significant challenges due to the complexity and variability of these factors. Electricity must be produced at the time it is demanded, which requires power system managers to schedule in advance the power plants that will produce electricity each day. This necessitates predicting each day's hourly energy demand ahead of time. Accurate forecasts are crucial to smooth power system operation. The cost of electricity is a key element in determining a country's competitiveness, and improving demand forecasts can significantly reduce costs in liberalized electricity markets.

Recent advances in statistical and machine learning methods have contributed significantly to improving forecast accuracy in this field. The current models used by power system operators provide 24-hour forecasts with an error of less than 2% [1, 2]. Maintaining and improving this margin of error involves continuous work to update and refine the forecasting models.

The effect of temperature has been considered in multiple ways in electricity demand prediction models. To review the literature on the effect of weather conditions on demand, it is necessary to keep in mind that the relationship can vary greatly depending on the country in question. An acceptable solution for one power system may not be valid for another. In France, for example, the effect of temperature is crucial because winter heating relies mainly on electricity [3]. In Spain, the effect of temperature is important in winter for heating, but it is even more critical during the summer months for cooling.

This thesis aims to investigate and analyze the current state of forecasting problems in the electric power market, focusing on demand forecasting, supply forecasting from renewable sources, and price forecasting. By providing a comprehensive overview of recent contributions and methodologies, this research bridges the gap between theoretical research and practical applications in electricity forecasting. Specifically, it focuses on improving the reliability and accuracy of critical forecasts in the electric power market, with a particular emphasis on the Peninsular system in Spain.

1.1. Methodological approach:

This section outlines the methodological procedures adopted to ensure a robust and scientific approach to addressing research questions.

- Literature review:

A comprehensive review of the existing literature in the field of electric power market forecasting is conducted to understand current methodologies and identify research gaps.

- Data collection:

Real-world data sets are gathered from relevant sources, including meteorological data, electricity demand data, renewable energy generation data, and electricity price data from European countries.

- Algorithm development:

Methodologies are designed to optimize the selection of meteorological variables to improve the forecasts of electricity demand.

Algorithms are proposed to enhance the combination of probabilistic predictions for the forecasts of renewable energy generation.

Models are developed to analyze the dynamics of hourly electricity prices in European countries and recommend suitable forecasting approaches.

- Testing and Validation:

Extensive testing and validation of the developed methodologies and algorithms developed are carried out using real-world data sets.

- Performance Evaluation:

The performance of the developed methodologies and algorithms is evaluated in terms of prediction accuracy, reliability, and computational efficiency.

The results are compared with existing forecasting methods to assess the improvements achieved through the proposed approach.

- Documentation and Dissemination:

The findings, methodologies, and results obtained throughout the research process are documented.

The dissemination of findings is carried out through academic publications and conference presentations to contribute to the broader research community.

1.2. Motivation and research objectives:

Electricity demand, supply, and prices are dynamic and are influenced by various factors. Understanding and accurately forecasting these variables is vital for effective market operations and planning. This thesis seeks to improve the accuracy of forecasting in the electric power market. Recognizing the need for better forecasting tools, my research focuses on three key areas: predicting electricity demand, forecasting renewable energy generation, and understanding electricity price dynamics.

The aim of this research work is to provide stakeholders with robust forecasting tools to make informed decisions and navigate the complexities of the electric power market.

1.2.1. Research objectives

1. What are the most effective techniques to forecast electricity demand?
   - Identify key meteorological variables that influence demand.
   - Develop and test methodologies for optimal selection of these variables.
2. How can probabilistic forecasts of renewable energy generation be improved?
   - Develop an algorithm to combine probabilistic predictions with advanced statistical techniques.
   - Assess the accuracy and reliability of the combined forecasts.
3. What are the best approaches to forecasting electricity prices in European markets?
   - Analyze the dynamics of hourly electricity prices across multiple European countries.
   - Evaluate different time-series models for predicting future prices.

1.3. Research structure

This thesis was structured into seven sections: the introduction sets the context and outlines research objectives; Section 2 provides an overview of the electric power market, emphasizing its complexity and the significance of forecasting, with a focus on the European and Spanish electricity systems; Section 3 introduces the basic forecasting model for electricity demand, detailing input variables and the mathematical framework utilized; Section 4 explores the optimal selection of weather stations for electric load forecasting, with a specific application to the Spanish system; Section 5 explores contributions to forecasting renewable energy generation, addressing the aggregation problem; Section 6 examines contributions to price forecasting, highlighting differences among European countries; and finally, Section 7 presents conclusions, summarizes findings, and suggests directions for future research in electric power market forecasting.

2. UNDERSTANDING THE SIGNIFICANCE OF FORECASTING IN THE ELECTRIC POWER MARKET

2.1. Overview of the electric power market: importance and complexity

The electric power market is a complex and dynamic system that plays a crucial role in the functioning of modern economies. It is an essential component of contemporary civilization, driving economic activities and enabling the operation of diverse sectors. In today's interconnected world, electricity is not merely a convenience but a fundamental necessity, powering everything from homes and industries to critical infrastructure and technological advancements. Understanding the electric power market involves exploring a field of immense importance and complexity, where intricate dynamics of supply, demand, and pricing drive a country's economy.

Forecasting the demand or price for electricity, as well as the stochastic generation of renewable energy, is a complex and challenging task. In recent years, significant advancements have been made in the forecasting of the electric power market through the use of advanced statistical and machine learning methods.

Sophisticated mathematical models are carefully designed to capture the details in supply, demand, and pricing dynamics. Using techniques such as time series analysis, econometrics, and machine learning, these models offer insights into historical trends and future trajectories. Established methodologies, such as ARIMA time series models, combined with the advent of new machine learning algorithms has revolutionized

forecasting practices, enabling analysts to extract actionable insights from vast and heterogeneous datasets. Through techniques like data mining and artificial intelligence, market participants gain deeper insights into underlying trends and emerging patterns, facilitating proactive decision-making amidst uncertainty.

2.2. The European electricity market

2.2.1. The origin of electricity markets

The origin of electricity markets dates to the early 20th century when the first regulated market was established in the United States. In 1920, the Federal Power Commission was created to oversee the interstate sale of electricity, with the aim of ensuring fair pricing and promoting competition within the industry [4, 5].

In Europe, the development of regulated electricity markets was a more gradual process. The establishment of the European Economic Community (EEC) in 1957 played a pivotal role in driving market liberalization and fostering the creation of competitive electricity markets across the continent. The objective of the EEC of creating a unified market for goods and services, including electricity, spurred efforts to remove trade barriers and encourage competition [4, 5].

Electric energy is one of the most important issues for the European Union. In the late 1980s, the European Union's approach to the energy sector changed significantly, influenced by developments in the United States and the United Kingdom and the positive experiences of these countries. During the 1980s and 1990s, American companies embraced free competition and a free market approach. These successful examples of market liberalization encouraged European leaders to gradually adopt competitive markets. Additionally, Argentina and Chile were among the first South American countries to pursue privatization of the electricity industry in 1982.

The electricity sector in the European Union was liberalized in the mid-1990s to provide better conditions for electricity producers and consumers in terms of prices and services. During this process, various regional spot markets were created, such as Nord Pool Spot in Nordic countries, EPEX SPOT in France, Germany, and Central European countries, and OMIE for the Iberian Peninsula (Spain and Portugal). These markets have operators to manage the spot market by buying and selling electricity between consumers, producers, suppliers, and traders. In the Iberian Peninsula, the responsible entity for the matching of electricity is the Iberian Electricity Market (MIBEL), and daily market regulation is handled by the Iberian Electricity Market Operator (OMIE).

2.2.2. The European electricity market today

Today, the European electricity market is the largest interconnected network for trading electricity, encompassing over one thousand independent participants. This complex ecosystem of organizations, actors, regulations, and infrastructure ensures reliable production and supply of electricity across the continent, while also facilitating the flow of electricity and maintaining competitive prices. At its core, the European electricity market operates on the principles of liberalization, fostering competition among different electricity suppliers and enabling market-driven price determination.

In Figure 2-1 shown a timeline detailing key developments in the European Union's energy policy from 1950 through 2022. Here's a breakdown of the key points and their implications:

1. European Coal and Steel Community ECSC, (1950): Marks the beginning of European integration with a focus on energy as the starting point. The ECSC was aimed at regulating the coal and steel industries, foundational to rebuilding post-war Europe.

2. Euratom: The European Atomic Energy Community, (1957): It was introduced as an initiative to coordinate the Member States' research programs for the peaceful use of nuclear energy. The mention of threats to cut off oil supplies may refer to geopolitical strategies influencing Europe's energy policies.
3. Energy Market Liberalization, (1990): The EU began liberalizing the energy market to encourage competition among operators across Europe, involving the separation of production, transportation, and distribution activities and the introduction of market prices. Member States, however, retained significant control over their energy mix decisions.
4. Combating Climate Change, (2000): Emphasis on reducing greenhouse gas emissions, notably CO2 from anthropogenic sources, as a significant contributor to global warming.
5. Transition to Renewable Energy, (2005): The EU started transitioning from fossil fuels to renewable energy sources, reflecting a broader commitment to sustainable energy.
6. Energy-Climate Package, (2008): Introduced as "3x20" targeting three goals for 2020: reducing greenhouse gas emissions, increasing renewable energy usage, and improving energy efficiency. The success of these initiatives was described as relative.
7. EU Energy Objectives for 2030, (2014): The EU set new goals for 2030, building upon previous targets and focusing on more sustainable energy practices.
8. European Green Deal (2020): Aimed at achieving net-zero greenhouse gas emissions by 2050, with an interim goal of at least a 55% reduction by 2030 compared to 1990 levels. This is a significant step up in ambitions to address climate change.

9. Energy Sovereignty (2022): Due to uncertainty from Russia (likely referring to political or supply issues), the EU prioritized "energy sovereignty" to ensure a more secure and independent energy supply.

This timeline highlights the EU's evolving approach to energy policy, from initial market integration and regulatory efforts to a strong focus on sustainability and climate change, culminating in the pursuit of energy independence and sovereignty.

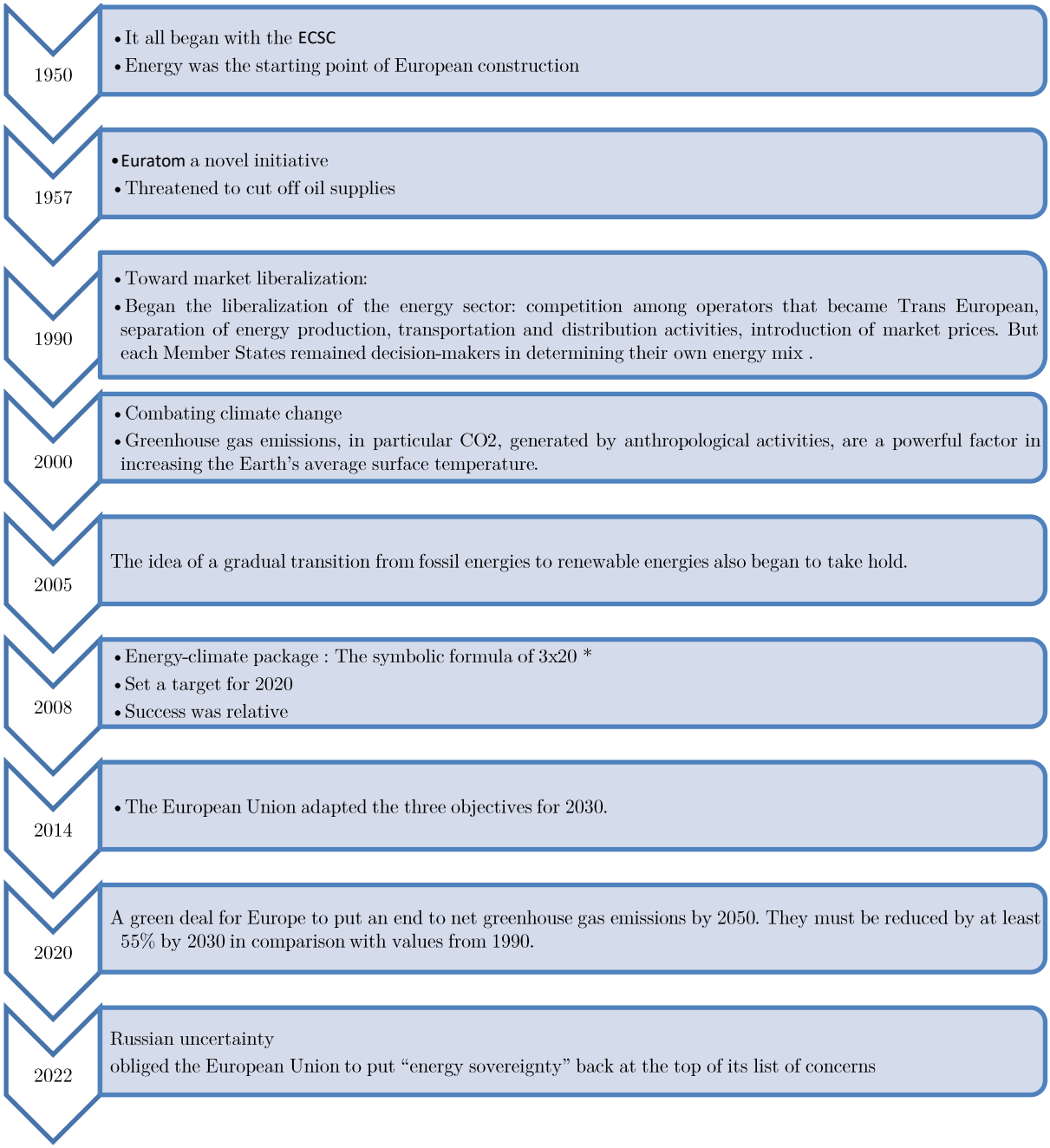

Figure 2-1: Europe's Energy History

The European electricity market currently faces several challenges, influenced by both global and regional dynamics. Some of the significant issues include the following:

1. Rising Energy Prices: Disruptions in global supply chains have significantly affected energy prices, particularly for natural gas, which has subsequently influenced electricity prices. This chain reaction has contributed to a cost-of-living crisis, exacerbating concerns about energy security. The limited availability of natural gas due to geopolitical tensions, logistical challenges, and supply-demand imbalances has amplified the volatility of global energy markets, driving up costs and posing challenges for consumers and policymakers. As a result, there is a renewed focus on finding resilient and sustainable energy solutions to navigate these uncertainties.
2. Dependence on Imports: Many European countries rely heavily on energy imports, particularly natural gas. The need to reduce this dependence has led to initiatives to diversify energy sources, including the accelerated adoption of renewables.
3. Energy Transition and Renewable Integration: Increasing the share of renewables is essential for sustainability, but the intermittent nature of renewable sources, such as wind and solar, creates challenges for grid stability. Balancing supply and demand with a high percentage of renewables requires advanced grid management and storage solutions.
4. Market Structure and Regulation: The European market operates on a marginal pricing model, where the cost of the last unit produced sets the price for all electricity. This model has been criticized for causing high electricity prices when fossil fuel prices spike.
5. The Iberian Exception: This is a specific measure taken by Spain and Portugal due to their limited connection to other European energy markets. The two countries secured permission from the European Commission to temporarily cap the price of natural gas used for electricity generation to protect consumers from price volatility.

This measure aims to lower electricity prices and provide stability, particularly given the regional dependence on natural gas.

6. Cross-border coordination: Coordination between countries is essential for managing the energy grid, yet differences in national regulations and market structures can hinder efficient cross-border trade and transmission.

7. Energy Security: Ensuring a steady and sufficient energy supply is increasingly challenging given geopolitical tensions, fluctuating fuel supplies, and extreme weather events.

Addressing these issues requires a combination of policy reforms, technological innovation, and international cooperation to secure a stable, resilient, and sustainable European electricity market.

2.3. The Spanish electricity system

The Spanish electricity system comprises a set of organizations and companies responsible for managing the country's power line network and all technical elements necessary to supply energy to users, from production plants to consumption points. This system involves both the physical flow, which includes the material process of electricity production and supply, and the economic flow, related to its purchase and sale on the market.

The goal of the Iberian Electricity Market (MIBEL) is to provide electricity through transmission and distribution networks with economic efficiency. This system includes the physical flow (production, transmission, and distribution of electricity), regulated by the system operator, and the economic flow that arises from the opportunity cost of the generators.

The physical flow of electricity encompasses the path of electrical energy from production to consumption Figure 2-2:

1. Production: This begins at power plants managed by companies such as Endesa and Iberdrola. Production involves converting various energy sources, such as water and wind, into electricity using specific technologies.

2. Transmission: The next step is power transmission, managed by operators such as transmission system operators (TSO), independent system operators (ISOs) and independent transmission operators (ITOs). In Spain, the TSO model is used, with red eléctrica de españa (REE) overseeing the transmission network.

3. Distribution: At distribution points, the transmission lines connect to distribution lines, where the voltage levels are reduced to suitable levels for industrial and residential use. Spain has five major electricity distributors (Endesa, Iberdrola, E-Redes Distribución, Unión Fenosa and Viesgo Distribución) and over 300 smaller independent distributors. Distribution involves transferring electricity to consumption points while maintaining quality and operating and expanding distribution networks.

4. System operation: REE coordinates the overall system to ensure smooth physical flow. Provides the operation of the system as the most crucial activity in the sector, guaranteeing quality and a safe supply [6].

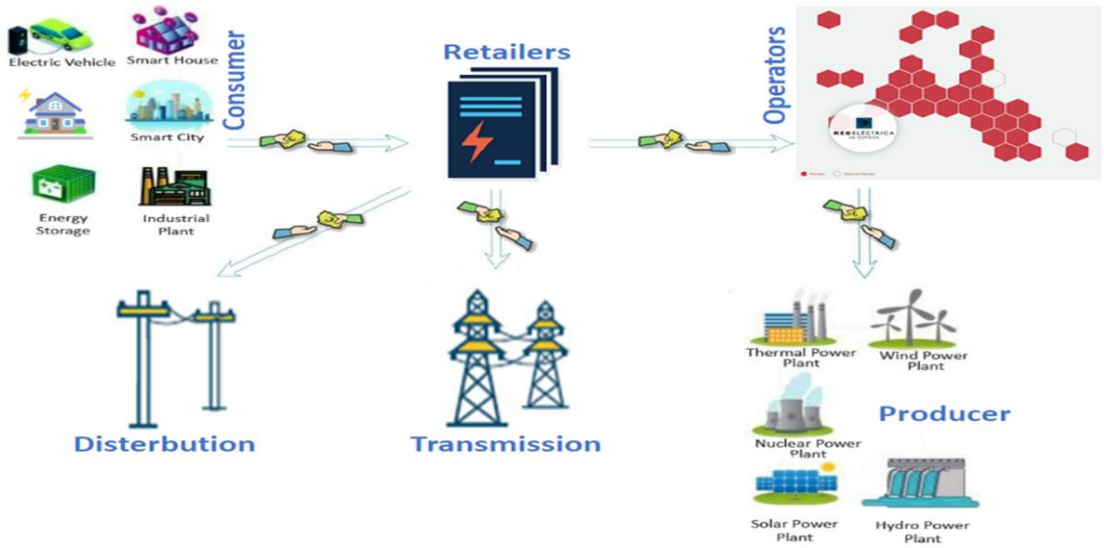

Figure 2-2: The physical flow of the electricity distribution.

2.3.1. The Spanish electricity market

In Spain, the wholesale electricity market, commonly referred to as the electricity pool, serves as a marketplace where electricity generators and marketers engage in trading energy by specifying their prices and desired sales volumes. This market operates within MIBEL, the Iberian electricity market that integrates Spain and Portugal into the broader European Union energy framework.

Market segments in Spain:

1. Day-ahead market: This segment handles the largest volume of transactions. Participants submit their offers by 10am daily. Buyers (marketers and eligible consumers) indicate their required energy volume and desired price, while sellers (producers) specify their supply availability and pricing. The Iberian Market Operator (OMIE) utilizes the EUPHEMIA algorithm to align the Iberian market with other European markets. This algorithm matches supply and demand curves to determine the equilibrium price, setting the hourly market rate for the next day's electricity supply.

2. Bilateral contracts: These contracts also hold a significant market share. They involve direct agreements between large producers and consumers, allowing them to negotiate terms that meet specific needs. This over the counter (OTC) arrangement provides stability and predictability.
3. Auxiliary markets:

- Intraday market: Enables trading closer to consumption time, allowing market participants to adjust their positions through several trading sessions per day. This flexibility helps manage unexpected changes in supply or demand.
- Adjustment Services Market: Balances the system by providing ancillary services, including secondary and tertiary regulation and deviation management, ensuring stable supply and demand.
- Capacity Markets: Offers financial incentives to maintain sufficient capacity to meet peak demand and emergencies, helping stabilize the energy supply.

European market integration:

The various market structures in Spain, guided by OMIE in the day-ahead market, ensure efficient trading and transparent pricing while fostering a deeper integration with European electricity markets. MIBEL operates within a network of interconnected European markets, such as EPEX spot, Nord Pool Spot, N2EX, and IPEX, enabling cross-border electricity trading through their respective system operators. These operators manage cash markets and coordinate electricity transactions between system participants, ensuring seamless energy flow across borders. This network of market operators collectively contributes to a more integrated European energy market, improving competition, efficiency, and reliability while supporting energy security.

2.4. Day-ahead market

The day-ahead market facilitates electricity transactions for the following day, where market participants submit offers to buy and sell energy based on their forecasted needs. Market agents, including producers and buyers, provide these offers for every hour of the next day. The market operator, OMIE, then consolidates these data to predict the electricity demand curve the following day. (Figure 2-3)

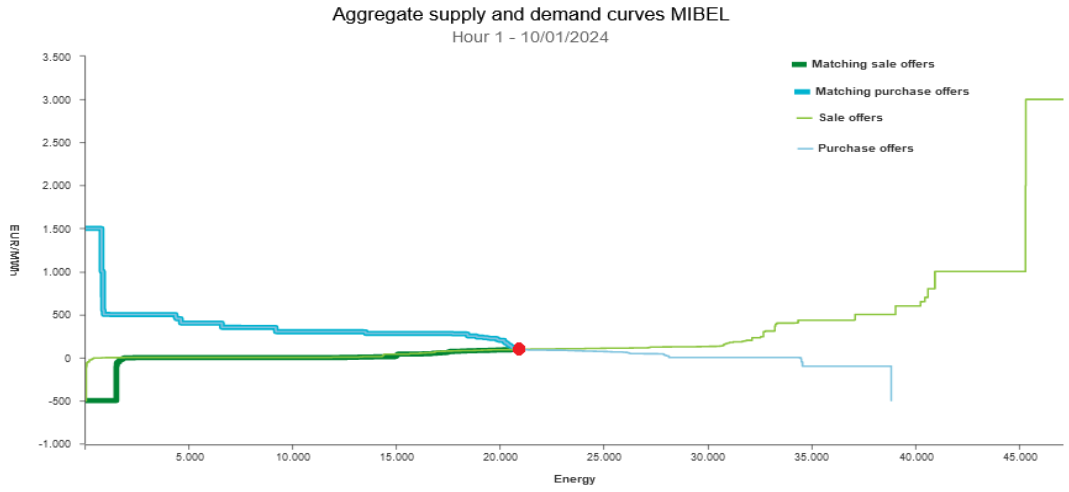

Figure 2-3: Aggregate supply and demand curves MIBEL for hour 1 of 10.01.2024 [7]

2.4.1. Market matching process

The market matching process works as follows.

1. Submission of offers: Market participants provide separate hourly offers (24 per unit), either as buyer or seller. Generators propose selling prices for the electricity they produce, while buyers state the maximum price, they are willing to pay.
2. Auction process: OMIE organizes the submitted data, creating a supply curve in ascending price order and a demand curve in descending price order. The intersection point between these two curves determines the market clearing price and volume for each hour of the following day.
3. Market clearing and pricing: Offers are accepted to the left of the intersection point, setting the price and volume for that particular hour. This point is where

the market achieves equilibrium, ensuring that supply meets demand at the optimal price.

4. Technical limitations management: After the daily market launch and resolution of the valuation, REE begins to analyze the technical limitations of the network. Using grid and electrical system flow models, it resolves congestion by adjusting the generation schedule while maintaining balance with demand.

The day-ahead market facilitates the integration of Spain's electricity market into the broader European network by aligning with the EUPHEMIA algorithm.

Daily markets are regulated in six auction sessions in the MIBEL region and a continuous European cross-border market. Additionally, in the system operation section, two additional tools are utilized: the deviation management system and the adjustment service.

2.4.2. Intraday markets

After completion of the daily market matching process, the intraday market begins its operations. In this market, the system agents have the opportunity to buy and sell electricity in six sessions. These agents can adjust their offers and obligations up to four hours before the actual market, ensuring alignment with their forecasts.

As the intraday market progresses, it adapts to reflect the actual demand volume on the day of distribution, providing increased liquidity as the delivery time approaches. This flexibility is essential to optimize efficiency and ensure the smooth operation of the electricity market. Agents have the option to negotiate within the same price zone or with other regions to improve overall efficiency, particularly if there is available interregional capacity.

Offers are submitted to a centralized platform, facilitating exchanges between bidding areas, including cross-border transactions. This market plays a crucial role in regulating production and consumption one hour before energy delivery, thereby reducing energy

losses attributed to demand and estimation errors. This aspect is particularly significant for renewable energy sources, where accurate forecasting and real-time adjustments are essential to maximize efficiency and minimize waste (Figure 2-4).

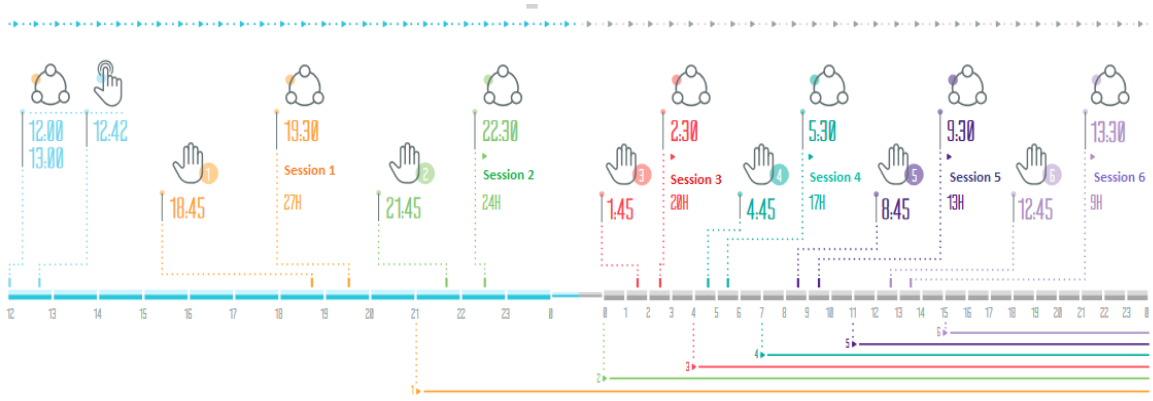

Figure 2-4: Time sequence of the daily and intraday market in MIBEL [8]

2.5. Marketing

Marketers play a vital role in the electricity market by purchasing energy from the wholesale market and supplying it to consumers. The determination of the type of transaction, whether through daily market operations, installment agreements or bilateral contracts, is based on forecasts of customer consumption patterns. The delivery of energy to consumers requires the utilization of transportation and distribution networks.

Marketing activities are conducted under conditions of free competition, and marketers are required to acquire the necessary energy while adhering to payment requirements, access fees, and voluntary price agreements with retailers. According to European legislation, marketers are required to provide labels that explain the origin of the energy supplied and the environmental impact associated with different energy sources.

In Spain, marketers supply electricity through three primary mechanisms:

- Reference supply: This involves the provision of electricity to small consumers under the Voluntary Price for Small Consumers (PVPC) scheme, which is calculated by REE based on daily and hourly market prices. Reference marketers are subject to a maximum price cap, comprising the total energy cost, access tariffs, and business management fees.
- Contracts in the liberalized market: Marketers offer electricity supply contracts in the liberalized market, providing consumers with flexibility and choice in selecting their energy provider.
- Supply of last resort: This option is available to vulnerable or transient consumers who may face difficulties in securing electricity supply through traditional means. Vulnerable consumers are offered a 25% discount, while highly vulnerable individuals receive a 40% discount on their electricity bills.

2.6. Forecasting problems

Electric energy possesses numerous advantages, including ease of use, low pollution, and portability through wiring. However, a significant drawback lies in its inability to be stored in large quantities, which poses a major challenge in engineering. Matching production with consumption requires predicting consumption to plan production accordingly. Using historical demand data and variables influencing it, electricity demand can be predicted.

A deeper understanding of demand patterns is crucial to improving the quality of future forecasts. Quality prediction is essential both in the short term, for system performance and market operations, and in the long term, for constructing new infrastructure such as factories or supply networks. Uncertainty can be mitigated by collecting more information and refining mathematical methods.

On the other hand, accurate forecasts of short-term power generation from renewable energy sources are vital for system operators. Such forecasts enable better decision

making on energy trading, hedging strategies, and infrastructure investments, ultimately minimizing operational costs and maximizing revenue.

Accurate forecasts of electricity prices are indispensable for market agents. Precise price forecasts provide crucial insights for power generators, enabling optimization of production schedules and informed investment decisions in new generation capacity. Similarly, electricity retailers benefit from accurate price forecasts for strategic pricing and hedging strategies, ensuring competitive offerings to consumers while mitigating financial risks associated with volatile market conditions. Energy-intensive industries rely on precise price forecasts to effectively manage operational costs, optimize production schedules, and make strategic decisions about energy procurement strategies. Additionally, accurate price forecasts empower consumers to make informed choices regarding energy consumption patterns, incentivizing demand-side management initiatives and promoting energy efficiency measures.

In general, the ability to make accurate predictions is indispensable to manage and operate a national electrical system, affecting operational efficiency, economic performance, environmental compliance, and system reliability. This thesis outlines various contributions within the context of operating the Spanish electrical system, addressing critical issues such as short-term demand forecasting for daily system operations, probabilistic predictions of wind energy production, and the behavior of hourly electricity prices in Europe. Despite the challenges associated with predicting these elements and their impact on the electricity market, the complexities of accurately forecasting short-term electricity demand are crucial to ensuring reliable daily operations of the power grid. Similarly, probabilistic forecasts of wind energy production are vital due to the variable nature of wind, posing challenges for grid integration. Understanding the dynamics of hourly electricity prices across European markets is essential for market participants, highlighting the difficulties in predicting

price fluctuations and their significant implications on the electricity market's economic environment.

3. BASIC MODEL

3.1. Introduction

In this chapter, we will dive into the data sources and models utilized throughout this thesis. We aim to provide a comprehensive overview of the modeling techniques that form the foundation of our research. This exploration will offer insight into the robustness and reliability of the data-driven approaches adopted in our study, setting the stage for the subsequent analysis and findings presented in this thesis.

3.1.1. Motivation and literature review

Short-term demand prediction is one of the key components for proper operation and optimal planning in any electric power system. The system operator, who manages any generation, transmission and distribution network, must have computer tools that allow predicting, with the highest possible accuracy, electrical demand in the coming hours or days, to coordinate all the agents involved in the energy market. In the Spanish electricity system, Red Eléctrica de España is the entity responsible for this task.

During the past two decades, the forecasting model devised by Cancelo and Espasa [1] has shown effective utility in predicting electricity demand in Spain. They proposed a reg-ARIMA model to predict daily electric demand in Spain. The model includes an extensive set of binary variables to model changes in demand on holidays and vacation periods. It also accounts for the non-linear relationship between demand and temperature through a piecewise linear function. The total number of parameters in the daily model is 185, ten of which correspond to the moving average part (there is no autoregressive part), 32 parameters correspond to climatic variables, and the rest (143 parameters) correspond to auxiliary variables modeling holidays and other calendar adjustments. The same model is estimated for each of the 24 hours and is

used to make predictions up to three days ahead. The 24-hourly models have the same basic structure, although their parameters are adapted to the particular characteristics of each hour of the day. A complete description of the model can be found in [9].

In neighboring countries like France, Dordonnat et al. [3] present a multivariate linear state space model for forecasting hourly electric demand. This model includes a stochastic trend component, along with fixed and dynamic regressive effects. Each equation is associated with a specific hour and has different coefficients and dynamic processes. This method demonstrates that temperature significantly impacts demand, subject to non-linear annual variations. The coefficients of the dynamic artificial variables are peculiar and surprisingly significant. The total number of parameters in the model is 37, of which seven are fixed, 27 are dynamic, and there are variances in the irregularities and parameters that model the level and slope of the stochastic process. The dataset used in the study is based on the hourly electricity demand in France. The quality of the predictions is satisfactory for one, two, and three days ahead for weekdays, but less satisfactory for special days, with errors more than three times those of ordinary days.

The complex structure of artificial variables used in [9] to characterize the peculiarities of different special days is rewarded with higher prediction quality for these days. Using dynamic coefficients to measure the effect of special days in [3] is an intelligent way to eliminate or reduce their effects in the model but does not achieve accurate predictions for these days. However, with only a small number of parameters, the model can make good predictions for most normal days.

Cottet and Smith [10] develop a Bayesian technique to estimate coupled multi-equation regression models using Markov Chain Monte Carlo methods. The results show that weekly, seasonal, meteorological, and dynamic effects are significantly different for different times of the day, confirming the multi-equation model used in the work.

During the last few years, professors Jesús Juan and Eduardo Caro, members of the ETSII- UPM This predictor is based on a reg-ARIMA time series model, which includes the effect of temperature and the peculiar characteristics of each day (working days, national or regional holidays, vacation periods, time change days, etc.). Forecasts are calculated with a fifteen-day horizon, although the most commonly used are those with a horizon of less than 48 hours.

Taking into account the prediction horizon and the special characteristics of the series, it was decided to build univariate models for each of the 24 hours of the day. The structure of the 24 models is the same for all hours, although the value of the parameters varies from one hour to another. As these 24 models do not take advantage of the information about the upcoming hours, this deficiency has been corrected by improving the predictions through a subsequent correction that consists of using the correlation between the upcoming hours, which significantly improves the quality of the predictions. In the Figure 3-1 shows a screenshot of the speech forecaster for peninsular demand for the week of March 20, 2023. The blue and green lines represent the actual demand and the forecast demand, respectively. The 95% confidence interval of the predictions is represented by the yellow band, and at the bottom of the graph, the absolute errors for each hour are displayed. The two graphs in the right margin illustrate the prediction quality quantified by the MAPE and ECM metrics for each hour.

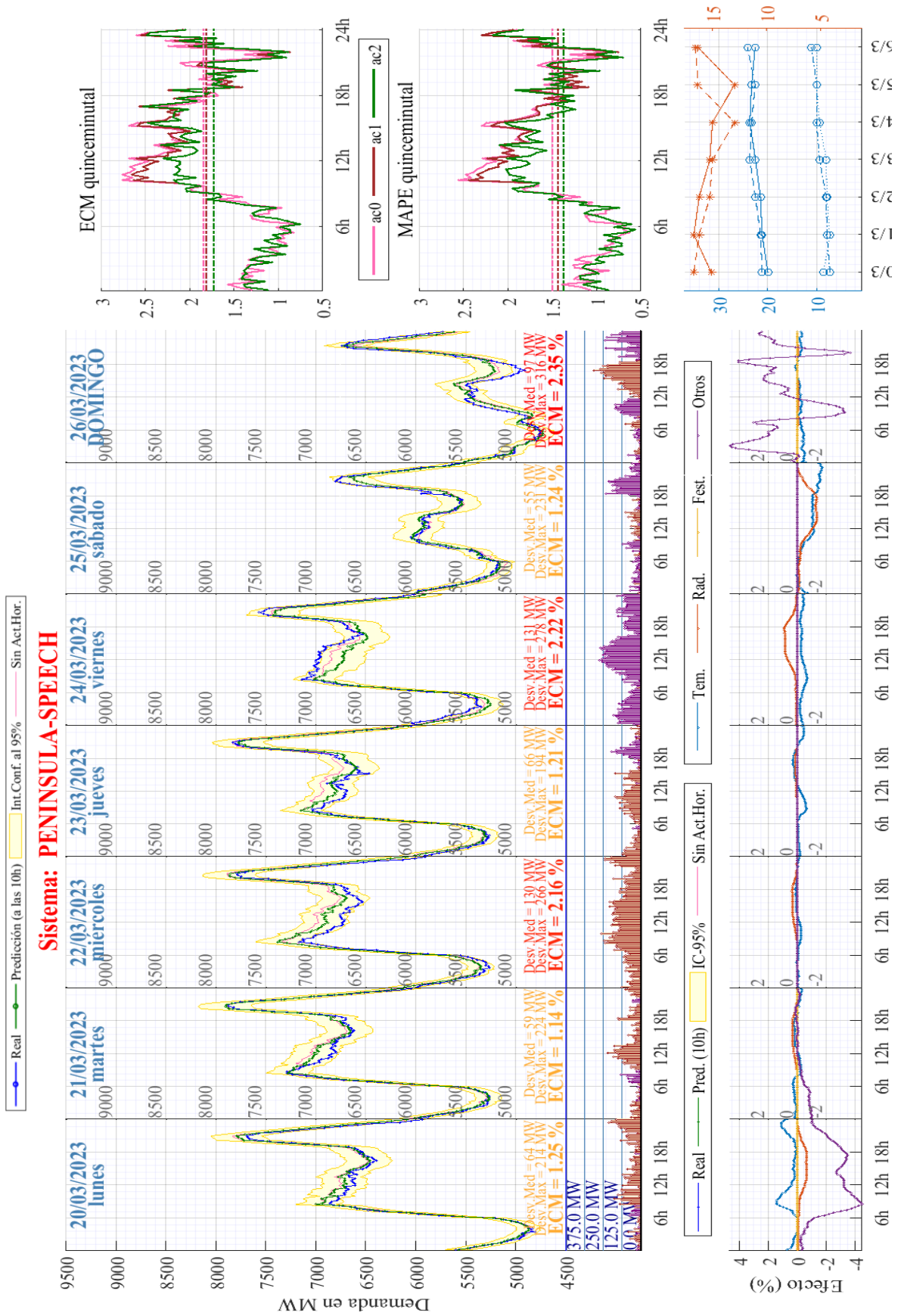

Figure 3-1: Real-time demand prediction by the ETSII-UPM forecaster.

3.1.2. Structure

In this chapter, the structure is as follows: Firstly, a brief description is provided in section 0 about the input data utilized by the electrical demand forecaster.

3.1.3. Inputs variables

The following sections outline the input variables required by the peninsular demand prediction model for its proper functioning.

3.1.4. Weather forecast for AEMET

One of the input variables for the model is the forecast maximum and minimum temperatures for the days for which prediction is desired. The program is designed to utilize the files provided by the Spanish meteorological agency (AEMET). These data can be accessed on the website [11] (Figure 3-2).

Figure 3-2: AEMET weather forecast consultation on its official website.

In Figure 3-3, the content of the file is provided:

- Description: The meteorological variable provided is the forecasted maximum and minimum temperature at 2 meters above ground level, in °C. These forecasts are provided for provincial capitals and other Spanish cities.
- Update: Daily files with predictions for a 10-day horizon. This data is obtained from the 00h run of the model, which is received around 07:05 UTC.

DATOS METEOROLÓGICOS PREVISTOS
DE CIUDADES ESPAÑOLAS

TEMPERATURAS MÁXIMAS A 2m. EN GRADOS CENTÍGRADOS
PREVISTAS DESDE EL 2023-03-31 HASTA EL 2023-04-09

CAPITALES DE PROVINCIA Y CIUDADES	TEMPERATURAS DÍAS 31	01	02	03	04	05	06	07	08	09	Estación	coordenadas
A Coruña	17.6	15.7	15.8	19.5	19.5	19.7	21.6	23.1	16.4	16.9	1387	43.3658N : 8.4214W
Lugo Aeropuerto	17.0	15.4	14.8	18.8	18.5	21.0	25.5	25.3	20.9	22.9	1505	43.1114N : 7.4575W
Oviedo	18.8	13.9	13.4	16.3	15.7	18.7	22.2	27.6	19.7	20.3	1249X	43.3533N : 5.8742W
Santander	18.9	15.2	14.1	14.4	14.3	15.8	17.8	21.4	18.6	16.6	1111X	43.4911N : 3.8006W
Bilbao Aeropuerto	20.7	14.9	14.8	16.2	15.8	18.4	21.7	26.6	24.6	22.3	1082	43.2981N : 2.9064W
San Sebastián Aeropuerto	23.1	16.5	15.6	16.1	14.8	17.1	20.0	24.9	23.1	20.0	1014A	43.3569N : 1.7922W
Pontevedra	17.0	17.5	19.4	21.6	23.9	24.2	26.5	25.0	22.0	23.7	1484C	42.4383N : 8.6158W
Ourense	19.4	19.3	20.6	22.5	25.1	25.4	28.3	28.1	25.7	27.8	1690A	42.3253N : 7.8597W

Figure 3-3: Predicted maximum temperature file.

3.1.5. ECMWF weather forecast

In recent years, much more comprehensive information on meteorological variable predictions has become available, thanks to the European ECMWF model, which is considered the most complete and reliable model by the scientific community. It is the global model with the highest resolution and quality currently available: it has a resolution of one point every 9 kilometers. These prediction data can be freely accessed at [12] (Figure 3-4).

The information contained is as follows:

- Longitude (lon variable)
- Latitude (lat variable)
- Time instance (time variable)
- Temperature (2_metre_temperature_surface variable)
- Cloud cover (Total_cloud_cover_surface variable)

- Radiation (Surface_solar_radiation_downwards_surface variable)
- Wind NS (10_metre_U_wind_component_surface variable)
- Wind WE (10_metre_V_wind_component_surface variable)

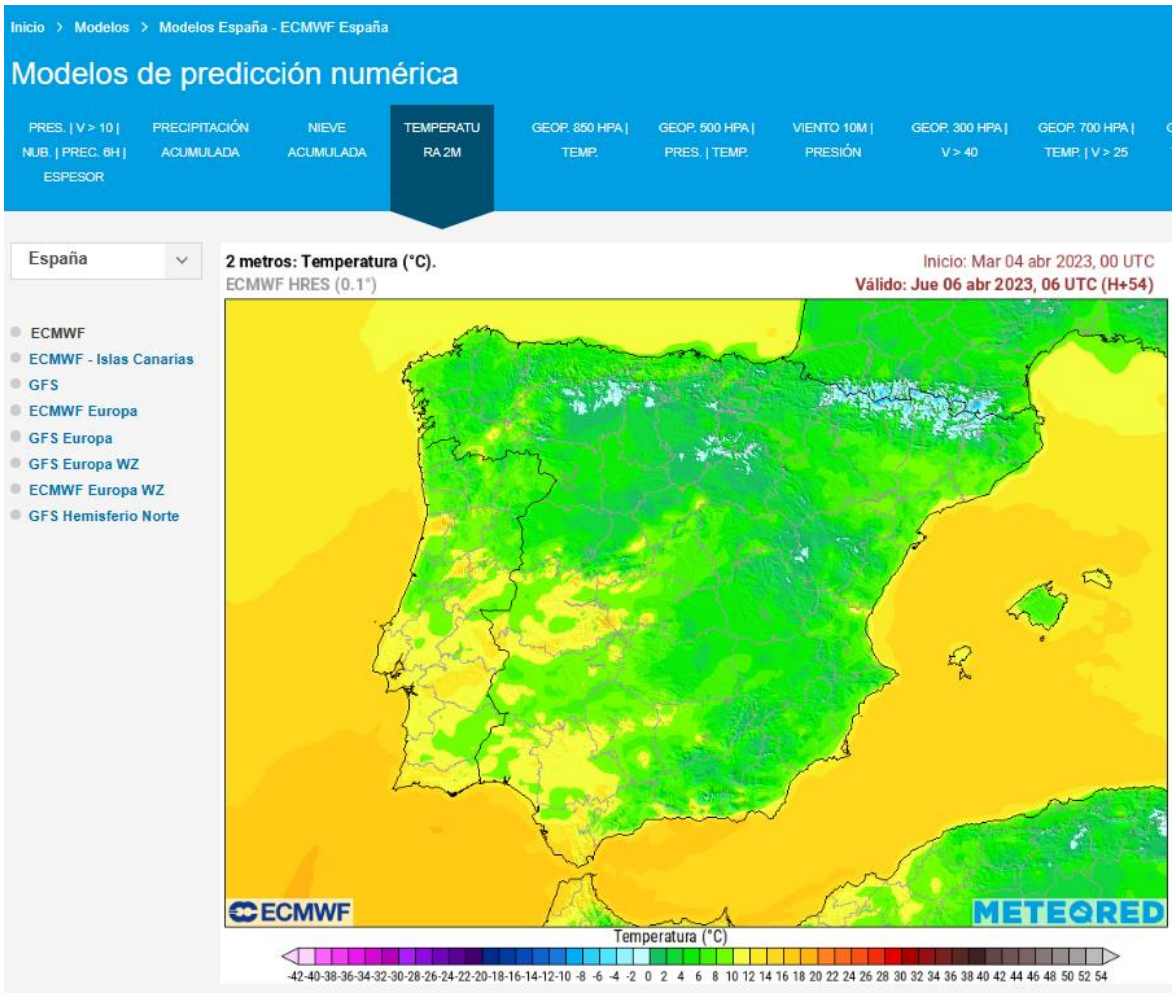

Figure 3-4: ECMWF model temperature forecast.

The information contained in these files is extensive, as the data is stored in various hypermatrices with the following dimensions:

- Latitude dimension: 89 values
- Longitude dimension: 141 values
- Time dimension: 36 values

Therefore, considering the two daily files received and the six meteorological variables contained, a total of 5,421,168 values are received each day. The following Figure 3-5,

Figure 3-6, Figure 3-7 and Figure 3-8 show the information contained in one of the GRIB files.

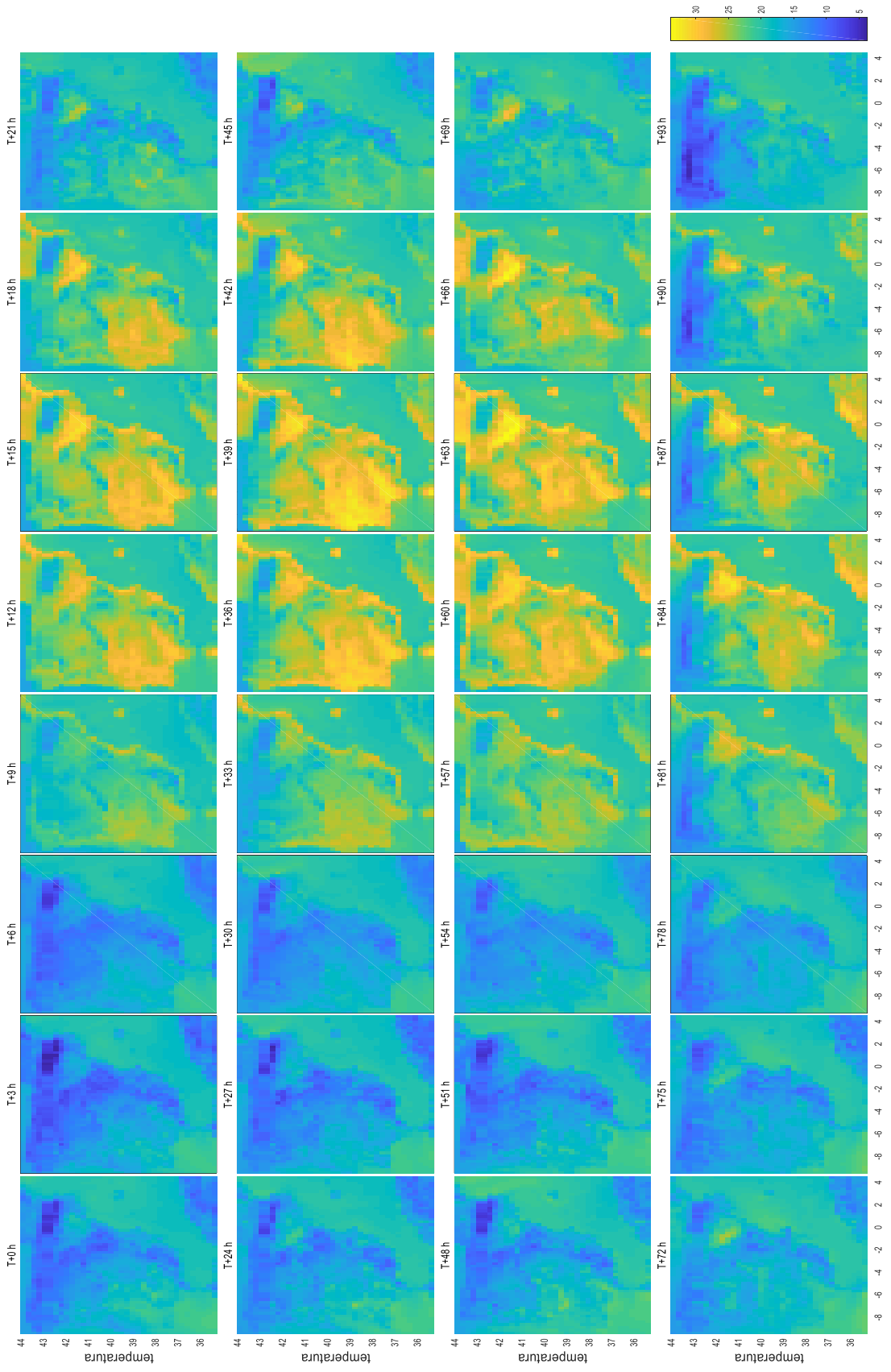

Figure 3-5: Prediction of meteorological variables: temperature.

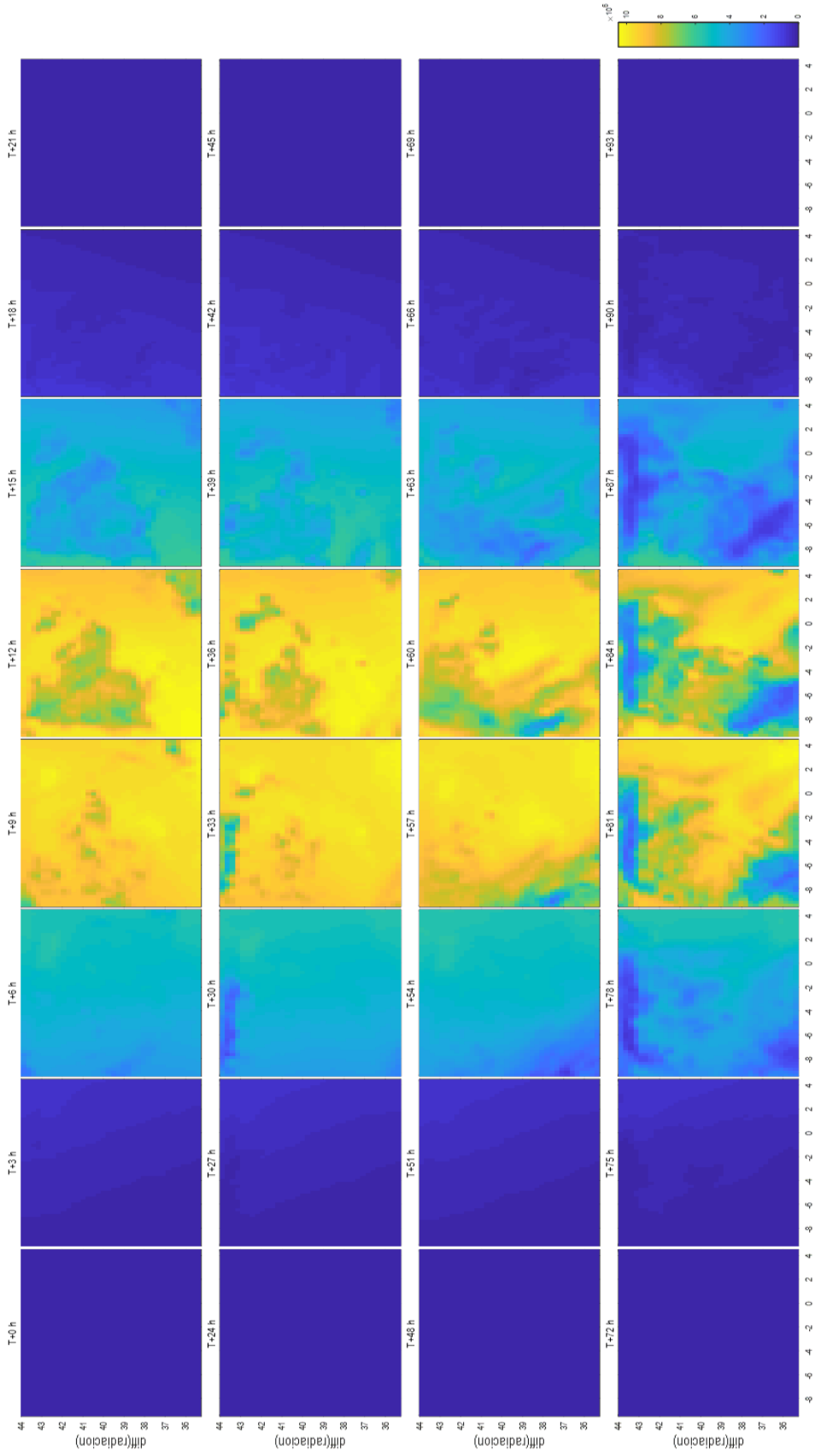

Figure 3-6: Prediction of meteorological variables: radiation.

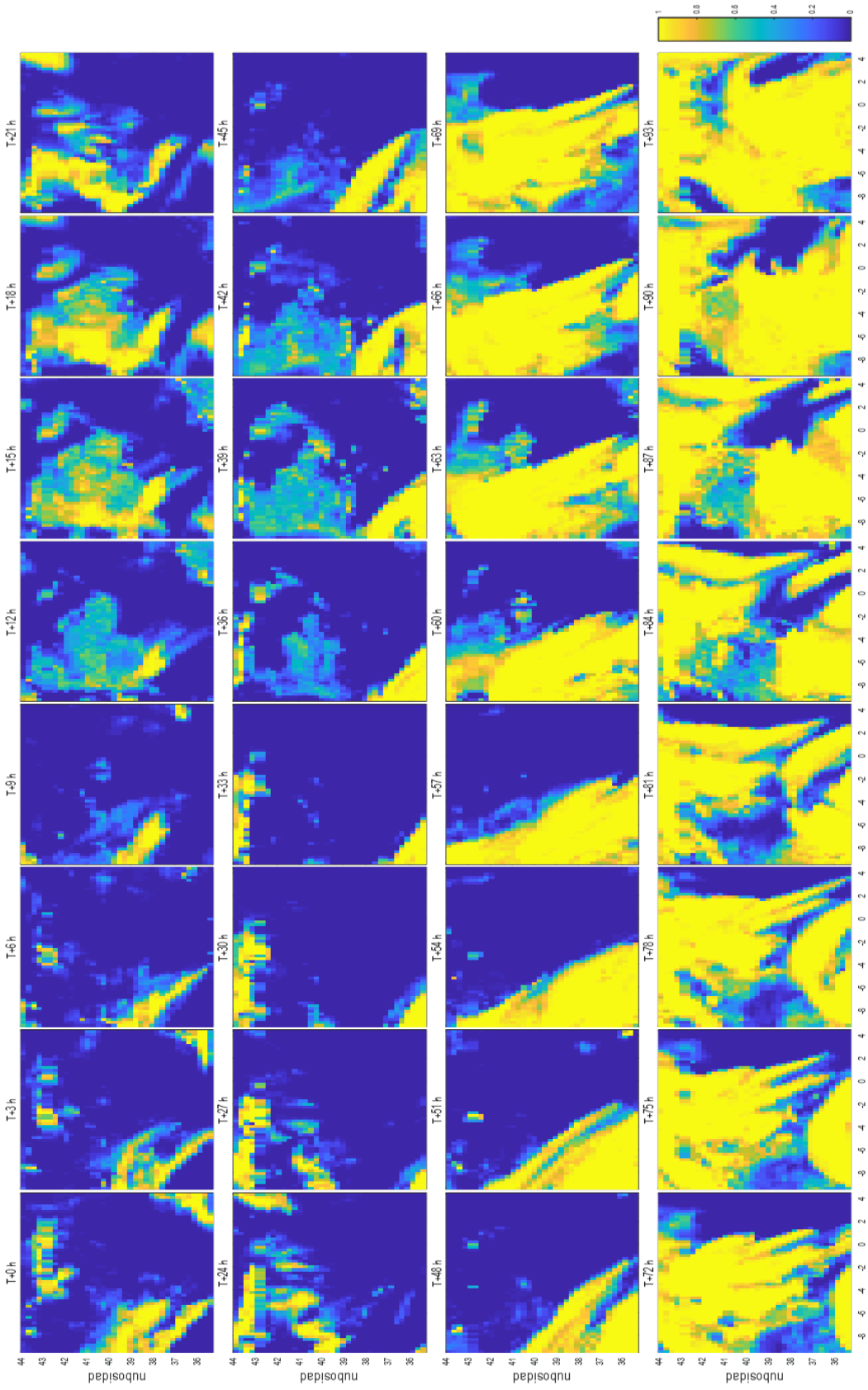

Figure 3-7: Prediction of meteorological variables: cloudiness.

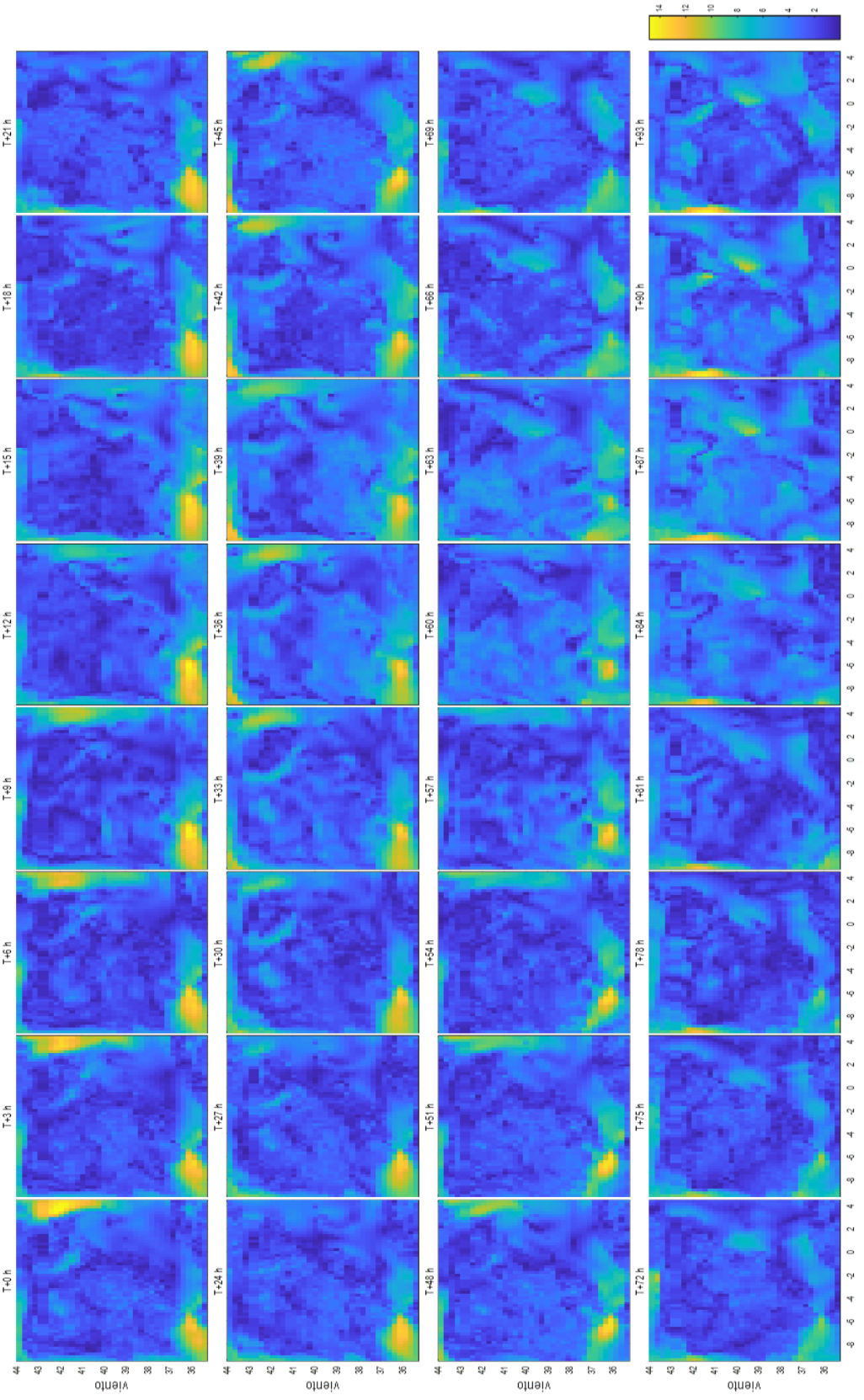

Figure 3-8: Prediction of meteorological variables: wind modulus.

Currently, the solar radiation information contained in the GRIB files generated by the ECMWF model is utilized to enhance the quality of predictions for electrical demand in the peninsular system.

3.1.6. Observed meteorological data

On the other hand, observed meteorological information is available, collected at AEMET weather observation stations. These values can be accessed online through the following website [13] (Figure 3-9).

Figure 3-9: Observed weather information from the AEMET website.

The information contained is as follows (Figure 3-10):

The meteorological variables provided include wind direction, wind speed (km/h), current temperature (ºC), maximum temperature (ºC), minimum temperature (ºC), atmospheric pressure (hPa), insolation, and precipitation (l/m2). This data is provided for provincial capitals and other Spanish cities.

	A	B	C	D	E	F	G	H	I	J	K
1	IDEMA	FINT	UBI	DV	VV	TA	TAMAX	TAMIN	PRES	INSO	PREC
2	76	2023-04-04T00:00:00	BARCELONA/AEROPUERTO	350	2.5	10.1	11	10	1013.5	0	0
3	367	2023-04-04T00:00:00	GIRONA/COSTA BRAVA	300	1.5	7.7	8.1	7.7	997.7	0	0
4	1014A	2023-04-04T00:00:00	SAN SEBASTIÁN/FUENTERRABIA	60	3.5	10.6	10.8	9.6	1018.2		0
5	1082	2023-04-04T00:00:00	BILBAO/AEROPUERTO	60	0.6	8.2	8.2	7.8	1014.8	0	0
6	1111X	2023-04-04T00:00:00	SANTANDER CMT	107	3.5	9.9	10.1	9.9	1012.4	0	0
7	1249X	2023-04-04T00:00:00	OVIEDO	162	0.8	9.3	9.8	9.2	978.1	0	0
8	1387	2023-04-04T00:00:00	A CORUÑA	72	1.4	11.6	12	11.6	1009	0	0
9	1484C	2023-04-04T00:00:00	PONTEVEDRA	17	0.7	12.4	12.5	12.3	1000.5	0	0
10	1505	2023-04-04T00:00:00	LUGO/ROZAS	64	0.3	6.7	7.3	6.7	964	0	0
11	1690A	2023-04-04T00:00:00	OURENSE	188	0.3	10.5	11.1	10.5		0	0
12	2030	2023-04-04T00:00:00	SORIA	127	1.2	4	4.6	4	891.1	0	0
13	2331	2023-04-04T00:00:00	BURGOS/VILLAFRÍA	64	4.9	2.7	3.2	2.3	913.2	0	0
14	2400E	2023-04-04T00:00:00	PALENCIA-AUTILLA PINO	76	5.5	5.4	6.2	5.1			0
15	2422	2023-04-04T00:00:00	VALLADOLID	322	0.9	7.5	7.7	7.5	929.2	0	0
16	2444	2023-04-04T00:00:00	ÁVILA	154	1.1	6.9	8.2	6.9	886	0	0
17	2465	2023-04-04T00:00:00	SEGOVIA	58	0.5	6.4	7	6.4	899.4	0	0
18	2614	2023-04-04T00:00:00	ZAMORA	29	0.7	7.9	9	7.9	938.2	0	0
19	2661	2023-04-04T00:00:00	LEÓN/VIRGEN DEL CAMINO	360	2.8	5.2	6	5.2	910.5	0	0
20	2867	2023-04-04T00:00:00	SALAMANCA/MATACAN	160	1.9	7.3	8.3	7.2	922.7	0	0
21	3129	2023-04-04T00:00:00	MADRID/BARAJAS	120	1	11.4	12.9	11.2	945.2	0	0
22	3168D	2023-04-04T00:00:00	GUADALAJARA	45	2	10.4	11.3	10.4	928.9	0	0
23	3260B	2023-04-04T00:00:00	TOLEDO	300	1.1	12.9	13.7	12.9	952.3	0	0

Figure 3-10: Observed weather file.

This input variable is currently not used by the prediction model.

3.1.7. Observed demand

One of the most important input data is the observed demand, which consists of the values of the time series itself to be studied and predicted. These data are available on the web at [14] (Figure 3-11).

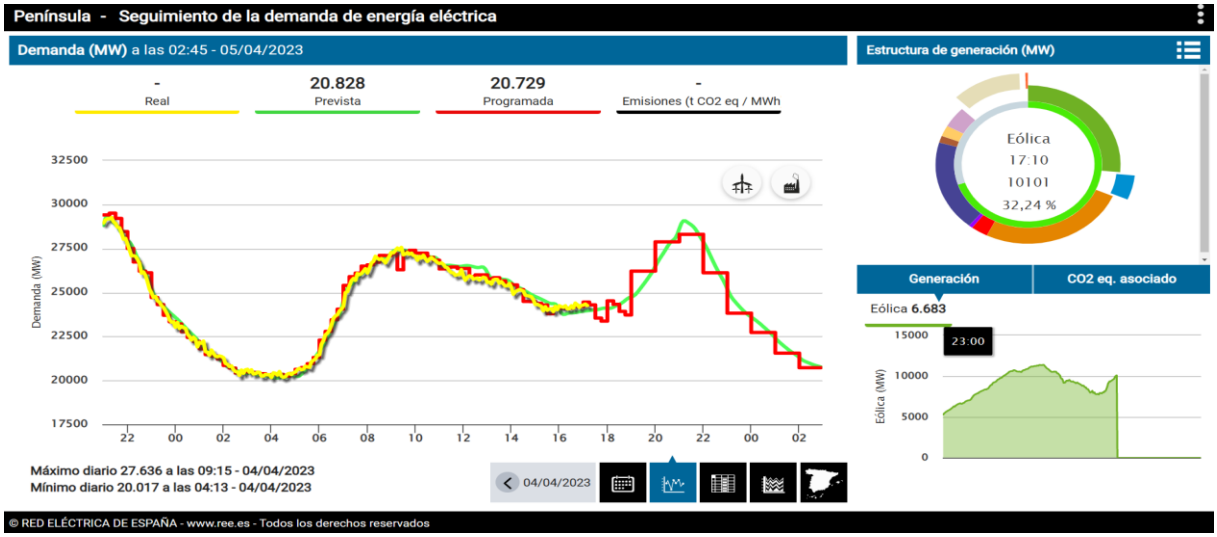

Figure 3-11: Observed demand from REE's website.

For the operation of the developed forecaster, plain text files are used (Figure 3-12), which show the observed demand with hourly data for different regions.

- Real-time energy demand values. Each file contains real demand values corresponding to the hours of the current day up to the time of reception.
- Regions and Systems: Files are received from four zones: Peninsula, Canary Islands, Balearic Islands, and Ceuta Melilla.
- Update: Demand data are received every hour, adding one line per system to the file.

```
================================
Datos de dia: 29-03-2023

Servidor: FUSE
================================
AREA     ANDOCC   DEMANDA  29-03-2023 00:00:00    515.063
AREA     ANDOCC   DEMANDA  29-03-2023 00:15:00    492.798
AREA     ANDOCC   DEMANDA  29-03-2023 00:30:00    484.116
AREA     ANDOCC   DEMANDA  29-03-2023 00:45:00    481.036
AREA     ANDOCC   DEMANDA  29-03-2023 01:00:00    461.340
AREA     ANDOCC   DEMANDA  29-03-2023 01:15:00    455.378
AREA     ANDOCC   DEMANDA  29-03-2023 01:30:00    453.932
AREA     ANDOCC   DEMANDA  29-03-2023 01:45:00    431.561
AREA     ANDOCC   DEMANDA  29-03-2023 02:00:00    440.838
AREA     ANDOCC   DEMANDA  29-03-2023 02:15:00    438.035
```

Figure 3-12: Observed demand obtained by file.

3.2. Mathematical model

3.2.1. Periodic Reg-ARIMA model

In this section, we briefly explain the mathematical model implemented in the electrical demand forecasting software currently used by REE to calculate hourly demand predictions from one to ten days in advance.

The hourly demand time series exhibits significant daily seasonality. The time of day affects both the mean and the autocovariance function of the series. Under these conditions, a single ARIMA model is not sufficiently adaptable to account for the complexity of the hourly process. Several authors have suggested using separate models for each hour of the day as an alternative.

Following this advice, the evolution of electrical energy demand is modeled using 24-hour Reg-ARIMA models. Hereafter, the variable $y_{t,h}$ corresponds to the logarithm of

consumption for day t and hour h. The following two equations define the Reg-ARIMA model for hour h:

$$y_{t,h} = c_h + \boldsymbol{\alpha}_h^T \boldsymbol{x}_t + \boldsymbol{\beta}_h^T \boldsymbol{z}_t + u_{t,h} \quad (3\text{-}1)$$

$$\phi_h(B)\Phi_h(B^7)\nabla^d \nabla_7^D u_{t,h} = \vartheta_h(B)\Theta_h(B^7)w_{t,h} \quad (3\text{-}2)$$

where the logarithm of the electric consumption for hour h of day t (variable $y_{t,h}$) is computed in (3-1) as the summation of a constant c_h, two regression terms, and correlated disturbances $u_{t,h}$. Regression vectors $\boldsymbol{x}_t$ and $\boldsymbol{z}_t$ model both the thermic influence and the holidays effect, respectively, and their values are assumed to either known or forecasted in advanced. Despite values in both vectors are daily updated, the vectorial parameters $\boldsymbol{\alpha}_h$ and $\boldsymbol{\beta}_h$ are estimated independently for each hour. Disturbances $u_{t,h}$ follow an $ARIMA(p,d,q)(P,D,Q)$ process with weekly seasonality (3-2): where B is the backshift operator ($B^k u_{t,h} = u_{t-k,h}$); the seasonal difference operator $\nabla_7 = (1 - B^7)$; the regular difference operator $\nabla = (1 - B)$; the regular and seasonal auto-regressive polynomials ($\phi_h(B)$ and $\Phi_h(B^7)$, respectively); and the regular and seasonal moving-average polynomials ($\vartheta_h(B)$ and $\Theta_h(B^7)$, respectively). Term $w_{t,h}$ represent the independent zero-mean Gaussian-distributed errors with variance σ_h^2. The Box-Jenkins methodology [15] has been applied to estimate the previous mathematical model.

3.2.2. Modeling the influence of temperature

The profound influence of temperature on energy consumption is widely recognized. Effective modeling must consider several key factors: (i) the temperature's varying impact on consumption across different seasons; (ii) the spatial dimension must be considered in the mathematical model for large systems; and (iii) the effect of temperature is not solely instantaneous because the temperature on one day can have a significant impact on demand in the following days.

The nonlinear relationship between temperature and consumption has been captured using spline regression techniques [16].

In essence, this method involves dividing the temperature range into intervals, with each interval corresponding to a polynomial and defined by a set of nodes. The approach guarantees that the polynomials seamlessly connect at these nodes $\{x_i^*: i = 1, 2, \dots, r\}$, ensuring continuity across the entire function as well as its first and second derivatives. The mathematical formulation of the spline regression model for the variable x is expressed as follows:

$$b_0(x) = 1 \;\; ; \;\; b_1(x) = x \;\; ; \;\; b_{i+1}(x) = R(x, x^*) \quad i = 1, 2, \dots, r \tag{3-3}$$

$$\begin{aligned} R(x, x^*) = &\left[\left(x^* - \frac{1}{2}\right)^2 - \frac{1}{12}\right]\left[\left(x - \frac{1}{2}\right)^2 - \frac{1}{12}\right] \cdot \frac{1}{4} \\ &- \left[\left(|x - x^*| - \frac{1}{2}\right)^4 - \frac{1}{2}\left(|x - x^*| - \frac{1}{2}\right)^2 + \frac{7}{240}\right] \cdot \frac{1}{24} \end{aligned} \tag{3-4}$$

where x is a value between 0 and 1. The regression-spline model for the variable x is constructed using equations (3-3) and (3-4).

Where the forecasted temperature is the variable T. As expected, if observations of temperature at different geographical points are available, the locations considered most representative from the perspective of electricity consumption need to be chosen. After evaluating several options, it was determined that the most practical explanatory variable for weather was the average of the daily maximum and minimum temperatures of the ten most representative cities. Instead of observed real data, the suggested method considers the weather forecasts from AEMET.

$$x = (T - T_{min})/(T_{max} - T_{min}) \tag{3-5}$$

The mathematical model employed also considers the non-instantaneous impact of temperature on energy consumption. As mentioned earlier, the demand on day d depends not only on the temperature of that day but also on the temperatures of previous days ($t-1$, $t-2$, . . ., $t-k$). Therefore, the linear term of the model for hour h corresponding to the temperature effect $g_{h,d} = \alpha_L^T x_d$ can be written as:

$$g_{h,t} = \alpha_{h,0} + \sum_{i=1}^{r+1} \alpha_{h,i}^{0} b_i(x_t) + \sum_{i=1}^{r+1} \alpha_{h,i}^{1} b_i(x_{t-1}) + \ldots + \sum_{i=1}^{r+1} \alpha_{h,i}^{k} b_i(x_{t-k}) \tag{3-6}$$

The total number of parameters in this component of the model is $(r+1)(k+1)+1$ where r is the number of nodes and K is the number of lags.

3.2.3. Modeling the influence of special days

Saturdays and Sundays are different from each other and significantly different from the rest of the weekdays. Among the five working days, there are also some differences, particularly on Mondays and Fridays. Holidays show a very significant reduction in demand, sometimes up to 30% during certain hours. Data analysis reveals that the demand profiles for holidays vary from one to another. The demand profile for a specific holiday, such as May 1st, changes depending on the day of the week it falls on. Additionally, a holiday affects the demand on one or more days of the surrounding week. Proper modeling of these days is crucial to reducing the overall prediction error, as errors in dynamic models tend to propagate to subsequent days.

The special days are classified into m types or groups, which we will refer to as $G_1, G_2, \ldots, G_m$. We define the binary variables z_{di} as follows:

$$Z_{ti} = \begin{cases} 1, & d \in G_i \\ 0, & d \notin G_i \end{cases} \tag{3-7}$$

and $I_{t,j}$ the day of the week indicator:

$$I_{t,j} = \begin{cases} 1, & mod(d-j,7) = 0 \\ 0, & mod(d-j,7) \neq 0 \end{cases} \tag{3-8}$$

To estimate the effect on demand of the days preceding a holiday, we consider the auxiliary variables $U_{t,i}^{k}$, where i corresponds to the type of day and k to the number of days prior to the holiday to consider:

$$U_{ti}^{k} = \begin{cases} 1, & t+k \in G_i \\ 0, & t+k \notin G_i \end{cases} \quad k \in \{1, 2, \ldots, k_U\} \tag{3-9}$$

Similarly, $V_{(d,i)}^{k}$ are the variables that identify the days following a holiday:

$$V_{(t,i)}^{k} = \begin{cases} 1, & t-k \in G_i \\ 0, & t-k \notin G_i \end{cases} \quad k \in \{1, 2, \dots, k_V\} \tag{3-10}$$

Finally, P_t is a number from 0 to 1 that represents the percentage of the population or demand, relative to the national total, for the region or localities where day t is a holiday. For special days that affect the entire population, $P_t = 1$. Using the above variables, the effect of special days on demand can be expressed through the following linear function:

$$f_{h,t} = \sum_{i=1}^{m}\sum_{j=1}^{7} \beta_{hij} \cdot Z_{ti} \cdot I_{tj} \cdot P_t + \sum_{i=1}^{m}\sum_{j=1}^{7}\sum_{k=1}^{k_U} \gamma_{hij}^{k} \cdot U_{ti}^{k} \cdot I_{tj} \cdot P_t + \sum_{i=1}^{m}\sum_{j=1}^{7}\sum_{k=1}^{k_V} \delta_{hij}^{k} \cdot V_{ti}^{k} \cdot I_{tj} \cdot P_t \tag{3-11}$$

With this formulation, three sets of parameters appear: β_{hij} which measures the increase or decrease in demand for hour h on a special day of group i falling on weekday j, γ_{hij}^{k} which measures the change in demand for hour h, k days before or after a holiday of group i falling on weekday j; and the same for the days following the holiday. The total number of parameters required for this modeling for each hour is $7 \cdot m \cdot (k_U + k_V + 1)$. If the number of groups is large, the number of parameters will also be large. The values of k_U and k_V (the number of days before and after the holiday that are affected) may depend on the type of holiday and especially on the weekday on which the holiday falls that year. To account for this, these values can be written as k_{Uij} and k_{Vij}, and can take values from the set {0, 1, 2} depending on each case. In total, the number of parameters for this component, depending on the number of groups, can range from 100 to 200.

Increasing the number of groups has advantages: it allows for a more detailed discrimination between different holidays. However, there are disadvantages as well: the number of degrees of freedom (data) used to estimate some parameters is very limited, and if you want to estimate all combinations of holiday type and weekday, it is necessary to estimate with series of large lengths, exceeding 10 years.

3.2.4. Hourly correction

The model described up to this point makes predictions for each hour of the day independently. However, the series has an hourly frequency, so a temporal dependence between the demand of successive hours is expected, which the aforementioned model does not capture. This section proposes a simple way to correct the predictions of the univariate hourly models using information from the demand of immediately preceding hours.

Let ε_t be the vector of dimension 24 that contains the errors or random component of the 24 univariate models for day t. If the univariate hourly models are correctly specified and under the usual assumptions, for each hour h, the autocorrelations of the error series $\varepsilon_{h,t}$ are zero. However, the vectorial process ε_t may exhibit nonzero autocorrelations when considering cross-correlations between errors of different hours, specifically between those corresponding to the final hours of one day and the initial hours of the following day. (Note: For the sake of simplicity in explanation, we refer to days, but the approach can be generalized by commencing the vectorial process from the hour deemed most appropriate for prediction purposes).

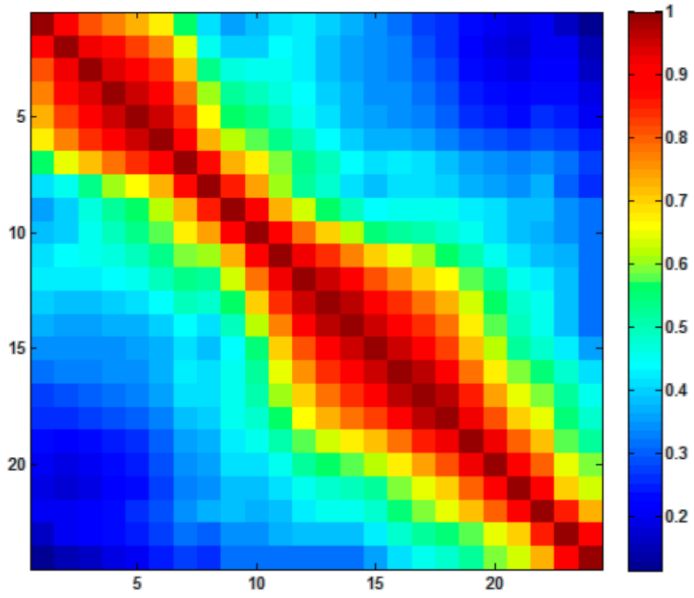

Figure 3-13: Matrix of correlation coefficients between the errors of each daily series.

We denote $\Gamma_k = cov(\varepsilon_{t+k}, \varepsilon_t)$ as the autocovariance matrices of the process. We assume that $\Gamma_k = 0$, for k $\geq$ 2, then we have:

$$\varepsilon_t = \Gamma_1 \cdot \Gamma_0^{-1} \cdot \varepsilon_{t-1} + e_t \tag{3-12}$$

This implies that the errors of day t can be corrected by knowing the errors of the previous day $t-1$. Calling y_{d-1} the predictions of demands y_t for day d obtained with the univariate models, we have:

$$y_t = y_t^{t-1} + \varepsilon_t \tag{3-13}$$

Thus, corrected predictions $\hat{y}_t^{t-1}$ due to multivariate autocorrelation can be immediately obtained using the following expression:

$$\hat{y}_t^{t-1} = y_t^{t-1} + \Gamma_1 \cdot \Gamma_0^{-1} \cdot \varepsilon_{t-1} \tag{3-14}$$

where e_t represents the new prediction errors [2].

3.3. Conclusion

In conclusion, the effective management of power systems relies heavily on accurate short-term forecasts, spanning from one hour to one week, to ensure stability and optimize dispatching. Load forecasting stands as a pivotal component in the day-to-day trading operations. This chapter has explored the model employed by the Spanish Transmission System Operator (TSO) to generate hourly forecasts for up to 10 days ahead. Viewing hourly series as periodically correlated processes, the model incorporates temperature as a significant explanatory variable and acknowledges the influence of holidays on demand patterns.

Having predictions with a low error level has beneficial implications at economic, energy, and environmental levels. If the system operator has accurate predictions, the volume of reserves (generating agents that must be ready to produce electricity in real-time if necessary to achieve supply-demand balance) could be significantly reduced, positively impacting the economic resources used to manage the system. Additionally, since reserve power plants generally use fossil fuels to provide the required flexibility,

a reduction in reserve volume has an advantageous impact on the pollutant emissions resulting from electricity generation, thus improving environmental conservation. Finally, if high-quality demand predictions with several days of horizon are available, the system operator and other market agents can plan their operations with a greater temporal margin to optimize the energy resources used, leading to an overall improvement in the energy efficiency of the system.

4. OPTIMAL SELECTION OF WEATHER STATIONS FOR ELECTRIC LOAD FORECASTING AND ITS APPLICATION TO THE SPANISH SYSTEM

4.1. Introduction

For effective planning and operation of any electric power system, it is crucial to have a reliable software tool that provides accurate short-term power consumption forecasts. Temperature significantly influences electricity usage, making the selection of appropriate weather stations essential to improve forecast accuracy. Short-term load forecasting has been a very active area of research in recent decades, and a significant number of studies have been devoted to this area, addressing the problem from different mathematical perspectives [18, 19]: regression analysis, artificial neural networks, fuzzy logic, and time series models, among others.

Because weather is a major driving factor of electric demand, most load forecasting models include information on meteorological variables such as temperature, humidity, and solar radiation, among others. Specifically, the hourly load demand exhibits a strong non-linear relationship with the ambient temperature; in winter, electricity demand increases due to heating devices, decreases for spring or autumn, and increases for summer due to air-conditioning equipment. The correlation between temperature and demand is so strong that some work exploits this relationship to detect anomalous temperature data [20]. For large networks, a unique weather station is not sufficient to represent the ambient meteorological conditions of the entire area [21].

The load forecasting software used by any TSO considers meteorological information from one or more weather stations located throughout the corresponding power network. It is common practice to integrate ambient temperature information from several locations into the mathematical model by computing the average value [2, 9] or using a selection based on experience or population statistics. In fact, the temperature information weighted by load and economy is not necessarily better than the equally weighted average [22].

To our knowledge, minimal research effort has been devoted to the creation of novel methodologies to appropriately select weather locations to increase the accuracy of the forecast (as stated in [23]). In recent years, some studies have shown that an enhanced model for temperature information can be obtained using advanced methodologies. In reference [24], several methods have been proposed and compared, such as linear and exponential combination, geometric mean, MAPE-based combination, genetic algorithms as in [25], and two-fold combination, among others. Fan et al. [21] proposed an alternative approach: Make use of multiregional load forecasting to create smaller systems with higher temperature-load relationships. A wavelet-squared coherence approach was proposed in [26]. Moreno-Carbonell et al. [25] proposed the use of genetic algorithms to analyze data from the global energy forecasting competition of 2012 and 2014. Ziel and Lim [27] addressed the problem of selecting weather stations by analyzing the goodness of fit to a cubic regression. In [23], two main questions were addressed: (i) how many weather stations should be used and (ii) which ones should be considered. The mathematical technique of singular value decomposition was employed in [28], and Nedellec et al. [29] proposed a station selection method based on minimizing a V-fold cross-validation criterion. Some of these studies are devoted to modeling the effect of the COVID pandemic [30]. Recently, work [26] presented a new method for selection and combination of weather stations based on Wavelet Squared Coherence that aims to improve the performance of forecast models for electric load.

We propose a weather station selection framework for electric load forecasting that aims to optimally select the number and location of temperature information to increase prediction accuracy. The proposed algorithm has been adapted to the Spanish TSO electric load forecasting software to identify the optimal number of weather locations to be used and their specific geographical locations. It has been observed that the optimal selection obtained outperforms the previous model [2, 9]. Additional details can be found at [94].

4.1.1. Contribution

This contribution of this chapter is twofold. First, we propose an algorithm to determine the optimal selection of weather stations (identifying both the optimal number and location of temperature information) based on (i) an initial reduction of problem complexity by computing a demand time series without holiday effects, which drastically decreases the computational cost, and (ii) a posterior incremental search algorithm. Second, the developed methodology is extensively tested using several case studies and two databases. The developed model is currently being used by the Spanish TSO on a daily basis to compute load forecasts.

4.1.2. Structure

The remainder of this chapter is organized as follows. In section 4.2 we propose an algorithm for optimally choosing a set of weather stations. Section 4.3 provides three insightful case studies using actual data from the Spanish mainland system. Finally, Section 4.4 provides the relevant conclusions.

4.2. Optimal selection of weather stations

As detailed in Section 3.2.2, one of the key factors in improving forecast accuracy is appropriate modeling of temperature information. Regarding the temperature

database, the procedure works as follows: (i) the TSO obtains daily weather forecasts from AEMET, the meteorological agency in Spain; (ii) the daily maximum and minimum temperature forecasts for the city with the largest population in each insular system are extracted from the meteorological forecaster's files; (iii) the extracted temperature information is mathematically transformed using the spline regression technique, detailed in equations (3-3)-(3-5); (iv) finally, the estimated mathematical model (3-1)-(3-2) is used to calculate electricity consumption predictions.

During the last decades [2, 9], the Spanish TSO has used the temperature-related regressor data obtained by computing the average value of the daily maximum of the ten most representative cities on the Spanish mainland. Figure 4-1 depicts the non-linear relationship between daily demand and maximum daily temperature for working days, for the ten most representative cities in Spain.

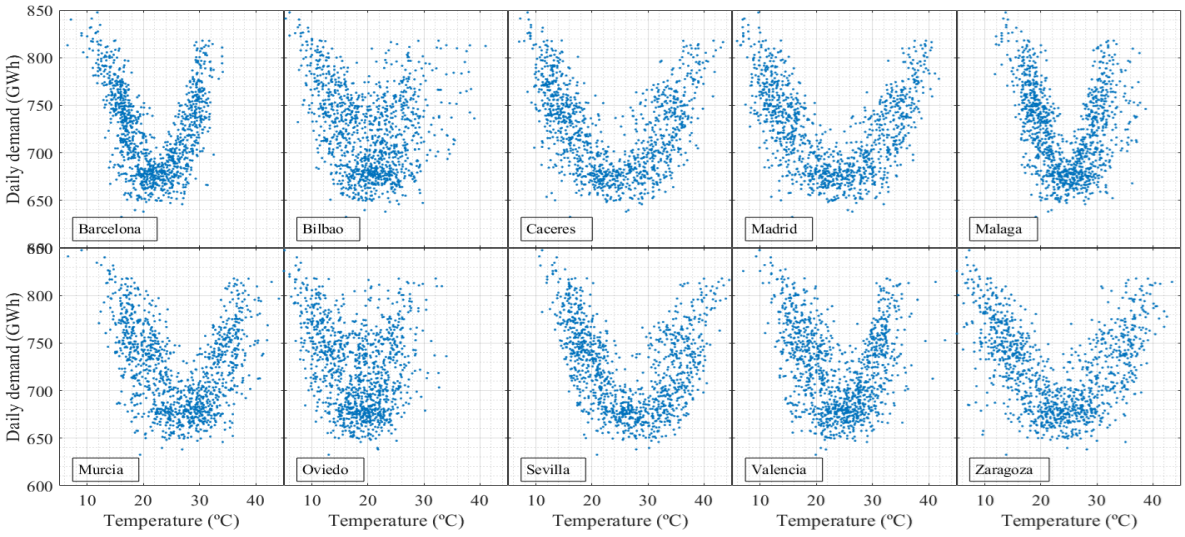

Figure 4-1: Scatterplot denoting the non-linear relationship between demand of working days (Y axis, in GWh) and temperature (X axis, in ^{o}C).

From Figure 4-1, it can be observed that the relationship is tighter in some locations (such as Barcelona or Madrid), and the U shape is not well defined in other weather stations (such as Bilbao or Oviedo). These ten plots lead us to wonder whether there is an optimal subset of these locations with a higher accuracy performance than

including all of them on average. In this section, an algorithm is proposed to select the optimal set of weather stations to be included in the model.

Once the twenty-four hourly models (3-1)-(3-2) are estimated, the obtained parameters related to the spline-regression model (3-3)-(3-5) for the thermal effect are analyzed. This allows us to study the effect of temperature as a function of the hour (subscript h) and temperature (variable T in equation (3-5)). Figure 4-2 shows the thermal effect on Spanish electricity consumption (Z-axis), as a function of the hour (Y-axis) and the maximum temperature (X-axis).

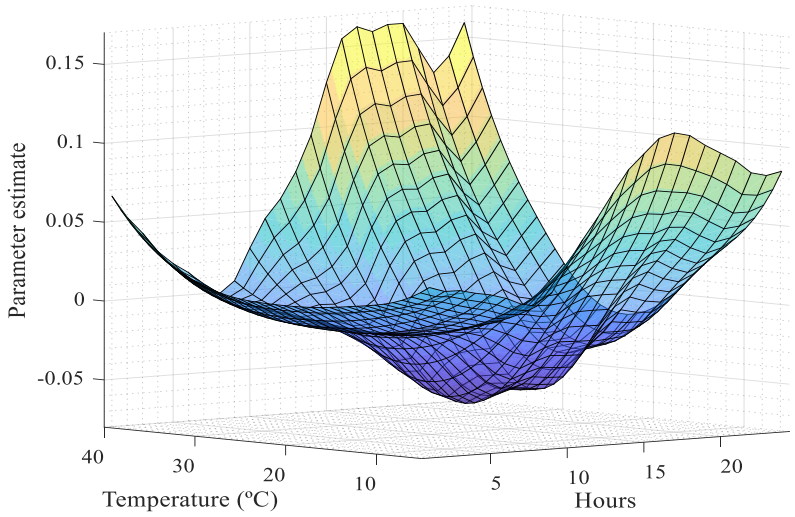

Figure 4-2: Thermal effect on Spanish electricity consumption (Z-axis), as a function of maximum temperature (X-axis) and time (Y-axis).

From Figure 4-2, the following observations can be made:

- Depending on the time of day, the impact of temperature on demand varies significantly.
- Demand is less influenced by temperature during the night than during the day.
- Consumption increases as the temperature rises in the warmer months (left side of the X-axis).
- Demand increases as the temperature drops in the colder months (right side of the X-axis).

- Energy consumption is not significantly affected by temperature changes during milder weather seasons (central part of the X-axis).

4.2.1. Method 1: exhaustive analysis

To determine the optimal selection of weather stations, a basic procedure consists of an exhaustive analysis of all possible combinations. With respect to the Spanish electric power system, in the last decades, the TSO traditionally makes use of the temperature information for ten cities [2, 9]. Thus, if a subset of K weather stations is selected out of ten, the number of possible dispositions is the binomial coefficient "10 choose K," computed as $nchoosek(10, K) = 10! \,/\, (K! \cdot (10 - K)!)$

Because the optimal value for parameter K is not known a priori, all possible values for K (from one to ten) should be explored. Consequently, the total number of possible combinations to be explored is computed as $\sum_{K=1}^{10} nchoosek(10, K) = 2^K - 1 = 1023$. Once all possible combinations have been analyzed individually, the optimal selection of weather stations is the one with the lowest out-of-sample forecasting errors.

4.2.2. Computational effort and feasibility

The computational effort required to estimate the forecasting model detailed in Section. depends on the technical specifications of the computer used. In this work, a desktop PC with a multi-threading octa-core i7-6700 3.41 GHz Intel processor and 32 GB of RAM has been used, taking advantage of parallel computation techniques (which increased the parameter estimation speed by approximately 700%). The CPU time required to estimate the 24-hourly Reg-ARIMA models and the subsequent evaluation of forecasting performance using an out-of-sample one year test period is approximately 150-180 minutes to complete.

From a practical perspective, testing all possible combinations is not feasible; it would require more than 110 consecutive days of continuous CPU operation. In this study, a methodology to reduce the computational effort is proposed.

Each hourly Reg-ARIMA model employs 284 regressors: 16 regressors for temperature and 268 regressors to model special day effects. The associated 284 parameters are estimated using maximum likelihood [15], employing the implemented estimate function of MATLAB R2017a, econometrics toolbox [23], which is based on solving a large non-linear optimization problem with constraints, with more than 4300 datapoints. The estimation of a single hourly model takes approximately 40-50 minutes to complete. A significant computational effort is required for the estimation of parameters related to holidays and special days.

Because the main purpose of this study is to analyze the temperature location effect on demand, the effect of special days is secondary. Therefore, the estimation of the parameters related to special days constitutes a significant computational cost, which represents no profit for this study. Because special days can neither be eliminated nor disregarded, in this work, we propose a technique to drastically reduce the computational effort without compromising the accuracy of the obtained results.

4.2.3. Modified demand time series without the holidays effect

To reduce the computational effort, we propose estimating model (3-1)-(3-2) using the electric load values as the response variable after removing the special days effect. For illustrative purposes, Figure 4-3 depicts the Spanish mainland hourly power demand during December 3rd-9th, 2018. In Spain, both December 6th and 8th are two public holidays (Constitution Day and Immaculate Conception Day, respectively). As it can be observed, there is a significant reduction of power demand from Thursday to Saturday, due to national holiday on Thursday and the so-called 'long weekend' effect. The affected days do not follow the weekly seasonal pattern, and consequently,

appropriate regressors must be included in (3-1)-(3-2) to model this particular behavior owing to special days.

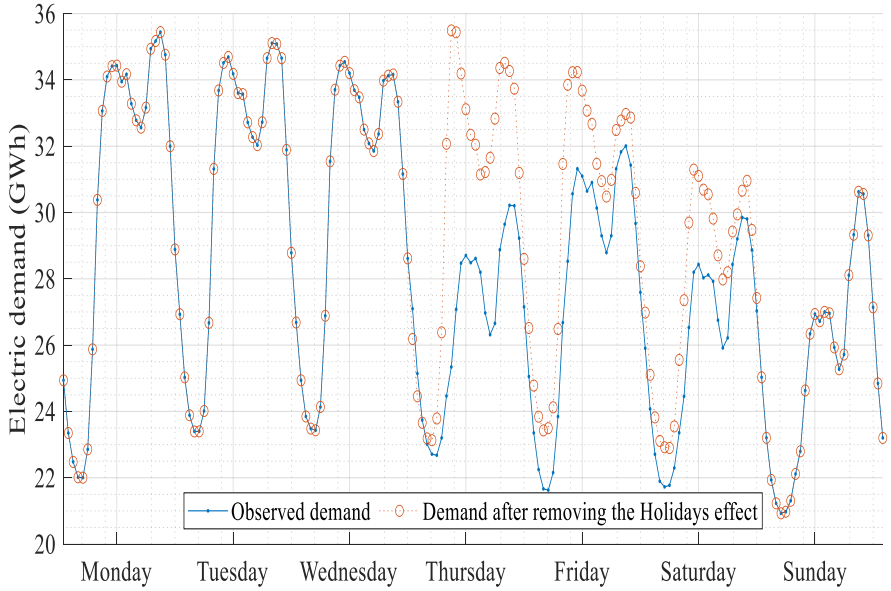

Figure 4-3: Observed demand for December 3rd-9th, 2018 and demand after removing the holidays effect.

Once model (3-1)-(3-2) has been estimated, the parameter vector $\boldsymbol{\beta}_h$ allows quantifying the effect of each special day over the hourly demand. Thus, since the impact of the public holidays December 6$^{\text{th}}$ and 8$^{\text{th}}$ over the demand has been estimated, this effect can be removed from the original observed demand, leading to a 'synthetic' demand without the influence of the holidays (orange line plotted in Figure 4-3). It should be noted that: (i) the obtained "demand without holidays effect" shows a clear weekly seasonal cyclic behavior, without the sporadic disruption of public holidays; (ii) this demand does contain the unaltered effect of temperature; and (iii) this time series can now be analyzed with model (3-1)-(3-2) without the need to include the term $\boldsymbol{\beta}_h^T \boldsymbol{z}_t$, because no special days are present any more. Additionally, because the effect of special days is not present in this modified demand time series, the requirement of 11 years of history (see Section) is no longer required. Consequently, the computational cost of model estimation has been drastically reduced because the number of regressors has

been decreased from 284 to 16 (96% reduction), and the historic data can be reduced from 11 years to 1-2 years (85% reduction).

The proposed algorithm works as follows:

Step 1) Solve model (3-1)-(3-2), estimating the Reg-ARIMA parameters and parameter vectors $\boldsymbol{\beta}_h$ and $\boldsymbol{\alpha}_h$. The estimated values of vector $\boldsymbol{\beta}_h$ are stored in vector $\tilde{\beta}_h$.

Step 2) Compute the demand without holidays effect (denoted as $y'_{t,h}$), as the difference between the observed demand and the special-day-effect reduction.

$$y'_{t,h} = y_{t,h} - \tilde{\boldsymbol{\beta}}_h^T \boldsymbol{z}_t \tag{4-1}$$

Step 3) Estimate the following model (for any specific selection of weather stations):

$$y'_{t,h} = c_h + \boldsymbol{\alpha}_h^T \boldsymbol{x}_t + u'_{t,h} \tag{4-2}$$

$$\phi_h(B)\Phi_h(B^7)\nabla^d \nabla_7^D u'_{t,h} = \vartheta_h(B)\Theta_h(B^7)w'_{t,h} \tag{4-3}$$

After comprehensive testing, it has been observed that the computational effort required to estimate the 24 Reg-ARIMA models is approximately 10 minutes. Thus, an exhaustive analysis of the 1023 possible combinations would require approximately 170 hours (7.1 days), which is now a feasible amount of time.

4.2.4. Method 2: Incremental search

The main disadvantage of the exhaustive analysis proposed in Section 4.2.1 is that the computational effort increases exponentially as the number of available weather stations increases. For instance, if the number of available weather locations is 15 (instead of 10), the required CPU time is 227 days (instead of 7 days). Thus, it is impractical to analyze all possible combinations if the number of weather stations is higher. To overcome this limitation, an alternative algorithm is proposed.

To determine the best selection of temperature locations, we propose a procedure that involves progressively adding the location that causes the lowest prediction error. The proposed algorithm is as follows:

Step 1) Start the counter $k \leftarrow 0$ and the set $\Omega_0 \leftarrow \varnothing$

Step 2) Update the counter: $k \leftarrow k + 1$.

Step 3) Maintaining the set of selected weather stations Ω_{k-1}, compute the out-of-sample forecasting errors of all possible combinations of including a new weather station, using the model (4-2)-(4-3). The number of possible combinations is $K - k + 1$.

Step 4) The weather station which minimizes the forecasting error in (Step 3) is included in set Ω_k.

Step 5) If $k < K$, go to (Step 2). Otherwise, the algorithm ends.

Once the above algorithm is concluded, the optimal set of weather stations is the one which exhibits the lowest out-of-sample forecasting error.

The total number of evaluations is $\sum_{k=1}^{K} K - k + 1 = (K^2 + K)/2$, providing a computational cost drastically lower than that of the exhaustive analysis proposed in Section 3.2.1, which is based on a brute-force algorithm. The reduction in computational effort is computed using the following equation:

$$CPU\ reduction\ (\%) = \frac{2^K - 1 - \frac{K^2 + K}{2}}{2^K - 1} \cdot 100 \tag{4-4}$$

For instance, if the number of available temperature locations is 10, the reduction in computational effort is 95%. If the number of available stations is 20, the reduction in computational effort is 99.98%. Figure 4-4 provides the number of evaluations for Methods 1 and 2, and the reduction in computational cost of the incremental search compared with the exhaustive analysis.

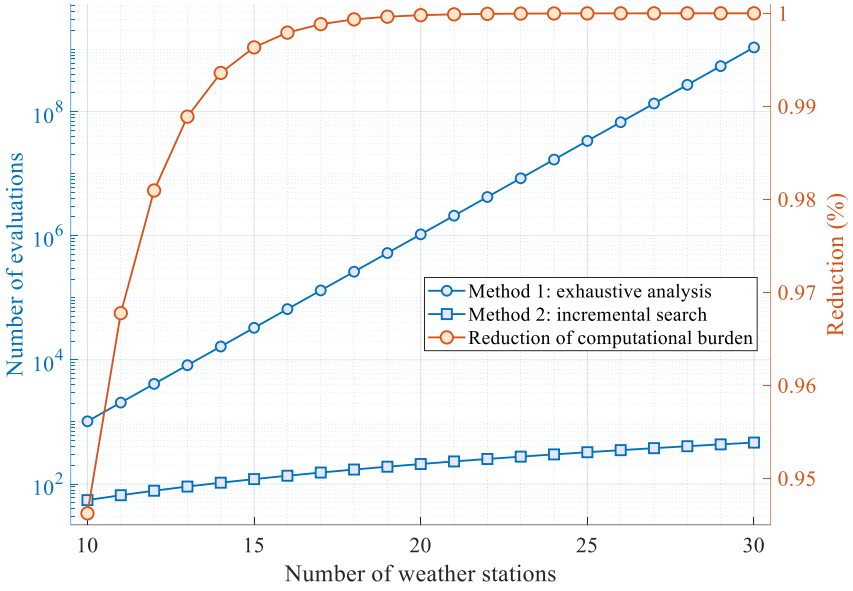

Figure 4-4: Number of evaluations for methods 1 and 2, and the reduction of computational cost.

4.2.5. Method 3: Decremental search

An alternative algorithm can be created by substituting incremental search with decremental search. Computational effort is equivalent. Note that the resulting final selection may not coincide with the selection obtained one using incremental search. Consequently, this decremental method can be used to either check the robustness of the incremental method solution or to obtain an alternative local optimal solution.

The decremental search algorithms works as follows:

Step 1) Start the decremental counter $k \leftarrow K$ and the full set $\Omega_0 \leftarrow \{1, 2, \ldots, K\}$

Step 2) Update the decremental counter $k \leftarrow k - 1$

Step 3) Maintaining the set of selected weather stations Ω_{k-1}, compute the forecasting errors of all possible combinations of removing a single weather station, using the model (4-2)-(4-3). Note that the number of possible combinations is $K - k + 1$.

Step 4) The weather station whose removal minimizes the forecasting error in Step 3) is eliminated from set Ω_k.

Step 5) If $k > 0$, go to Step 2). Otherwise, the algorithm ends.

Once the above algorithm is concluded, the optimal set of weather stations is the one which exhibits the lowest out-of-sample forecasting errors.

A flowchart of the proposed algorithms (incremental and decremental) and the methodology used to reduce the CPU time are shown in Figure 4-5.

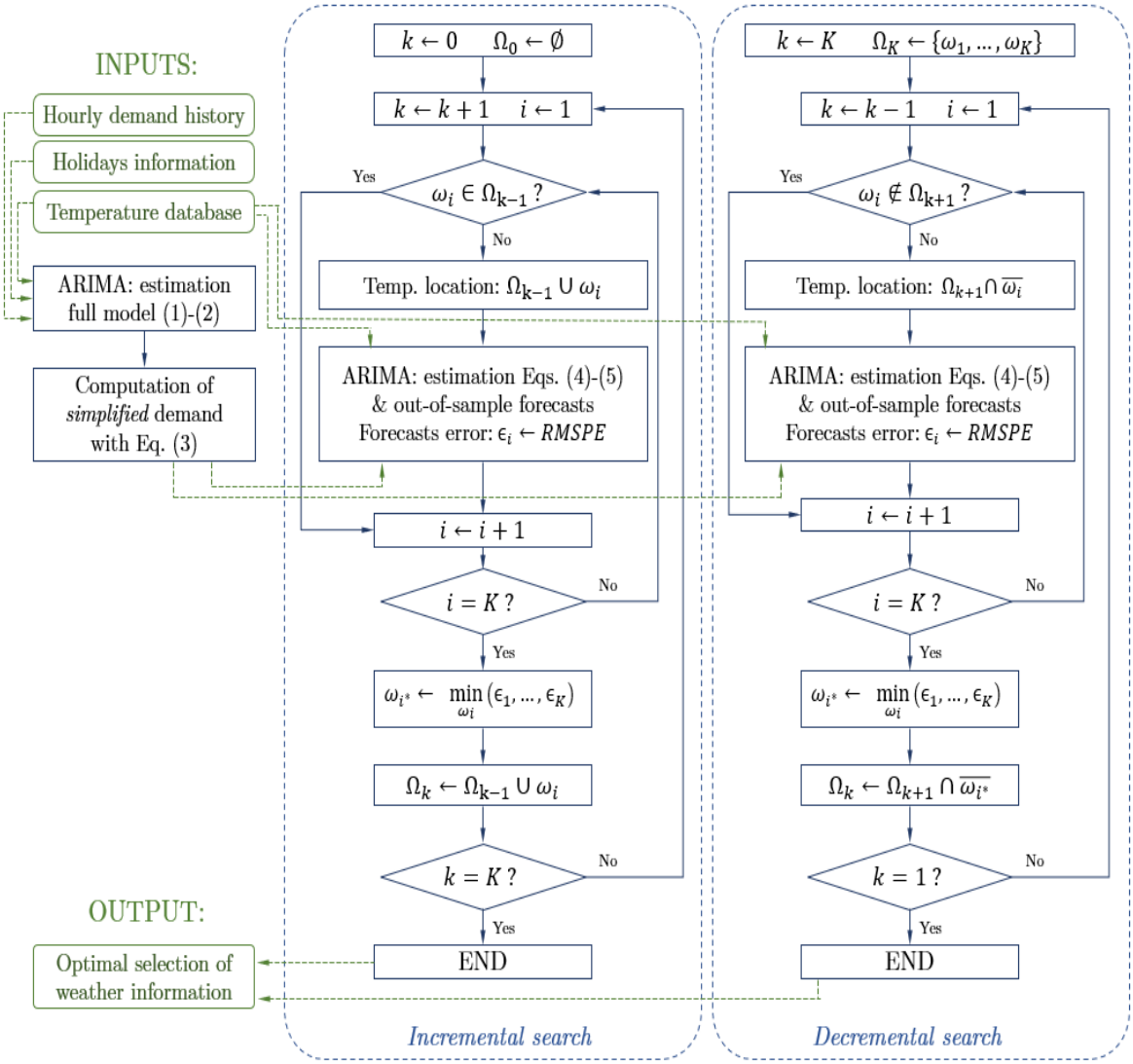

Figure 4-5: Flowchart of the proposed algorithm.

4.3. Case study

Following the methodology described in section 4.2, the performance of the proposed methodology has been tested using real data from the Spanish mainland electric power

system. As in [2], the metric error employed in this work corresponds to the RMSPE, defined as:

$$RMSPE = \sqrt{\sum_{d=1}^{n_d}\sum_{h=1}^{24}\left(\frac{y_{d,h}-y^*_{d,h}}{y_{d,h}}\right)^2 \cdot \frac{1}{n_d * 24}} \cdot 100 \qquad (4\text{-}5)$$

where values $y_{d,h}$ and $y^*_{d,h}$ are the observed and forecasted hourly Spanish demands at the h-th hour of the d-th day, respectively, and value n_d is the number of days considered in the study. Forecasts $y^*_{d,h}$ are computed using the estimated model (3-1)-(3-2).

4.3.1. First case study: analysis of 2018

The time period considered for estimating the parameters in model (3-1)-(3-2) is the 12-year period from 2006 to 2017. Such a large estimation period is required to estimate the effects on all special days. Once the complete model is estimated, the computational effort technique described in section 4.2.3 is applied, reducing the estimation period for model (4-2)-(4-3): from June 2016 to Dec. 2017. The electric data have been provided by the Spanish TSO. This information is open-source and can be publicly accessed through: https://demanda.ree.es/demanda.html. Concerning the temperature model, weather information has been provided by AEMET. To evaluate the forecasting performance of each configuration, the Reg-ARIMA model is employed to compute one day-ahead forecasts from January 1, 2018, to December 31, 2018.

4.3.1.1. Case A: Exhaustive analysis

The extensive analysis algorithm proposed in Section 4.2.1 has been applied to estimate the model (4-2)-(4-3) for the 1023 possible selections and computing the out-of-sample forecasting for the prediction period. The global RMSPE error for each possible weather station selection is plotted in the boxplot of Figure 4-6 (left plot), as a function of the number of considered temperature locations. Note that the reference

model corresponds to the model with ten temperature locations (the RMSPE is equal to 1.36%). The right plot in Figure 4-6.

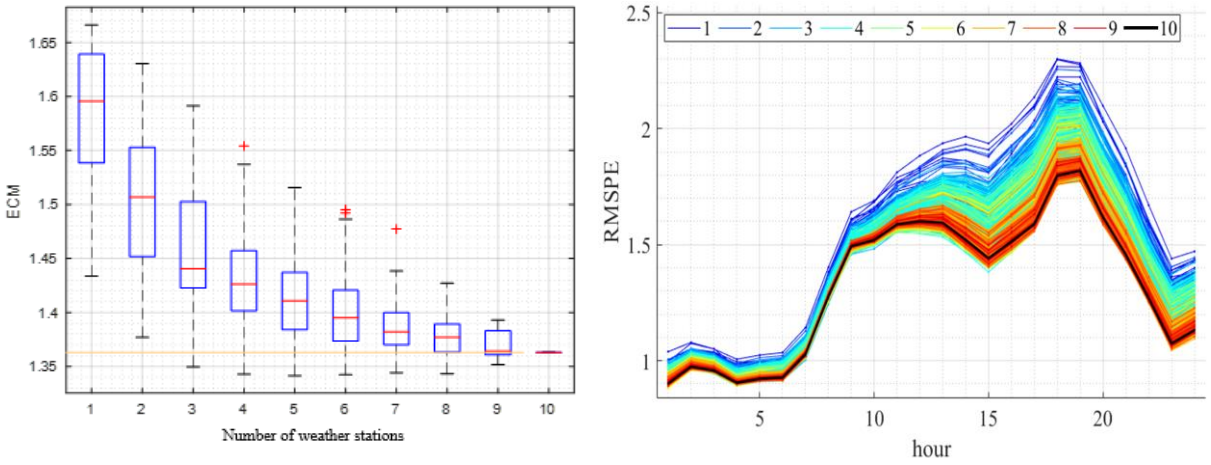

Figure 4-6: Exhaustive analysis: (left plot) boxplot of RMSPE errors, as a function of the number of weather stations considered; (right plot) hourly RMSPE. Color code: number of weather stations considered.

From Figure 4-6 (left plot), it can be observed that: (i) none of the possible combinations with one or two weather stations can improve the forecasting accuracy; (ii) some configurations considering from three to nine weather stations can reduce the prediction errors; (iii) in particular, more than 25% of the combinations with $n = 8$ and $n = 9$ are more accurate than the reference model with $n = 10$.

From Figure 4-6 (right plot), it can be observed that (i) the forecasting error during night hours is not significantly influenced by the weather station selection employed, whereas (ii) the prediction error from 12 noon until 12 midnight highly depends on the selected temperature locations.

Table 4-1 provides the forecasting errors (RMSPE column) of the reference model (*n = 10*) and the 20 configurations with higher prediction accuracy. The first column indicates the number of weather locations considered, and columns from 2nd-11th specifies the weather locations included in the mathematical model (in the following order: Barcelona, Bilbao, Cáceres, Madrid, Málaga, Murcia, Oviedo, Sevilla, Valencia,

and Zaragoza). The last two columns provide the out-of-sample forecasting error and the position out of 1023 (sorted by decreasing accuracy).

Table 4-1: The reference configuration and the twenty configurations with lower forecasting errors.

Method 1: Exhaustive analysis												
	Weather station										Forecasting accuracy	
n	1	2	3	4	5	6	7	8	9	10	RMSPE	Position
10	x	x	x	x	x	x	x	x	x	x	1.363	(79th)
5	x			x	x			x		x	1.342	1st
6	x		x	x	x			x		x	1.342	2nd
4	x			x				x		x	1.343	3rd
8	x		x	x	x		x	x	x	x	1.343	4th
7	x		x	x	x			x	x	x	1.344	5th
7	x		x	x	x		x	x		x	1.345	6th
4	x			x			x	x			1.345	7th
5	x			x	x		x	x			1.346	8th
6	x			x	x		x	x		x	1.347	9th
7	x	x	x	x	x			x		x	1.347	10th
8	x	x	x	x	x			x	x	x	1.348	11th
5	x	x		x	x			x			1.349	12th
5	x		x	x	x					x	1.349	13th
7	x		x	x		x	x	x		x	1.349	14th
7	x		x	x			x	x	x	x	1.349	15th
6	x		x	x				x	x	x	1.349	16th
5	x			x			x	x	x		1.349	17th
4	x	x		x				x			1.349	18th
7	x		x	x	x		x	x	x		1.349	19th
3	x			x				x			1.350	20th

From Table 4-1, it can be observed that Barcelona, Madrid, and Sevilla appear in (almost) all scenarios, whereas Murcia or Bilbao rarely appear, and Zaragoza, Málaga, and Cáceres appear in a percentage of 65%, 60%, and 55%, respectively. Note that the accuracy of the reference model (*n = 10*) is in position 79th (out of 1023 combinations).

4.3.1.2. Case B: Incremental search and decremental search

The algorithms described in Sections 4.2.4 and 4.2.5 are applied. Table 4-2 indicates the iteration number (first column), location considered at the k-th iteration (second column), and forecasting error (third column). The optimal location is denoted by a gray-colored row ($k = 5$ in both cases).

From Table 4-2 it is observed that (i) in both cases, the optimal selection includes the same locations; (ii) as the iteration process continues, the forecasting error is reduced as it approaches the value $k = 5$; (iii) the required CPU time has been 95.5% lower than method 1 (exhaustive analysis), since the number of required evaluations have been 45; and (iv) the optimal selection obtained using the three methods has been exactly the same.

Table 4-2: Methods 2 and 3: results for the period from Jan. 2018 until Dec. 2018

Method 2: Incremental search		
k	Locations considered	RMSPE
1	Mad	1.434
2	Mad-Barc	1.377
3	Mad-Barc-Sev	1.350
4	Mad-Barc-Sev-Zar	1.343
5	**Mad-Barc-Sev-Zar-Mal**	**1.342**
6	Mad-Barc-Sev-Zar-Mal-Cac	1.342
7	Mad-Barc-Sev-Zar-Mal-Cac-Val	1.344
8	Mad-Barc-Sev-Zar-Mal-Cac-Val-Ov	1.343
9	Mad-Barc-Sev-Zar-Mal-Cac-Val-Ov-Mur	1.352

Method 3: Decremental search		
k	Locations considered	RMSPE
9	Mad-Barc-Sev-Zar-Mal-Cac-Val-Ov-Mur	1.352
8	Mad-Barc-Sev-Zar-Mal-Cac-Val-Ov	1.343
7	Mad-Barc-Sev-Zar-Mal-Cac-Val	1.344
6	Mad-Barc-Sev-Zar-Mal-Cac	1.342
5	**Mad-Barc-Sev-Zar-Mal**	**1.342**
4	Mad-Barc-Sev-Zar	1.343
3	Mad-Barc-Sev	1.350
2	Mad-Barc	1.377
1	Mad	1.352

4.3.2. Second case study: analysis of 2019

Once the set of weather locations has been optimally selected (using data up to 2018), the forecasting accuracy has been tested using data from 2019. The complete model (3-1)-(3-2) has been used, and the traditional model with 10 locations (labeled as

"reference") is compared with the model using the optimal set of weather stations. The forecasting accuracy of each method has been quantified using hourly/monthly RMSPE (see Table 4-3 and Figure 4-7).

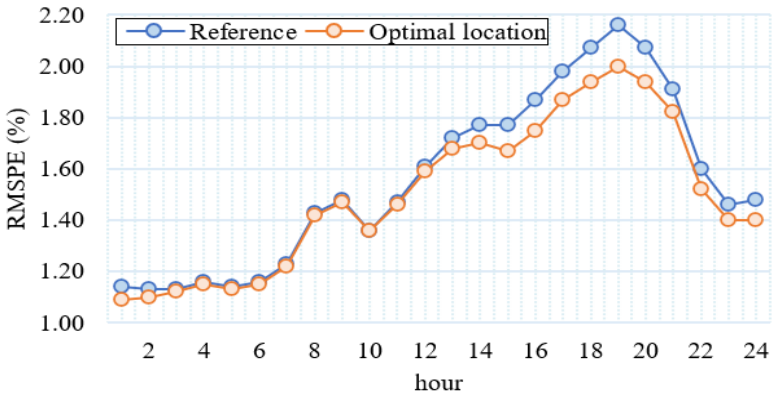

Figure 4-7: Hourly errors for the reference and optimal-location models. Prediction period: from Jan. 2019 to Dec. 2019.

From Table 4-3 and Figure 4-7, it can be observed that:

- The optimal location model provides significantly higher forecasting accuracy, reducing the hourly error by up to 7%.
- Specifically, greater improvements in accuracy are achieved during hours from 2 PM to 12 midnight. During these hours, the percentage of improvement ranges between 4.0% and 7.4%, with an average of 5.5%. The hourly behavior of percentage of improvement is reasonable, because the highest increments in accuracy are achieved during sunny hours with the highest influence of temperature.
- During the period between 3 AM and 11 AM, the improvement can be disregarded, because it is lower than 1%.
- The highest accuracy increments are obtained during summer months (June, July, and August) and February to March.

Table 4-3: Hourly and monthly errors for the reference and optimal-location models. Prediction period: Jan.-Dec. 2019.

Hour	h1	h2	h3	h4	h5	h6	h7	h8	h9	h10	h11	h12	h13	h14	h15	h16	h17	h18	h19	h20	h21	h22	h23	h24
RMSPE reference	1.14	1.13	1.13	1.16	1.14	1.16	1.23	1.43	1.48	1.36	1.47	1.61	1.72	1.77	1.77	1.87	1.98	2.07	2.16	2.07	1.91	1.60	1.46	1.48
RMSPE optim. loc.	1.09	1.10	1.12	1.15	1.13	1.15	1.22	1.42	1.47	1.36	1.46	1.59	1.68	1.70	1.67	1.75	1.87	1.94	2.00	1.94	1.82	1.52	1.40	1.40
Perc. Improvement (%)	4.4	2.7	0.9	0.9	0.9	0.9	0.8	0.7	0.7	0.0	0.7	1.2	2.3	4.0	5.6	6.4	5.6	6.3	7.4	6.3	4.7	5.0	4.1	5.4

Month	Jan	Feb	Mar	Apr	May	Jun	Jul	Aug	Sep	Oct	Nov	Dec
RMSPE reference	1.70	1.33	1.22	1.98	1.40	1.50	1.57	1.60	1.50	1.21	1.57	2.22
RMSPE optim. loc.	1.64	1.20	1.08	1.94	1.39	1.39	1.45	1.49	1.53	1.12	1.55	2.19
Perc. improvement (%)	4.0	9.7	11.5	2.0	0.3	7.3	7.4	6.8	-2.1	7.5	1.4	1.3

4.3.3. Third case study: ECMWF database

In this case study, an alternative database of temperature forecasts is used. The database is generated by the ECMWF [31], and the processed file contains the maximum daily temperature for the 38 cities, corresponding to the provincial capital cities in the Spanish mainland. It should be noted that the database source is different (thus, the forecasted weather information may be slightly different), and 28 temperature locations have been added. Consequently, the resulting optimal selection is expected to differ from that obtained in Section 4.3.1.

The exhaustive analysis algorithm cannot be applied here because the number of possible combinations is higher than 274 billion configurations (which would lead to a computation time greater than five million years). Therefore, the incremental search method has been applied. After running the incremental search algorithm indicated in Section 4.2.4, Table 4-4 provides the selected location at each step of the iterative process, whereas Figure 4-8 shows the RMSPE of each configuration analyzed at each iteration.

From Figure 4-8 and Table 4-4, it can be observed that: (i) seven locations out of 38 is the number of weather stations considered in the optimal selection that provides the best forecasting accuracy; (ii) the geographical location of the optimal selection using the ECMWF database has some common patterns with the optimal selection obtained using the AEMET database.

Table 4-4: Incremental search algorithm (method 2): iterations employing the ECMWF database.

k	Added city	RMSPE
1	Madrid	1.393
2	Barcelona	1.345
3	Córdoba	1.304
4	Castellón	1.288
5	La Coruña	1.278
6	Sevilla	1.275
7	Zaragoza	1.260
8	**Albacete**	**1.259**
9	Burgos	1.260
10	Almería	1.260
11	Málaga	1.260
12	Cáceres	1.261
13	Tarragona	1.260
14	Cádiz	1.262
15	Lleida	1.263
16	Ciudad Real	1.263
17	Asturias	1.263
18	Granada	1.264
19	Murcia	1.266
20	León	1.267
21	Girona	1.267
22	Toledo	1.268
23	Huelva	1.269
24	Alicante	1.271
25	Valladolid	1.273

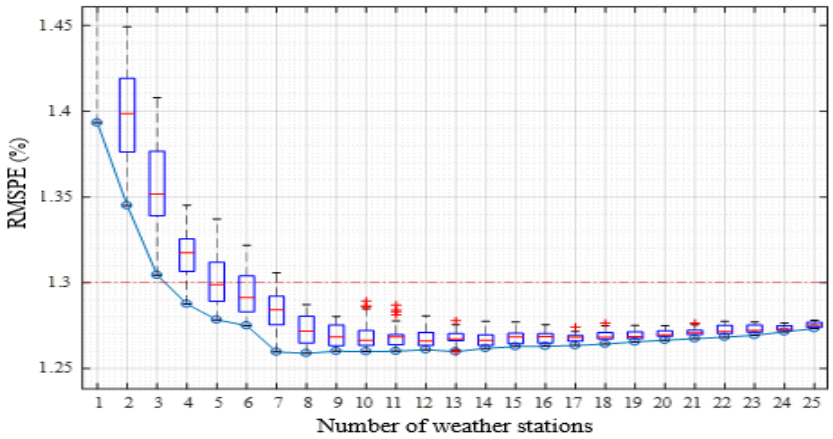

Figure 4-8: Incremental search algorithm (method 2): iterations employing the ECMWF database.

Finally, Figure 4-9 shows the hourly forecasting error of the following configurations: optimal selection (labeled as "7 loc"), the reference configuration (labeled as "10 loc"), and the configuration using just a single weather station (the Spanish's main city, Madrid, labeled as "1 loc"). From this figure, it can be observed that an appropriate selection of weather stations influences the hours between 9 AM and midnight the most, whereas the forecasting accuracy between 1 AM and 8 AM is not significantly affected. The average improvement is 2.6%, with an average improvement of 5% between 2 PM and 8 PM, both included.

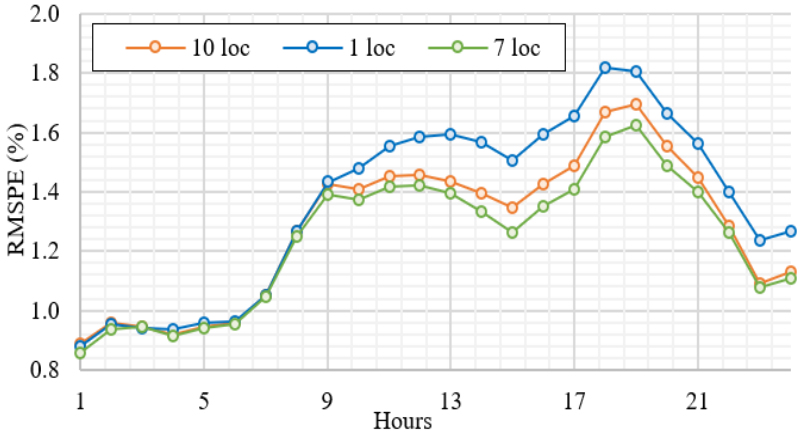

Figure 4-9: ECMWF: hourly errors for the ref. model (orange), just one loc. (blue) and optimized-locations model (green).

4.4. Conclusion

Temperature is one of the most important drivers of electric load, and selecting the right station or combination of stations is crucial for reducing the forecasting error. In this study, we propose an algorithm that determines the optimal selection of weather locations based on (i) an initial reduction in problem complexity which decreases drastically the computation effort using a simplified demand time series without the holiday effect, and (ii) a posterior incremental/decremental search algorithm. The developed methods not only determine the optimal number of temperatures regressors to be used but also identify their optimal geographical location. This study employs the model which is currently in use by the Spanish TSO to make hourly forecasts up to 10 days ahead.

The proposed methodology has been exhaustively tested using three insightful case studies using real data from the Spanish mainland electric power network. Two different weather forecast databases have been used: the Spanish meteorology agency AEMET and the European weather forecast agency ECMWF. The global forecast accuracy increased by approximately 2-3%, denoting a higher enhancement between 2 PM and 8 PM (average increment of accuracy between 5.0-5.5%). The results of this chapter have been published in [94, 97, 98, 100].

5. CONTRIBUTIONS TO RENEWABLE ENERGIES FORECASTING: THE AGGREGATION PROBLEM

5.1. Computation of prediction intervals of wind energy

The integration of renewable energy sources, such as photovoltaic or wind power, into existing electric power systems is critical for the advancement of sustainable energy development. To mitigate the challenges of the inherent variability of wind power production, accurate probabilistic forecasting methods must be developed.

5.1.1. Motivation

Due to the recent increase in energy prices derived from petroleum-based fuels worldwide and cutting-edge research in wind turbine design optimization, wind energy has emerged as a renewable energy source that is proliferating worldwide. Consequently, the installed wind power capacity and the wind power supplied to the electricity market continue to increase. However, due to the stochastic and volatile nature of wind energy, predictive mathematical models that allow any electric power system to be safely operated must be developed [32].

Two fundamental approaches exist for short-term wind energy forecasting: physical models and statistical models [33]. Physical models consider the specific conditions of the wind farm site and consider physical conditions to tailor wind predictions for that area. These models typically utilize mesoscale or microscale models to calculate the incident wind speed on wind farm turbines and then derive energy predictions using the power curve. Physical models have the advantage of considering local factors that affect wind power production, such as terrain, temperature, and atmospheric

conditions, making them suitable for longer forecasting horizons [34]. Statistical models, on the other hand, rely on historical data of variables as input and may also incorporate weather prediction values from atmospheric models. These models correlate past energy production or other measured historical values with meteorological data to make predictions. Statistical models provide "local" approximations of the complex reality of wind power production and are generally better suited for short-term forecasting, ranging from 1 to 5 hours. However, their performances may vary under different conditions, and they might not capture the physical interactions between wind and the specific characteristics of a wind farm [35].

To ensure reliable wind power predictions, the system operator typically employs multiple forecasting models in parallel. In this technique, first introduced by Bates and Granger [36], forecasts are combined to achieve more accurate and robust predictions. By leveraging the strengths of both physical and statistical models, forecasters can enhance prediction accuracy across varying forecasting horizons. Physical models may provide better results for longer horizons, where detailed site-specific data are essential, while statistical models may offer superior performance for shorter horizons, where historical patterns are more relevant. Combining these models enables more reliable predictions and improves the overall management of wind power resources [37]. Additional details can be found in [95].

5.1.2. Literature review

The field of forecast combinations has undergone extensive research in recent years. Numerous studies have focused on the development and evaluation of combined models for wind power forecasting, contributing to ongoing advancements in the field. Boyu He et al. proposed a combined model for short-term wind power forecasting based on the analysis of numerical weather prediction data, demonstrating improved forecasting capabilities through comprehensive data analysis [38]. Hanifi et al. critically reviewed

various wind power forecasting methods, providing a comprehensive overview of past developments, current approaches, and future prospects in the field [39].

Furthermore, Lin et al. [40] introduced a multimodel combination approach for probabilistic wind power forecasting, forming a robust methodology to handle uncertainties in wind power predictions. Furthermore, recent research efforts have focused on developing novel hybrid models for wind power forecasting. Duan et al. [41] proposed a novel hybrid model based on a non-linear weighted combination, effectively improving short-term wind power forecasting capabilities through advanced modeling techniques.

Tascikaraoglu and Uzunoglu [42] comprehensively reviewed the combined approaches for the prediction of short-term wind speed and power, offering valuable insights into the application of various combined methods in wind power forecasting.

Moreover, Chen et al. [43] reviewed ultra-short-term wind power forecasting based on data decomposition-forecasting technology combination models, highlighting the significance of hybrid approaches in improving wind power predictions.

Li et al. [44] proposed a neural computation-based prediction model that integrates renewable energy sources, wind power and photovoltaics. Sun et al. [45] focused on short-term wind power, forecasting at multiple scales via variational model decomposition (VMD), K-means clustering, and long short-term memory (LSTM) principal computing, thereby comprehensively analyzing multiscale forecasting approaches for wind power prediction.

Yagang et al. [46] introduced a combined model utilizing the fast filtering algorithm (FCBF) and VMD for feature extraction from wind resource data that was integrated with a least squares support vector machine (LSSVM) for short-term wind speed prediction.

A hybrid probabilistic forecasting method was proposed that combined kernel density estimation (KDE) with copula functions to model the joint distribution of wind power forecast errors, leading to more accurate probabilistic forecasts [47].

Recent advances in wind power forecasting have led to various innovative techniques being adopted to improve accuracy and reliability. For example, a hybrid ensemble method was proposed that combines neural networks and extreme learning machines for the prediction of short-term wind power [48].

5.1.3. Contribution

The contribution of this chapter is the development of a practical method for optimally aggregating probabilistic forecasts and computing prediction intervals based on the applications of three techniques: the exponentially weighted moving average method for estimating the covariance matrix of prediction errors; the Berstein online aggregation method for optimally combining point forecasts; and the Johnson distribution for adapting the final distribution kurtosis. Using real-world Spanish wind production data, the performance of this method is exhaustively analyzed and has been proven to be accurate and reliable.

5.1.4. Structure

The remainder of the chapter is organized as follows. Section 5.2 details the proposed method for combining the predictions and computing the prediction intervals. Section 5.3 analyses the performance of the proposed combination approach using real-world Spanish wind energy data. Finally, section 5.4 provides some pertinent conclusions.

5.2. Proposed methodology: computation of prediction intervals

5.2.1. Forecast: punctual and probabilistic

The univariate hourly wind power production series observed at n equidistant time points is denoted by $y_1, y_2, \ldots, y_n$. In this document, both the punctual and the probabilistic forecasts are analyzed.

Variables and parameters:	
y_t	Observed wind power.
$\hat{y}_t$	Forecast wind power.
h	Prediction horizon
e_t	Forecasting error
r_t	Standardized forecasting error
$\hat{\tau}$	Forecasting error bias
$L_{t,i}$	Percentile of the interval forecast.
$\hat{x}_{i,t}$	Individual forecast to be optimally combined.
$\alpha_{i,t}$	Combination weight
$\hat{\Sigma}_t$	Covariance matrix of individual forecasts
$\hat{S}^2_{y,t}$	Covariance matrix of combined forecast

5.2.1.1. Punctual forecasts

Punctual forecasts are used is to predict the variable y_t for future instants. The prediction error is the disparity between an observed value and its forecast, expressed as $e_{t|T} = y_t - \hat{y}_{t|T}$, where $\hat{y}_{t|T}$ denotes the prediction made for y_t using the information available at time T. The observed prediction error $e_{t|T}$ depends on the prediction time T and the difference $h = t - T$, which is the lead time, also known as the prediction horizon.

To simplify the notation, we define $e_1, e_2, \dots, e_m$ as the discrepancy between the actual values y_t and the corresponding predicted values $\hat{y}_{t|t-h}$ during the evaluation or test period. For the sake of conciseness and without loss of generality, in this study, the forecasting horizon is set equal to $h = 24$ hours.

The metrics described in Table 5-1, including the bias, MAE, MAPE, RMSE and SD, are used to assess the accuracy of punctual forecasts in this chapter.

Table 5-1: Performance metrics for punctual forecasts

Bias	MAE	MAPE	RMSE	SD
$\hat{\tau} = \sum(e_t)/m$	$\sum(\lvert e_t \rvert)/m$	$\sum(\lvert e_t \rvert/y_t)/m$	$\sqrt{\sum(e_t)^2/m}$	$\sqrt{\sum(e_t - \hat{\tau})^2/m}$

5.2.1.2. Probabilistic forecasts

A probabilistic forecast is a prediction that includes an assessment of the uncertainty associated with that value. With respect to wind energy production, intervals in probabilistic forecasts represent a range within which the true outcome is likely to fall. The associated probabilities indicate the likelihood of the actual value falling within each specific interval.

The forecast experts offer prediction intervals for each hour of each day with different time horizons. Without loss of generality, in this work, we focus on the 5th, 10th, 15th, 50th, 85th, 90th, and 95th percentiles. Therefore, for instant t, the probability forecast is composed of seven values $L_{t,i}$, where i ranges from 1 to 7, corresponding to the 5%, 10%, 15%, 50%, 85%, 90%, and 95%, respectively, e.g., $P(y_t \leq L_{t,1}) = 0.05$.

To assess the accuracy of the probabilistic forecasts, two metrics can be computed: the coverage and the interval width:

- Coverage: The coverage refers to the accuracy with which the forecasted probability levels match the observed outcomes. It assesses how well the predicted probabilities reflect the actual frequency of events within the forecasted range. For example, the value y_t should be between $L_{t,1}$ and $L_{t,7}$ in 90% of the situations.

- Width: For a given coverage, the interval width refers to the distance between the inferior and the superior limits. For example, the width of the 90% prediction interval is computed as $|L_{t,7} - L_{t,1}|$.

In this work, we assume that the aforementioned probabilistic predictions have been provided (generated by an external agency).

5.2.2. Scheme of the proposed algorithm

Figure 5-1 shows the flowchart of the proposed methodology. The input data corresponds to both the historical real data and a set of individual probabilistic forecasts. The output data are the probabilistic forecasts based on an optimal combination of the input forecasts.

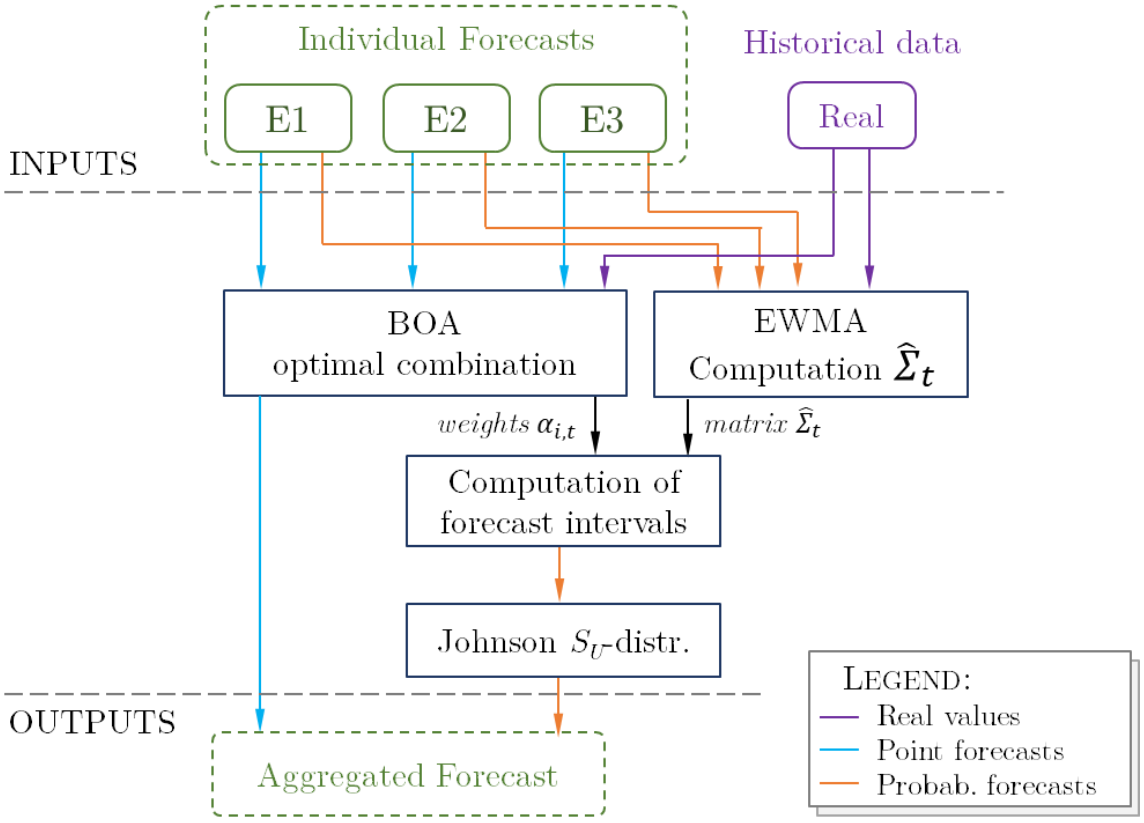

Figure 5-1: Flowchart of the proposed methodology.

The algorithm is detailed below:

Step 0) Receive the historical real data and the individual probabilistic forecasts.

Step 1) Compute the weights $\alpha_{i,t}\ \forall\, i,t$ using the Berstein Online Aggregation method (Section 5.2.3.2).

Step 2) Compute the variance matrix $\hat{\Sigma}_t$ using the exponentially weighted moving average technique (Section 5.2.5).

Note: Steps (1) and (2) can be performed simultaneously.

Step 3) Estimate the Johnson S_U-distribution to adapt the kurtosis (Section 5.2.4.1).

Step 4) Compute the forecast intervals using Eq. (5-6).

5.2.3. Combination of predictors

To predict the amount of wind energy produced at time t, denoted as y_t, we utilize a set of k predictors: $\hat{x}_{1t}$, $\hat{x}_{2t}$, ... $\hat{x}_{kt}$.

For the sake of conciseness and without loss of generality, three predictors are considered in this study: $\hat{x}_{1t}$, $\hat{x}_{2t}$ and $\hat{x}_{3t}$. The combined prediction $\hat{y}_t$ is expressed as a linear combination of individual forecasts:

$$\hat{y}_t = \alpha_{1t}\hat{x}_{1t} + \alpha_{2t}\hat{x}_{2t} + \alpha_{3t}\hat{x}_{3t} \qquad (5\text{-}1)$$

where the coefficients α_{1t}, α_{2t}, and α_{3t} are dynamic and recalculated online based on the observed errors in previous time intervals. Coefficients $\alpha_{i,t}$ are optimally computed to minimize the errors between the combined forecast $\hat{y}_t$ and the actual value y_t. Predictions with higher precision are given higher weights and those with lower accuracy are penalized.

5.2.3.1. Uniform weights

The technical literature is rich in procedures for searching for the optimal weights $\alpha_{1,t}$, $\alpha_{2,t}$, $\alpha_{3,t}$ assigned to each predictor at each time t. A basic solution is to assign equal and constant weights for every time t:

UNIF: $\alpha_{1,t}=\alpha_{2,t}=\alpha_{3,t}=1/3\ \forall t$.

Using the same weight for each predictor is equivalent to using the arithmetic mean of the three predictions.

According to the technical literature [49-52], the arithmetic mean sometimes outperforms other sophisticated combinations of predictions. This has been the subject of multiple explanations. In this work, the arithmetic mean is used as a benchmark for comparison purposes.

5.2.3.2. Bernstein online aggregation (BOA)

To optimally compute the weighting coefficients in the combined forecast in (5-1), the well-established BOA algorithm is employed in this part. This approach has been used in recent years for prediction problems related to the electricity market [53]. BOA is a recursive method that ensures predictions with minimum mean squared error, given certain general conditions. A simplified version of the algorithm is as follows:

$$\begin{cases} \Sigma_t = & (1-\lambda)\sum_{t=1}^{\infty}\lambda^{t-1}(\epsilon_{t-1}\epsilon'_{t-1}-1) \\ \square & = (1-\lambda)(\epsilon_{t-1}\epsilon'_{t-1}) + \lambda\cdot\Sigma_{t-1} \\ \alpha_{i,t} = & exp\left(-\eta L_{i,t}\left(1+\eta L_{i,t}\right)\right)\alpha_{i,t-1} \\ \square & \quad / \Sigma_{j=1}^{m}\ exp\left(-\eta L_{i,t}\left(1+\eta L_{i,t}\right)\right)\alpha_{i,t-1} \\ L_i = & l\left(y_t,\hat{y}_{i,t}\right) - \alpha_{1,t=1}l\left(y_t,\hat{y}_{1,t}\right) \\ \square & \quad + \alpha_{1,t=2}l\left(y_t,\hat{y}_{2,t}\right) + \alpha_{1,t=1}l\left(y_t,\hat{y}_{3,t}\right) \end{cases} \tag{55-2}$$

where $L\left(y_t,\hat{y}_{j,t}\right)$ is a loss function such as

$$L\left(y_t,\hat{y}_{j,t}\right) = \left(y_t-\hat{y}_{j,t}\right)^2 \tag{5-3}$$

and $\eta > 0$ is a parameter called the learning rate and set by the user. The procedure starts with $\alpha_{1,t} = \alpha_{2,t} = \alpha_{3,t} = 1/3$.

5.2.4. Interval width of aggregation

The three predictors $\hat{x}_{1t}$, $\hat{x}_{2t}$ and $\hat{x}_{3t}$ are assumed to be centered on $E[y_t - x_{kt}] = 0$, and the variance matrix is assumed to be $\hat{\Sigma}_t$:

$$\hat{\Sigma}_t = \begin{bmatrix} \hat{s}_{1,t}^2 & \hat{s}_{12,t} & \hat{s}_{13,t} \\ \hat{s}_{12,t} & \hat{s}_{2,t}^2 & \hat{s}_{23,t} \\ \hat{s}_{13,t} & \hat{s}_{23,t} & \hat{s}_{3,t}^2 \end{bmatrix} \tag{55-4}$$

The estimated variance matrix $\hat{\Sigma}_t$ can be used to estimate the variance of the combined forecast $\hat{y}_t$:

$$\hat{S}_{y,t}^2 = [\alpha_{1t}\, \alpha_{2t}\, \alpha_{3t}] \begin{bmatrix} \hat{s}_{1,t}^2 & \hat{s}_{12,t} & \hat{s}_{13,t} \\ \hat{s}_{12,t} & \hat{s}_{2,t}^2 & \hat{s}_{23,t} \\ \hat{s}_{13,t} & \hat{s}_{23,t} & \hat{s}_{3,t}^2 \end{bmatrix} \begin{bmatrix} \alpha_{1t} \\ \alpha_{2t} \\ \alpha_{3t} \end{bmatrix} \tag{5-5}$$

Equation (5-5) provides the variance of the aggregated forecast. Assuming a Gaussian approximation, the prediction interval with a confidence level of $(1 - \gamma)$ for the value y_t is obtained using:

$$\hat{y}_t - z_{\gamma/2}\hat{S}_{y,t} \leq \; y_t \; \leq \hat{y}_t + z_{\gamma/2}\hat{S}_{y,t} \tag{5-6}$$

where $z_{\gamma/2}$ is the value from the standard normal distribution $Z - N(0,1)$ with mean 0 and standard deviation 1, such that $P(Z > z_{\gamma/2}) = \gamma/2$.

Our numerical analysis reveals that the distribution of prediction errors resulting from the combination of the three predictors exhibits a symmetric distribution with notably greater kurtosis than the standard normal distribution. This high kurtosis underscores the inadequacy of this method in adequately capturing the unique characteristics of prediction errors within our model.

5.2.4.1. Johnson S_U distribution

To overcome this limitation, we replace the standard normal distribution percentiles with those obtained from the Johnson S_U-distribution system with unbounded support, as referenced in [54]. This novel approach improves the coverage results and more robustly handles the inherent uncertainties embedded within the system.

The Johnson S_U-distribution incorporates additional parameters to control skewness (γ) and kurtosis (δ). The following specific density function is used:

$$f_x(x) = \frac{\delta}{\sqrt{2\Pi(x^2+1)}} e^{\left[-\frac{1}{2}(\delta \log(x+\sqrt{1+x^2}))^2\right]}, \qquad x \in \mathbb{R} \tag{5-7}$$

This function corresponds to the Johnson distribution with a location parameter of zero, a scale parameter of one, a skewness parameter of zero, and a kurtosis parameter of δ. The specific density function is chosen based solely on the δ parameter, which quantifies the kurtosis of the distribution. In practical applications, the estimation of δ is derived from the data and typically falls within the range of 1 to 1.25.

To obtain the prediction intervals using this distribution, the parameter δ must be estimated. First, the standardized error is defined as follows:

$$r_t = (y_t - \hat{y}_t) \,/\, \hat{s}_{y,t} \tag{5-8}$$

where $\hat{y}_t$ is the combined prediction, the value y_t corresponds to the real value, and $\hat{s}_{y,t}$ is the estimated standard deviation of the prediction error. We propose approximating the probability distribution of the relative errors r_t by using the Johnson S_U distribution, $f_x(x)$. The maximum likelihood estimation of the parameter δ is determined by the expression:

$$\delta^2 = n \cdot \left(\sum_{t=1}^{n} \left[log\left(r_t + \sqrt{1 + r_t^2} \right) \right]^2 \right)^{-1} \tag{5-9}$$

Given the predicted value $\hat{y}_t$ and its estimated standard deviation $\hat{s}_{y,t}$, the prediction interval with probability (1− α) is obtained as follows:

$$\hat{y}_t - J_{\alpha/2}\hat{s}_{y,t} \leq \; y_{\;t} \leq \hat{y}_t + J_{\alpha/2}\hat{s}_{y,t} \tag{5-10}$$

where $J_{\alpha/2}$ represents the $(1 - a/2)$ percentile of the Johnson distribution in (5-7) using the parameter δ estimated by (5-9).

5.2.5. Exponentially weighted moving average technique

To compute the interval width of the aggregated forecast, the variance matrix $\hat{\Sigma}_t$ must be estimated. There are different procedures for estimating the covariance

matrix $\hat{\Sigma}_t$. In this work, the exponentially weighted moving average (EWMA) method is employed.

The EWMA method contemplates the possibility that the variance matrix will vary smoothly. The background idea is that there are moments when the variability is low and moments where the variability is higher. Periods of low variance are followed by days of low variability; similarly, periods of high variance are followed by days of high variability.

This model, widely used in multivariate time series analysis, depends on a smoothing parameter $0 < \lambda < 1$. Let ϵ_t be the column vector containing the observed errors from the three prediction methods at time. The covariance matrix $\hat{\Sigma}_t$ at time t is estimated using the following formula:

$$\begin{aligned} \hat{\Sigma}_t &= (1-\lambda) \cdot \sum_{t=1}^{\infty} \lambda^{t-1} (\epsilon_{t-1} \epsilon'_{t-1} - 1) \\ &= (1-\lambda) \cdot (\epsilon_{t-1} \epsilon'_{t-1}) + \lambda \cdot \hat{\Sigma}_{t-1} \end{aligned} \tag{5-11}$$

In this equation, the matrix at time t is obtained by updating the variance matrix at time t – 1, with the prediction errors ϵ_{t-1} observed at the most recent available time t−1.

The value of λ (the smoothing or discount parameter) is typically set to values like 0.94 or 0.96. When λ is close to 1, the variance matrix is updated very slowly. The optimal value depends on the dynamics of the errors and can be estimated using maximum likelihood.

5.2.6. Estimating the variance matrix including uncertainty

In this section, the prediction intervals of different models are utilized to calculate the prediction intervals for the combined model. By considering the estimated standard deviations of each model at a given time *t*, estimating the uncertainty associated with a linear combination of predictors at a specific time *t* becomes relatively easy.

We denote $\widehat{D}_t$ as the diagonal matrix that includes the standard deviations from the matrix $\hat{\Sigma}_t$:

$$\widehat{D}_t = \begin{bmatrix} \hat{s}_{1,t}^2 & 0 & 0 \\ 0 & \hat{s}_{2,t}^2 & 0 \\ 0 & 0 & \hat{s}_{3,t}^2 \end{bmatrix} \tag{5-12}$$

D_t^* is the diagonal matrix that contains the average standard deviations obtained from the prediction intervals:

$$D_t^* = \begin{bmatrix} s_{1,t}^* & 0 & 0 \\ 0 & s_{2,t}^* & 0 \\ 0 & 0 & s_{3,t}^* \end{bmatrix} \tag{5-13}$$

The method proposed in this section replaces the variances obtained from historical errors with the new variances provided in the prediction intervals. Let $\hat{\Sigma}_t^*$ be the new variance matrix at time t that includes the uncertainties provided in D_t^*. The following substitution is sufficient:

$$\hat{\Sigma}_t^* = D_t^* \widehat{D}_t^{-1} \hat{\Sigma}_t \widehat{D}_t^{-1} D_t^* \tag{5-14}$$

When calculating the prediction intervals for the linear combination described in the previous section, $\hat{\Sigma}_t$ is simply replaced with the updated $\hat{\Sigma}_t^*$. Notably, using only the matrix D_t^* as an estimator of the error covariance matrix is not recommended because it does not consider the high correlation between prediction errors. This leads to unrealistically narrow intervals that do not satisfy the coverage requirements.

5.3. Case study

To test the accuracy and performance of the proposed methodology, the hourly wind energy generation in the Spanish mainland system from 12 March 2020 to 14 January 2022 is analyzed.

5.3.1. Descriptive statistics

Figure 5-2 depicts the time series of the real hourly wind energy production in Spain, highlighting the wide-ranging variability of the recorded values. The minimum and maximum production levels are 0.181 GWh and 19.90 GWh, respectively, with an average hourly production of approximately 6.4 GWh and a standard deviation of 3.75 GWh. Furthermore, Figure 5-3 visually emphasizes the discernible asymmetry within the distribution, reflecting the underlying complexity of the dataset.

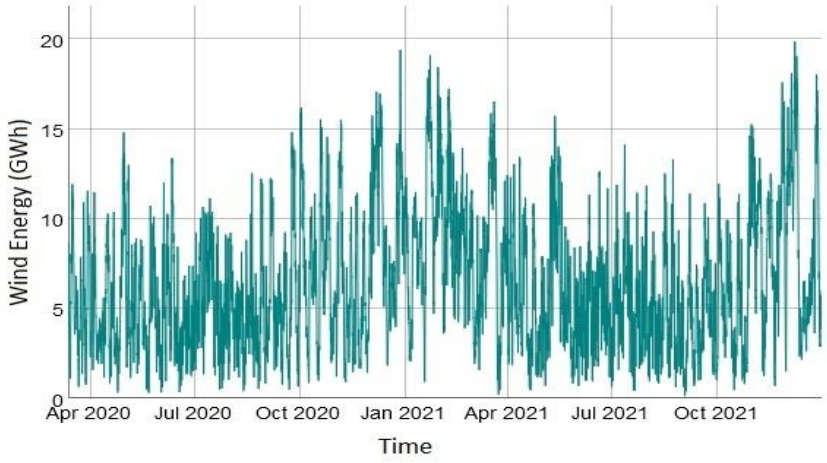

Figure 5-2. Hourly production of wind energy in the Spanish peninsula system.

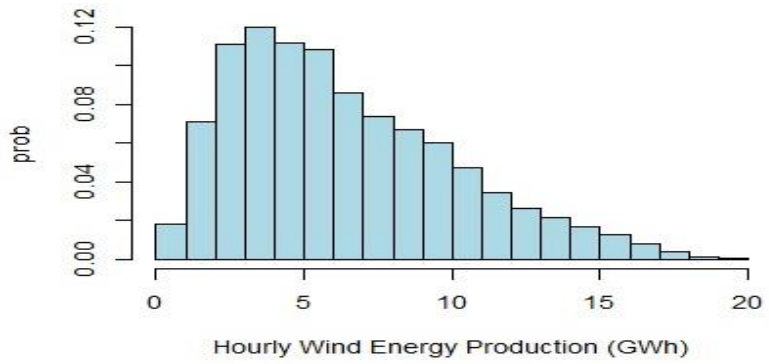

Figure 5-3. Histogram of hourly wind energy generated.

The time series of wind energy production exhibits strong autocorrelation coefficients, indicating a 24-hour periodicity associated with seasonality. This seasonality is considered during the subsequent error analysis.

5.3.2. Analysis of individual predictions

In this work, we examine the hourly wind energy predictions provided by three forecasting companies. For confidentiality reasons, we are unable to disclose further details about the predictive models employed to generate these forecasts. Throughout the article, we refer to these models as E1, E2, and E3.

To preserve privacy, the forecasting models are denoted as E1, E2, and E3, respecting confidentiality while maintaining the validity of the results. Figure 5-4 shows the observed and predicted wind power production values for a 24-hour horizon using three different models.

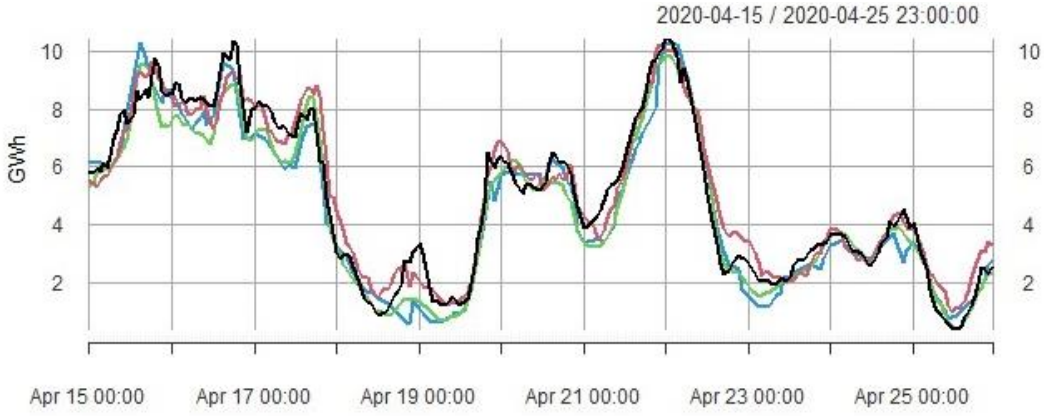

Figure 5-4. Hourly wind generation (black) and predictions (E1: red, E2: blue, E3: green).

The visual inspection and error analysis of the three models indicate that in most cases, their behaviors are generally very similar (Figure 5-3). As illustrated in Figure 5-4, the prediction curves closely track and follow the evolution of the actual production series. In the following sections, unless stated otherwise, 24-hour horizon predictions are employed.

5.3.2.1. Analysis of punctual individual forecasts

Among the 659 days examined, approximately 49 days (7% of the total) exhibited extreme errors. Nevertheless, the three models frequently provided similar predictions, while the actual series deviated significantly from the predicted values. This

discrepancy is likely attributed to disparities between the weather predictions provided by the atmospheric model and real-time weather conditions. On most days (93%), the prediction errors followed an approximately normal distribution, with a mean of zero and a standard deviation of approximately 0.8 MWh.

To summarize the behavior of each model and measure the accuracy of the prediction methods, the measures listed in Section 5.2.1.1 are used, with the results provided in Table 5-2.

Table 5-2: Basic descriptions of the prediction errors of the three models.

Name	E1	E2	E3
Bias	-0.1317	0.0676	0.1121
MAE	0.6056	0.5952	0.6842
MAPE	0.1350	0.1290	0.1529
RMSE	0.8172	0.8269	0.9154
SD	0.8065	0.8241	0.9085

Table 5-2 shows that all three methods have bias, with E1 and E3 exhibiting more pronounced biases. E1 underestimates the production, while E2 and E3 overestimate it. Overall, E1 and E2 exhibit similar behaviors over the period and perform better than E3.

Figure 5-5 illustrates the strong correlation among the prediction errors of the three models, displaying multiple scatter plots of these error series. This high correlation is further underscored by the fact that high and negative errors in one predictor correspond to similar errors in the other two models, particularly in the lower tail of the scatter clouds.

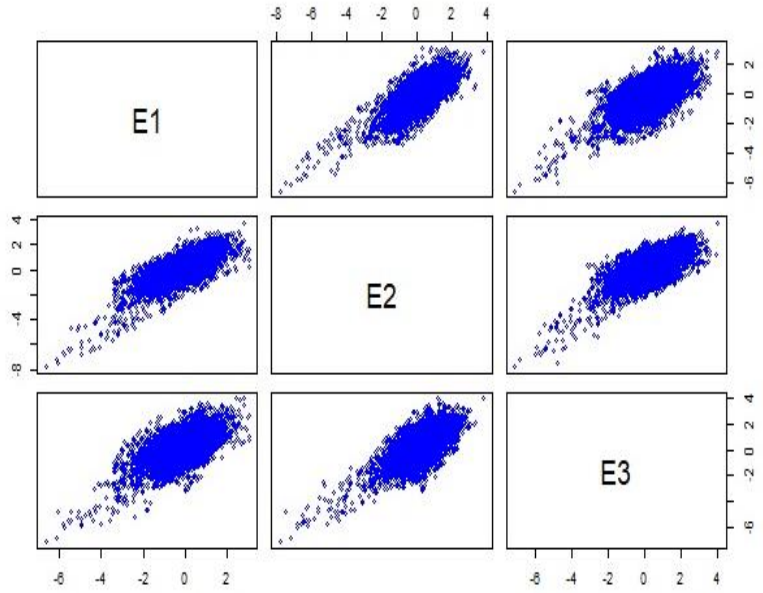

Figure 5-5. Scatter plots of prediction errors.

The monthly MAE values depicted in Figure 5-6 reveal the dynamic nature of the three models' evolutions. Notably, no single method consistently outperforms the others, as indicated by the absence of a consistent pattern of lower average MAE values across the graphs. Although E3 generally exhibits poorer performance, it demonstrates improved predictive capabilities in select months, such as May 2020 and April 2021. On the other hand, E1 and E2 alternate in terms of performance throughout the remaining months, sometimes resulting in significant deviations.

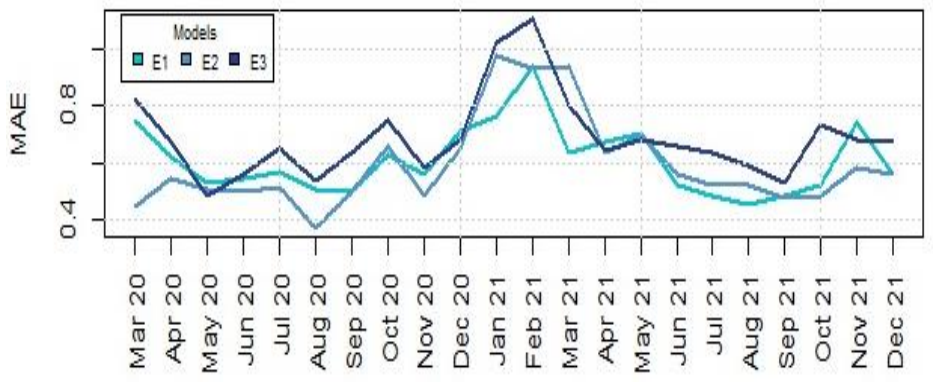

Figure 5-6. Monthly evolution of MAEs for the three models.

The fluctuating nature of the three methods' prediction errors indicates that a clear dominant solution is not present. Even if such dominance were present, the conditions

allow for the formulation of a strategy that amalgamates the predictions of all three methods, thereby assessing whether the resulting amalgamated prediction achieves better accuracy than any individual solution. In the following sections, the characteristics of an effective prediction model are described, and a methodology for refining predictions to enhance the performances of the original methods is introduced.

5.3.2.2. Probabilistic individual forecasts

The evaluation of prediction intervals involves coverage analysis, ensuring that observed values fall within the intervals at the specified percentage and minimizing the widths of these intervals. In the considered database, each probabilistic prediction consists of 7 values, which correspond to the 5%, 10%, 15%, 50% (point prediction), 85%, 90%, and 95% percentiles (see Figure 5-7).

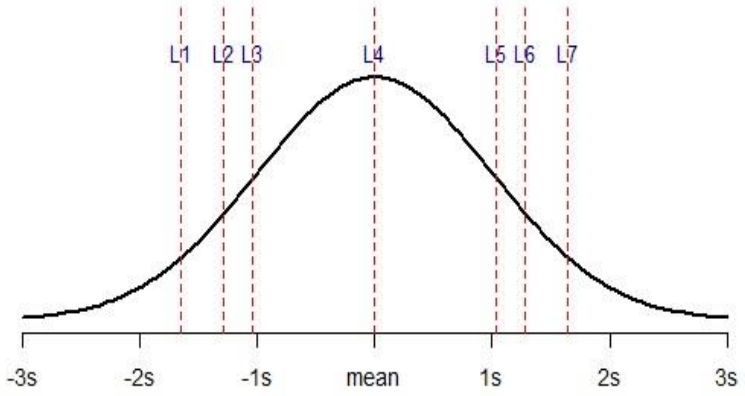

Figure 5-7. The normal PDF curve and the quantiles provided in the predictions.

The interval for y_t with a 90% probability is the interval (a_t, b_t), such that $y_t \in (a_t, b_t)$ with a probability of 0.90. The values a_t and b_t correspond to the 5% and 95% percentiles, respectively, provided in the probabilistic predictions. Intervals with 70% and 80% probability can be constructed similarly. Note that the prediction intervals provided are not necessarily obtained under the assumption of normality of the errors.

To evaluate the widths of the prediction intervals, we use standard deviations as a measure of model accuracy. If the coverage exceeds the established security level (1-α), the confidence intervals are wider than necessary and should be reduced to meet the

fixed probability level. In contrast, if the coverage falls below the theoretical value set, the prediction interval limits should be widened. In Figure 5-8, we present the time series of actual wind production (in black), its predicted values (in red), and the 90% prediction intervals (in blue and green dashed lines).

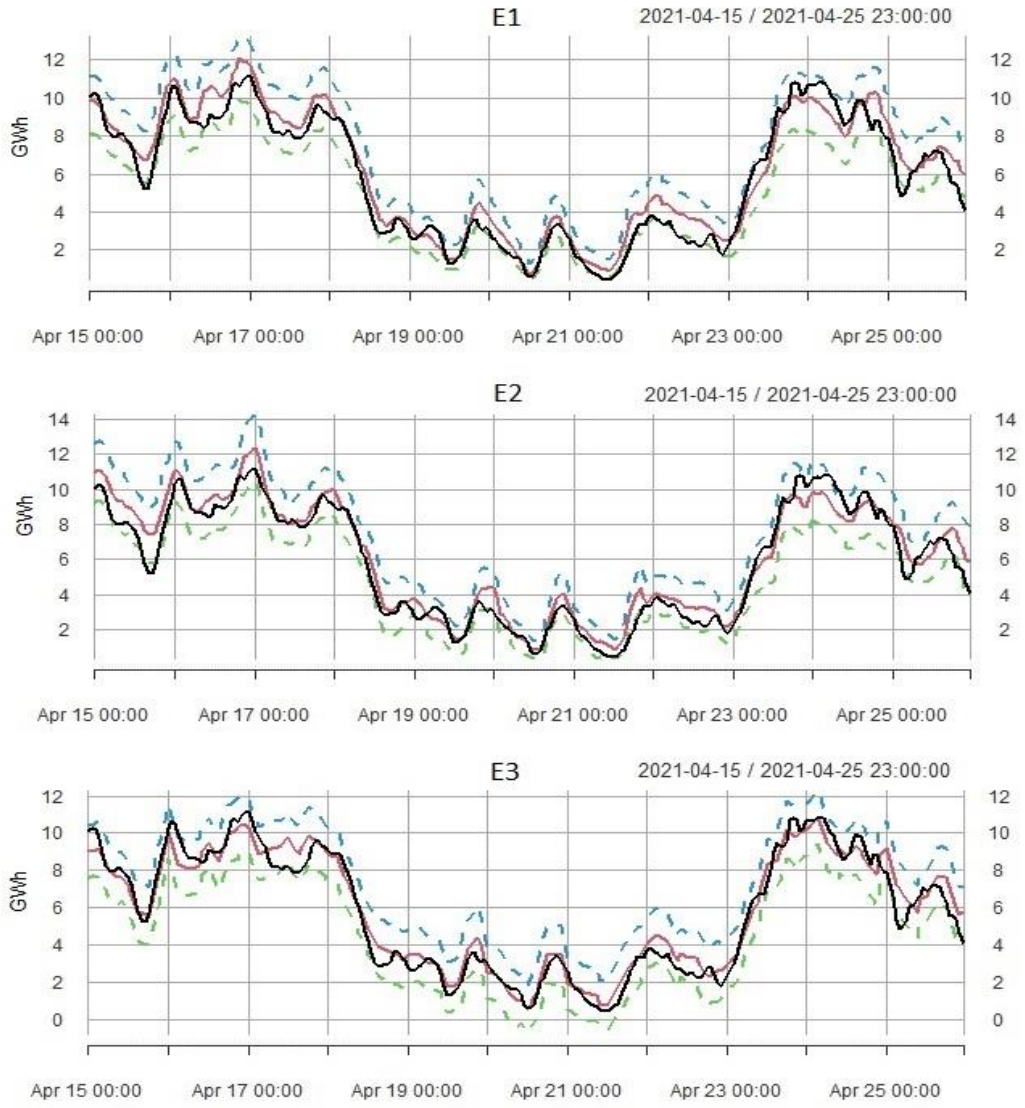

Figure 5-8. The time series of actual wind production (black), its point predictions (red), and the 90% prediction intervals (blue and green dashed lines) for the three models.

5.3.2.3. Prediction interval width: standard deviations

By equating the values to the prediction intervals under a normal distribution with mean $\bar{x}_t$ and standard deviation $\hat{s}_t$, we can approximate the percentiles using the following equations:

$$L_{t,1} = \bar{x}_t - 1.654\hat{s}_t \quad L_{t,2} = \bar{x}_t - 1.287\hat{s}_t \quad L_{t,3} = \bar{x}_t - 1.039\hat{s}_t$$
$$L_{t,4} = \bar{x}_t \qquad (5\text{-}15)$$
$$L_{t,5} = \bar{x}_t + 1.039\hat{s}_t \quad L_{t,6} = \bar{x}_t + 1.287\hat{s}_t \quad L_{t,7} = \bar{x}_t + 1.654\hat{s}_t$$

where the values $(-1.654, -1.287, -1.040, 0, 1.040, 1.287, 1.654)$ correspond to the percentiles of the standard normal distribution $N(0,1)$, with a mean of zero and a variance of one. The mean corresponds to the 50th percentile, and the value of $\hat{s}_t$ is estimated by least squares for each hour t (Figure 5-9).

$$\hat{s}_t = \sum_{i=1}^{7}(w_i \cdot L_{t,i}) \qquad w_i = z_i \,/\, \sum z_i^2 \qquad (5\text{-}16)$$

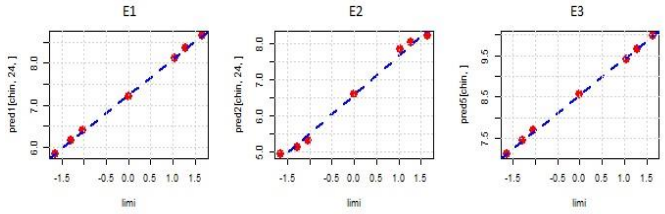

Figure 5-9. Estimation of s_t by least squares for the three models at a specific instant.

The mean of the estimated standard deviations for each model is shown in Table 5-3**.** In simplified terms, model E1 provides 95% of predictions with an accuracy of approximately $2 \times 0.76 = \pm 1.52$ GWh, model E2 has an average accuracy of ± 2.19 GWh, and model E3 has an accuracy of ± 1.70 GWh.

Table 5-3. Average standard deviation of intervals for the three models.

E1	**E2**	**E3**
0.7659	1.1015	0.8567

Table 5-3 illustrates that model E1 provides more precise intervals than does E2. The amplitude provided by the E3 model, whose intervals were obtained *post hoc* using the conformal prediction methodology, provides values between those of the first two

models. The intervals of the E3 model are constant throughout the analyzed period for each hour. This is kept in the document as an upper bound of the average standard deviation: intervals that adapt to local uncertainty are expected to provide a lower average width than that obtained using the conformal prediction method. Conformal prediction is a technique used in machine learning to create prediction intervals with controlled error rates. This approach helps to quantify the uncertainty associated with a prediction, allowing adaptable prediction intervals to be constructed in response to varying levels of uncertainty within the data.

To better assess the difference between the three methods, Figure 5-110 shows the average deviations of the intervals for each of the 22 months of the analyzed time window. Model E1 generally provides narrower intervals for all months than does E2. The increase in the standard deviation of the prediction intervals provided by Model E2 is remarkable for the months of December 2020 and January, February, and March 2021. Importantly, this corresponds to the period of the Filomena storm, in which the meteorological conditions were very singular and uncommon.

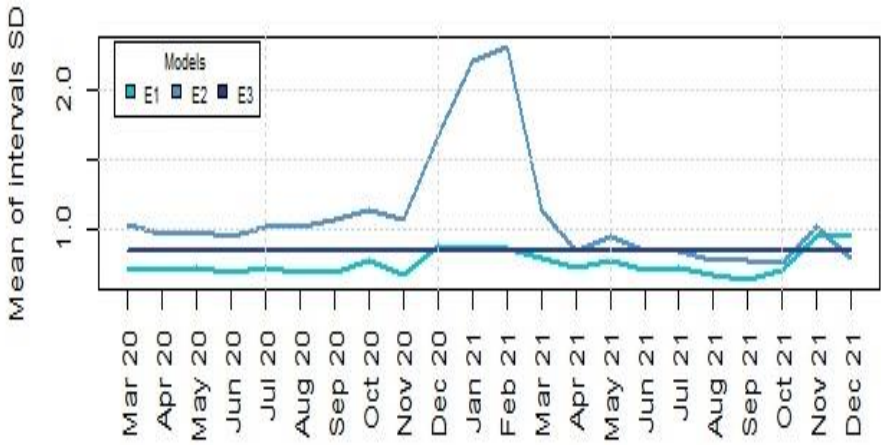

Figure 5-110. Average hourly standard deviations (GWh) of 24-hour horizon predictions by month.

Model E1 generally provides lower standard deviations, which implies narrower prediction intervals; this indicates that its predictions are more precise.

Model E2 provides much wider intervals for January and February than for the remainder of the year. These results are consistent with the prediction errors obtained

during that period. The average width is above the bound provided by the conformal prediction method. Therefore, these are not efficient intervals.

The amplitudes (standard deviations) of the intervals should be analyzed alongside the actual coverage (% of correct predictions) of the prediction intervals provided by the different models, which is discussed in the following section.

5.3.2.4. Coverage analysis

Coverage analysis is a crucial step in evaluating the performances of prediction intervals. Coverage analysis is conducted to determine the extent to which the provided prediction intervals accurately capture the true values. The evaluation criterion is straightforward: the historical analysis of the prediction intervals, with a given probability level of 1-α, should successfully encompass the actual value being predicted in a percentage of cases equal to $(1-\alpha)\cdot 100$. By comparing the predicted intervals with the observed values, we can assess the reliability and effectiveness of each prediction model.

Table 5-4. Percentage of times the actual value falls in each of the eight classes generated by prediction intervals.

Class	1	2	3	4	5	6	7	8
Interval	0-5	5-10	10-15	15-50	50-85	85-90	90-95	95-100
Exp	5.00	5.00	5.00	35.0	35.0	5.00	5.00	5.00
E1	6.83	6.049	6.15	37.5	32.6	4.07	3.48	3.33
E2	2.13	0.854	1.20	41.9	47.0	1.99	1.41	3.46
E3	3.67	3.982	3.88	33.3	36.6	6.01	6.10	6.46

Table 5-4 shows the percentage of times that the actual value of the variable of interest falls into each of the eight possible regions defined by the seven percentiles provided in the prediction intervals of each model. The first row ("exp") indicates the expected proportion of times that theoretically should be observed in each class. For instance, in "class 0-5", the actual value should be 5%.

The analysis of Table 5-4 for each model can be summarized as follows:

- Model E1: The observed frequencies in each of the eight classes are similar to the expected theoretical values. The lower classes 1, 2, 3, and 4 contain a higher percentage of true values than expected; consequently, the higher classes 5, 6, 7, and 8 contain true values less frequently.
- Model E2: The observed frequencies in each of the eight classes clearly differ from the expected theoretical values. The limits of the prediction intervals (or percentiles $L_{t,i}$, $i = 1,2, \ldots ,7$) do not correspond to the expected theoretical probabilities. The central classes 4 and 5 contain the true value 88.9% of the time, which is significantly higher than the expected 70%. On the other hand, classes 1, 2, 3 and 6, 7, and 8 contain the true value 11.1% of the time, which is much lower than the expected 30%.
- Model E3: The observed frequencies in each of the eight classes are similar to the expected theoretical values. This behavior is opposite to that of Model E1, as its prediction intervals more frequently contain the true values in the upper classes.

Table 5-5. The coverage of the prediction intervals at 70%, 80%, or 90%.

	cob70	cob80	cob90
E1	70.1	80.3	89.8
E2	89.0	92.1	94.4
E3	69.9	79.8	89.9

Comparing the coverage of the prediction intervals at 70%, 80%, and 90% of the models with the theoretical values (Table 5-5), illustrates that model E2 exhibits a significant discrepancy. While the other two models in this case closely approximate the expected values, model E2 is very conservative in its prediction intervals. This result is consistent with that observed in the previous section, where it was noted that model E2 provides wider prediction intervals. Models E1 and E2 provide 90% intervals with coverage very close to the theoretical values, but they are highly asymmetric.

5.3.3. Application of the proposed procedure

After the set of individual forecasts is analyzed (both point and probabilistic predictions) as described in the previous sections, the proposed procedure is applied as detailed in section 5.2.2.

5.3.3.1. Berstein online aggregation: case study

In the first step, BOA (section 5.2.3.2) is applied to compute the combination weights for each instant in the study period. In this case study, the BOA algorithm is implemented in the opera package in R [55]. Figure 5-11 shows the evolution of the weights assigned to each of the three models in combination during the study period.

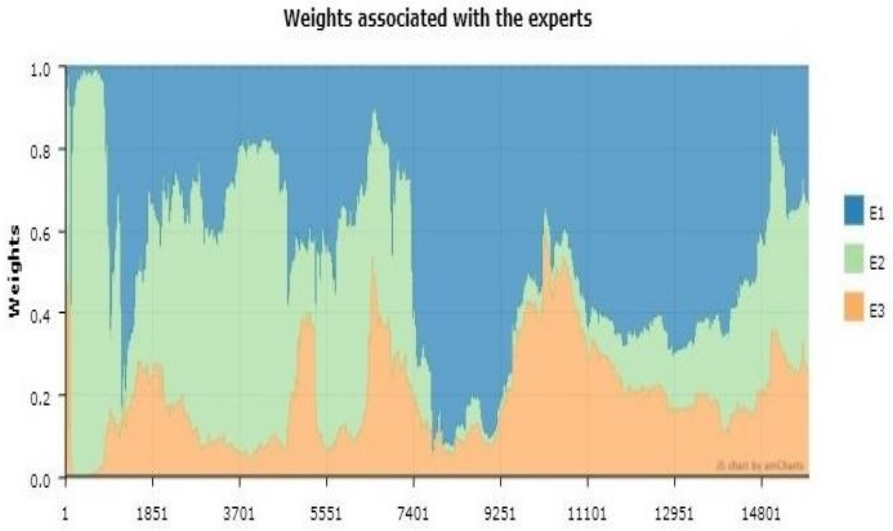

Figure 5-11. Weights assigned to each of the three methods in the BOA.

The relative importance of each model varies significantly. In the initial months, the weight of model E2 dominates the prediction, but it becomes negligible in the interval between approximately instants 7500 and 9500.

Once the optimal weights have been computed, the punctual combined forecast is computed using Eq. (5-1). The performance of the combined forecast is quantified by means of the monthly MAE in Figure 5-12. For comparison purposes, the performance of the uniform weights (section 5.2.3.1) is included in the analysis.

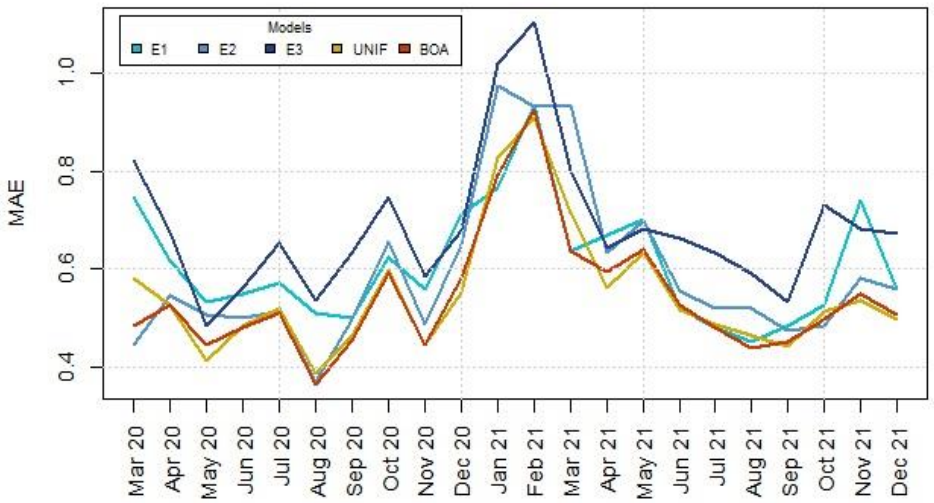

Figure 5-12. Monthly evolution of the MAEs for the three predictors and the aggregators UNIF and BOA.

Figure 5-12 shows the improvements in the aggregation models (UNIF and BOA) compared with the individual forecasts (E1, E2 and E3). The MAE values are consistently better in all months for both the UNIF and BOA aggregation techniques. Although UNIF and BOA exhibit little difference, the latter consistently performs better in almost all months. All three predictors (E1, E2, and E3, and hence, their combinations, yield significantly increased prediction errors during the months of January and February 2021. The global MSE considering the whole period is provided in Table 5-6.

Table 5-6. Global MSE for each method.

E1	E2	E3	UNIF	BOA
0.675	0.681	0.845	0.562	0.531

Table 5-6 shows that BOA outperforms all the individual forecasts. For the entire period, BOA exhibits an MSE value 20% lower than that of the best individual forecast.

5.3.3.2. EWMA method: case study

Once the BOA algorithm has been applied, the EWMA method is used to compute the dynamic variance matrix $\hat{\Sigma}_t$ at each time instant t. In this study, we use the EWMA *vol*() function from the MTS package in R to estimate the matrix $\hat{\Sigma}_t$. For illustrative purposes, Table 5-6 provides the estimated variance matrix for a specific instant. This matrix is computed for each time instant via Eq. (5-11).

Table 5-7. Estimated variance matrix using the EWMA procedure for a specific instant.

	E1	**E2**	**E3**
E1	1.1135	1.0441	0.4374
E2	1.0441	1.1078	0.4648
E3	0.4374	0.4648	0.3205

Then, both the BOA weights and the EWMA variance matrix $\hat{\Sigma}_t$ are employed in Eq. (5-5) for computing the standard error of the combined forecasts $\hat{S}_{y,t}$, which is required for computing the interval width.

5.3.3.3. Johnson distribution: case study

Once the standard error $\hat{S}_{y,t}$ has been computed, a set of quantiles from an adjusted Johnson S_U-distribution should be computed. To do so, first, the parameter δ is estimated using (5-9), and the quartiles are then obtained using (5-7). Finally, the prediction intervals are computed using (5-10). For illustrative purposes, a histogram of standardized errors of the combined forecasts is depicted in Figure 5-13, overplotting the CDF of the standardized normal distribution (blue dashed line) and the adjusted Johnson S_U-distribution (red dashed line) with a parameter $\delta = 1.092$.

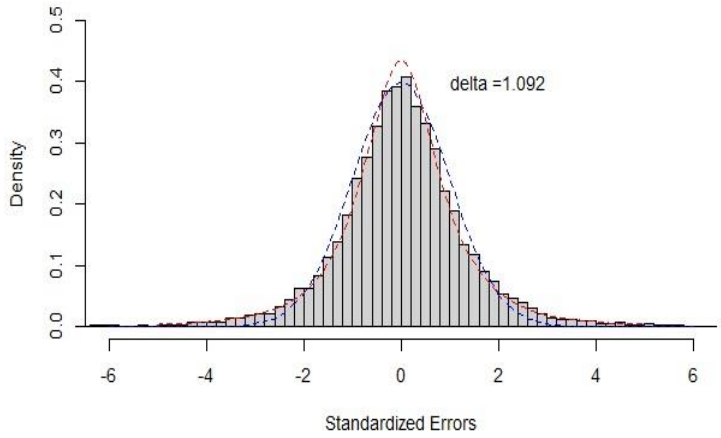

Figure 5-13. Histogram of BOA standardized prediction errors. Blue line: Gaussian distribution. Red line: Johnson distribution.

As depicted in Figure 5-13, the Johnson S_U-distribution substantially better fits the data than does the normal distribution. Consequently, employing this enhanced distribution yields improved prediction intervals, providing stronger coverage than intervals obtained using a normal distribution.

5.3.3.4. Coverage analysis: case study

The combination of predictions has demonstrated a significant reduction in point prediction errors (section 5.3.3.1). To assess the coverage of the aggregated forecasting intervals, Figure 5-14 depicts the coverage rates for the three individual models (E1, E2, and E3) and the two aggregated forecasts (UNIF and BOA).

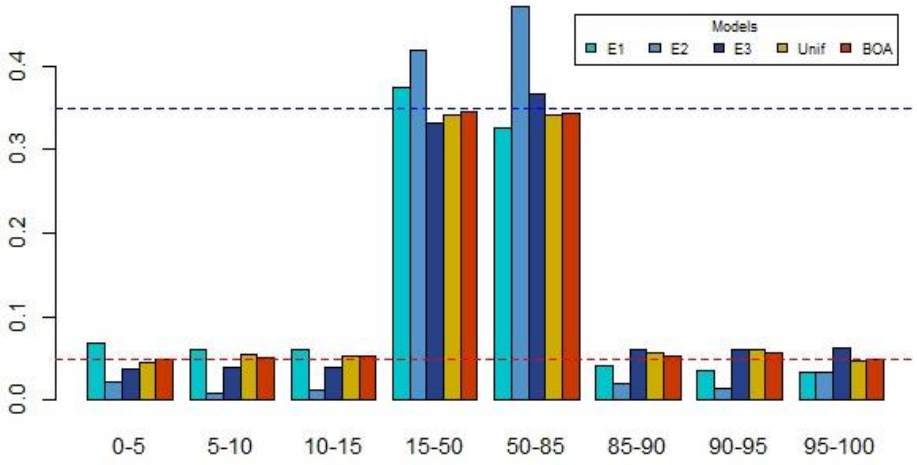

Figure 5-14. Bar chart of the coverage rates for the considered models.

The data depicted in Figure 5-14 highlight several notable trends in the coverage percentages across different aggregation intervals. Initial intervals, such as 0-5, 5-10, and 10-15, exhibit consistent and uniform coverage across all predictors and aggregators. However, subsequent intervals exhibit a discernible shift in coverage.

For instance, the 15-50 interval shows varying coverage percentages among the predictors. The UNIF and BOA aggregators display coverage percentages that closely correspond to the expected values in this interval, emphasizing their effectiveness in maintaining consistent coverage within this interval.

As the intervals progress into the higher range (50-85, 85-90, 90-95, 95-100), the coverage percentages for both predictors and aggregators exhibit more fluctuation. Notably, the UNIF and BOA aggregators demonstrate similar patterns of coverage across these higher intervals, suggesting their reliability in managing the aggregation of predictions. Overall, the observed coverage of the prediction intervals aligns well with the expected theoretical values. The performances of the UNIF and BOA aggregators particularly underscore their potential in enhancing the accuracy and dependability of the forecasting process.

5.3.3.5. Interval width analysis: case study

As stated above, once the coverage has been analyzed, the interval width must be explored. Figure 5-15 depicts the monthly evolution in average standard deviations for the UNIF and BOA aggregators, represented by orange and red lines, respectively, as well as for the individual predictors. The graph reveals a noteworthy decrease in standard deviation, indicating significant reductions in the widths of the prediction intervals. These improvements are evident at all times except for in February 2021. At this point, the aggregator employs the E2 model, which exhibits a large standard deviation and propagates it, increasing the error.

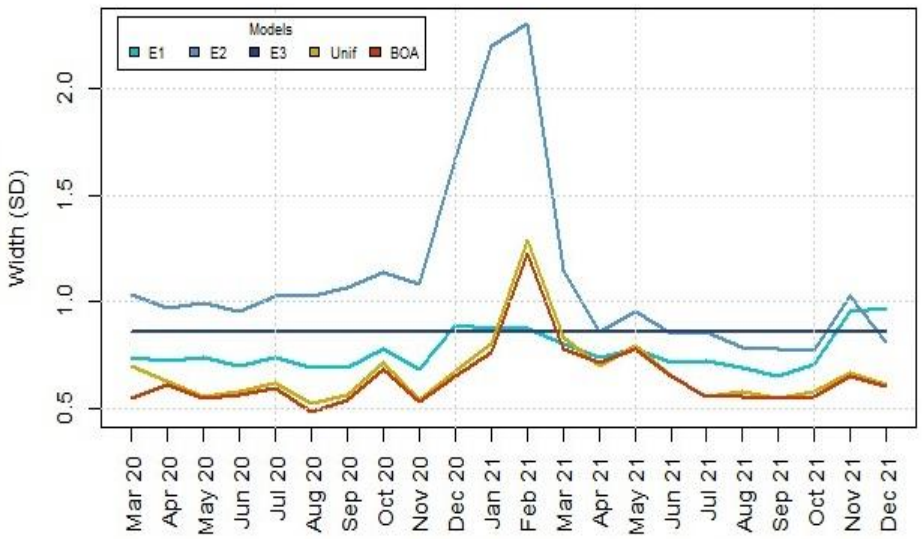

Figure 5-15. Monthly evolutions of the amplitudes of the prediction intervals for the three predictors and two aggregators: the UNIF and BOA.

The reduction in the width of the prediction intervals (average standard deviation) is highlighted in Table 5-8, which provides the average values of the standard deviations for the entire period. On average, the prediction intervals generated through the BOA aggregator are 16% narrower than those generated through the E1 predictor, which is the most accurate among the three.

Table 5-8. Amplitudes of the predictors and the UNIF and BOA aggregators.

E1	E2	E3	UNIF	BOA
0.7658	1.1015	0.8566	0.6643	0.6412

5.3.4. Case study: varying the prediction horizon

In the previous sections, the analysis focused on predictions with a 24-hour horizon. In this section, the analysis is extended to cover horizons ranging from one to forty-eight hours. Figure 5-16 presents the prediction error results obtained using statistical metrics (bias, MAE, MAPE, and RMSE) for each model as a function of the forecasting horizon.

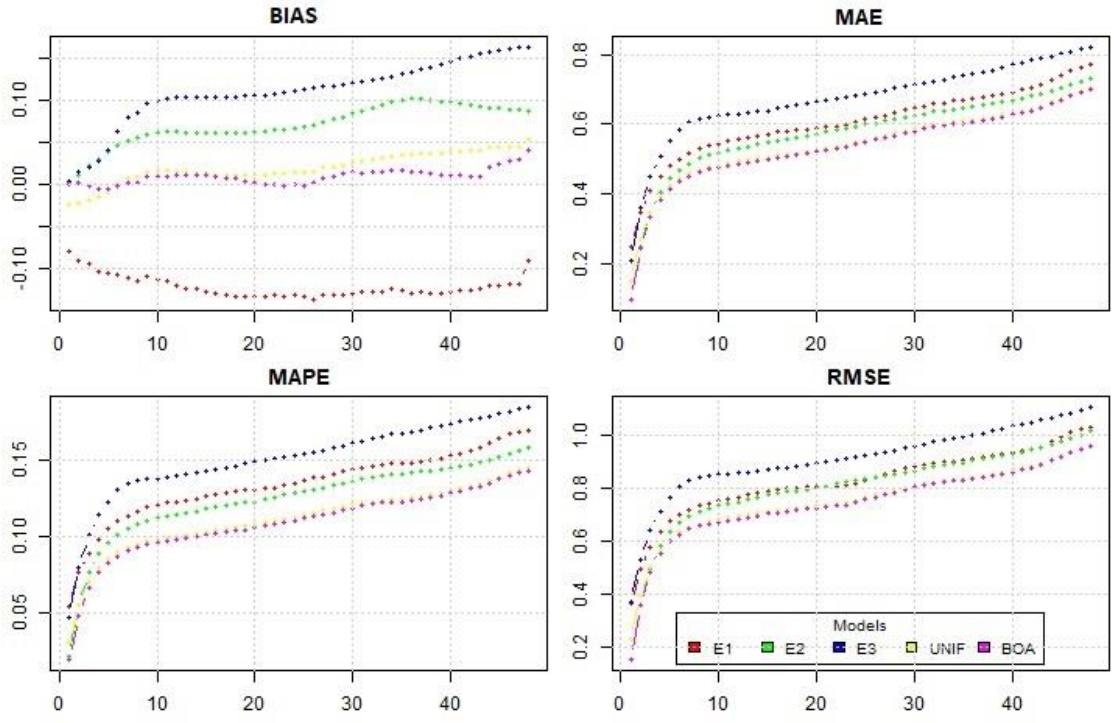

Figure 5-16. Bias, MAE, MAPE, and RMSE for prediction horizons ranging from 1 to 48 hours.

Figure 5-16 illustrates the following:

- The original E1, E2, and E3 models exhibit noticeable biases for horizons longer than five hours. E1 and E3 exhibit the most significant biases with opposite signs. The combination of BOA substantially reduces the bias.
- The MAE, MAPE, and RMSE metrics show similar trends. Beyond the one-hour horizon, the model with the highest error is E3, followed by E1 and then E2. The combinations of BOA and UNIF consistently provide lower errors.
- The BOA method was the best combination, followed by the uniform approach.
- In the plots of the MAE, MAPE, and RMSE, for all the models, two distinct sections can be distinguished: a step linear increase from 1 to 5 hours and linear growth with a significantly lower slope for predictions ranging from 6 to 48 hours.

Figure 5-17 evaluates the coverage and width of prediction intervals for the probabilistic predictions of the E1, E2, and E3 models, as well as the UNIF and BOA combinations.

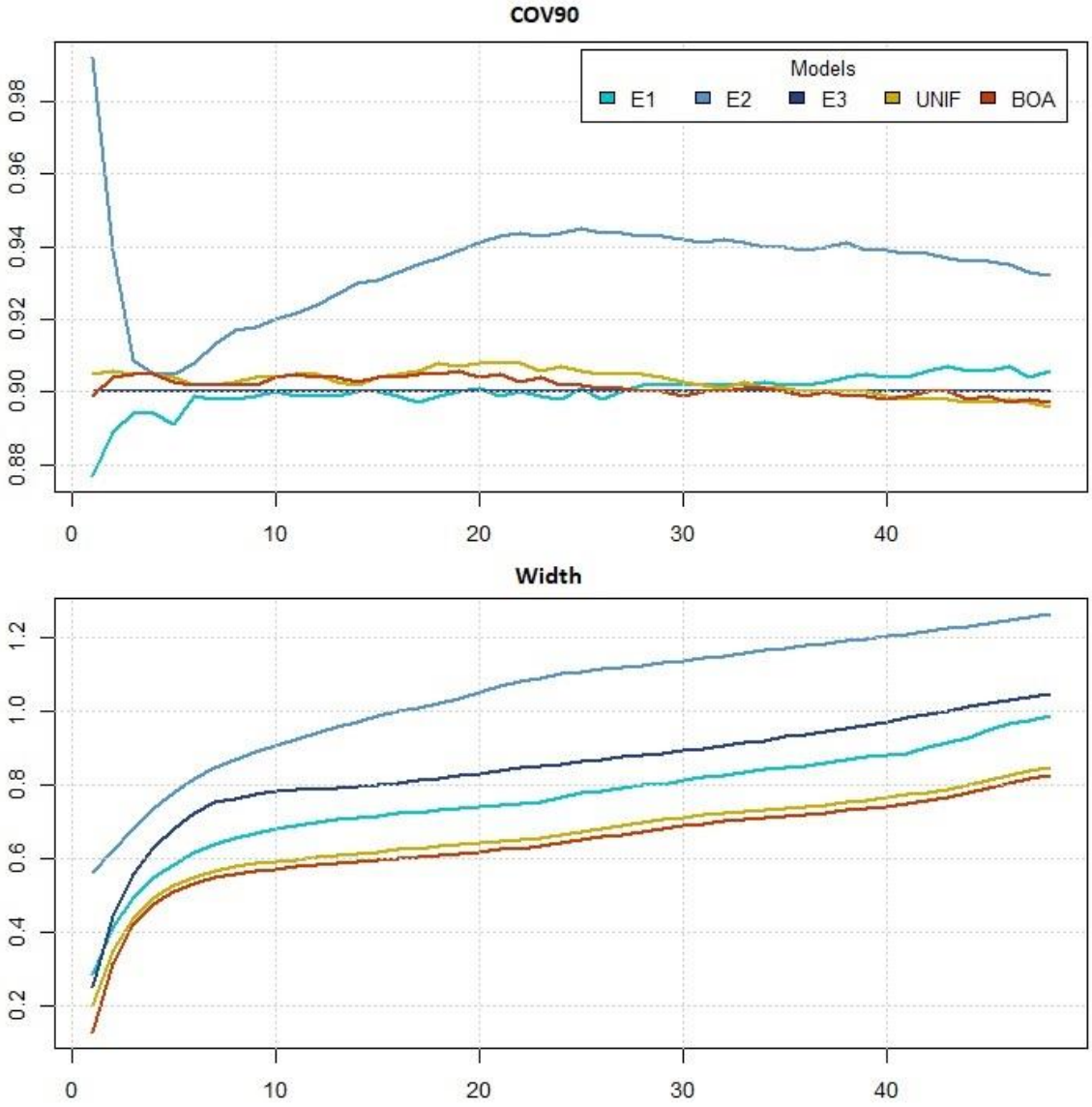

Figure 5-17. Coverage and width of prediction intervals for horizons ranging from 1 to 48 h.

Figure 5-17 shows that all the models except for the E2 model, which exhibits significantly deviant coverage, exhibit highly acceptable results for all 48 horizons. The probabilistic predictions based on the BOA and UNIF combinations significantly reduce the width of the prediction intervals. Concerning the coverage of E3, the interval was computed using conformal predictions; thus, the value of coverage was 90% for all horizons.

5.4. Conclusions

When addressing critical prediction issues, it is common to resort to various models that provide different predictions. The widespread consensus in technical literature suggests that the best prediction strategy is to combine the results of these predictors. In this work, a method for calculating prediction intervals from a predictor obtained through a linear combination of independent predictions is proposed.

The developed method is based on the application of three techniques. First, the Berstein online aggregation is applied to compute the optimal combination of point forecasts, denoting an outperformance compared with the individual predictions in terms of accuracy. Second, to appropriately estimate the prediction intervals, the variance matrix of the prediction errors is calculated using the exponentially weighted moving average method. Finally, the Johnson S_U-distribution is applied to improve the statistical properties of the aggregated predictions. Analyzing both the coverage and interval width shows that the proposed technique is computationally efficient and numerically accurate.

An exhaustive analysis was performed using Spanish wind power generation data by testing the accuracy of the point-aggregated forecasts and the reliability of the prediction intervals and by checking the coverage and interval width. The obtained results indicate that the proposed probabilistic combination method is both accurate and reliable: the forecasting error is lower than that of the individual predictions, and the coverage is better than that of the separate forecasts.

The results of the wind production prediction study demonstrate that combining different predictors is highly advantageous and significantly enhances individual predictions. The aggregated prediction intervals have appropriate coverage and significantly narrower widths than any of the intervals constructed with individual

predictors, thereby improving the quality of point forecasting. The chapter's findings were published in [95, 100]

6. CONTRIBUTIONS TO PRICE FORECASTING: DIFFERENCE AMONG EUROPEAN COUNTRIES

6.1. Introduction

This chapter aims to statistical analyze hourly electricity price series in six European countries: Denmark, France, Germany, Italy, Spain, and the United Kingdom, using time series models. The purpose of the analysis is to select a procedure to make predictions for the next day's 24-h prices. With the help of the selected models, the predictability of prices is compared for each country. The five most prominent countries in the European Union have been selected with Denmark.

6.1.1. Motivation and literature review

In many competitive electricity markets around the world, the dynamic behavior of hourly electricity prices is subject to significant uncertainty and volatility due to electricity demand, availability of generation sources, fuel costs, and power plant availability. Electricity markets have experienced a significant transformation around the world in the last few decades. The price of electricity set by the government each year is entirely determined by the market every day. In most countries, the price of electricity is arranged through a daily auction for each 24 h of the next day. The results of the daily market, based on free contracting between buying and selling agents, represent an efficient solution from the economic point of view but introduce huge uncertainty for the market participants: producers, sellers, and consumers.

In the European Union, the wholesale electricity market operates under the so-called 'uniform price' rule [56, 57]. In summary, the uniform pricing procedure is as follows:

The daily demand is first satisfied by the supply of technologies whose production costs are lower, allowing them to offer electricity at a lower price. In practice, these technologies are those that produce non-storable electricity, such as nuclear and renewables. If this supply is insufficient to meet the total demand, the unsatisfied part of the demand is covered by the technology among all others whose prices are lower, and so on. The final price is the price corresponding to the supply that satisfies the last fraction of the demand. This final price is largely related to the production costs of the most expensive technology entering the market supply. In this pricing system, all technologies are remunerated at the matching price, resulting in considerable magnitude benefits for those technologies that generate electricity at a lower cost.

Unlike most financial or commodity markets, the "spot market" of electricity is typically a daily market that does not allow continuous trading. This is because system operators require advance notice to verify that the schedule is feasible and conforms to transmission constraints. These deregulated prices have been characterized in all markets by having extremely high volatility.

Several elements explain the high volatility observed in electricity prices [58]. Probably the most important factor is the impossibility of storing electricity. Electricity cannot be physically stored directly, and production and consumption must be continuously balanced. Therefore, supply and demand shocks cannot be easily smoothed and directly affect equilibrium prices. The characteristics of demand and supply also play an essential role in the observed volatility. The electricity demand is highly inelastic because it is a necessary good and is highly dependent on the weather conditions. The characteristics of the supply pool in each market can also contribute to the volatility of a given demand. The relative insensitivity of demand to price fluctuations and supply constraints at peak times makes short-term electricity prices extremely volatile. Therefore, in markets where demand and supply curves are steep,

we can observe sharp price increases as the quantity demanded increases. Moreover, depending on the structure of the market and the market power of generators, for high levels of demand, only a few generators could satisfy the residual demand, and therefore market power could come into play through monopolistic or oligopolistic behavior of generators.

Most wholesale electricity markets use the 'new' uniform auction system to set the price. However, the recent experience and perceived poor performance of some decentralized electricity markets have led some regulators to 'revisit' the adoption of discriminatory or 'pay-as-you-bid' auctions. Under this rule, each market participant is remunerated according to the price of its bid. In the short term, less is paid for electricity, but clean energy is no longer incentivized. It is well known that discriminatory auctions are not usually superior to uniform auctions in the medium and long term [57, 59]. Both types of auctions are commonly used in financial market and other markets, and there is now a voluminous economic literature devoted to their study. The system of 'pay-as-you-bid' or discriminatory auctions resembles the old system of market operation prior to the liberalization of the electricity sector.

There is currently an intense debate in the European electricity sector about the best pricing system. Critics of the uniform auction system argue that some large utilities have the market power to artificially alter prices. The aim of our article is to statistically describe how electricity prices evolve in six countries using the uniform auction system. This comparative study may be useful in helping policy makers and market players evaluate the current pricing system in the European Union.

As mentioned above, the uniform pricing mechanism introduces huge uncertainty, which means an economic risk to the agents involved in the market. Logically, it is beneficial for any participant in the auctions to have a procedure for predicting prices when configuring their purchase or sale bids. Given the importance of electricity prices in the economy of a country [60], the prediction problem has been the subject of an

enormous research effort from the electricity companies with the support of specialists in statistics and finance from around the world. The statistical analysis performed, and the models constructed allow us to answer another question of special interest, which is to quantify the uncertainty associated with the price prediction in each country.

A significant number of references have been devoted to electricity price forecasting in the state-of-the-art technical literature [19, 61, 62]. In general terms, the proposed techniques can be grouped into three categories according to the forecasting framework: statistical models, time series methods, and artificial intelligence.

Concerning the time series approach, in the last years some studies have addressed the forecasting of electricity prices using a hybrid approach of statistical and regression models, based on a NARMAX model [63], or ARMAX models based on a linear regression where functional parameters operate on functional variables [64]. Other references employ dynamic trees and random forest statistical techniques [65].

Concerning the area of artificial intelligence, in recent years, some references have analyzed the techniques based on deep learning on hybrid platforms [66], ensemble learning [67], parametric and non-parametric approaches such as non-parametric and/or functional AR models [68], Hybrid ANN and Artificial Cooperative Search Algorithm [69], General Regression Neural Network and Harmony Search Algorithm [70], using the hybrid backtracking search algorithm and the ANFIS approach [71], and a comparative of different machine learning techniques such as random forest regressor models, deep neural networks, convolutional neural networks [72]. Additional details can be found in [96].

6.1.2. Contribution

The contribution of this chapter is twofold. First, the hourly price series of six most-representative European electricity markets have been described and modeled using ARIMA models and different versions of GARCH models. Secondly, a set of similarities

and differences has been drawn after the exhaustive comparison of the: (i) the estimated ARIMA/ GARCH parameters, (ii) the outliers' rate of appearance, and (iii) the evaluation of out-of-sample one-day-ahead forecasts.

6.1.3. Structure

The rest of this chapter is organized as follows. Section 6.2 describes the collection of data used in this study. Sections 6.3 and 6.4 model the daily price time series using ARIMA and GARCH techniques, respectively. Sections 6.5 and 6.6 are devoted to analyzing the data asymmetry and comparing the accuracy of the out-of-sample forecasts, respectively. Finally, Section 6.7 provides some relevant conclusions. The analysis performed is summarized using the flow chart in Figure 6-1.

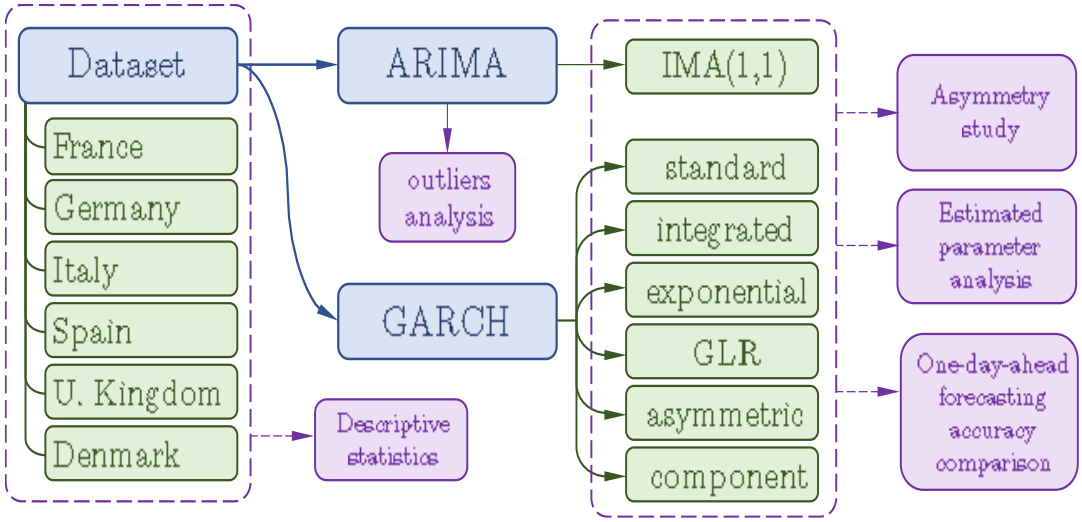

Figure 6-1: Flow diagram of the analysis performed.

6.2. Electricity prices dataset

6.2.1. Characteristics

There is a very general agreement about listing the main characteristics observed in the descriptive analysis of the price series, which is common to practically all liberalized electricity markets. The first is the existence of jumps and spikes, which is justified by

the difficulty of storing large quantities of energy to allow a smooth adjustment between supply and demand. The second is the strong seasonality due to the dependence of electricity demand on weather conditions and social and economic activities that generate daily, weekly, and annual cycles. Finally, another feature that is common to other financial markets is the existence of intense heteroskedasticity, which creates periods of high volatility [73-75].

6.2.2. Single-day-ahead coupling

Most of Europe is now part of the Single Day-Ahead Coupling (SDAC), which is a coordinated electricity price setting and cross-zonal capacity allocation mechanism that simultaneously matches orders from the day-ahead markets per bidding zone, respecting cross-zonal capacity, and allocation constraints between bidding zones. This allocates scarce cross-border transmission capacity efficiently by coupling wholesale electricity markets from different regions. It does so by simultaneously considering cross-border transmission constraints. Its goal is to create a single pan-European cross-zonal day-ahead power market. Every day of the year, at 12:00 CET, the daily market session takes place in which the prices and the volume of energy for the twenty-four hours of the following day are fixed in most European countries (Spain, Portugal, Germany, Austria, Belgium, Bulgaria, Croatia, Slovakia, Slovenia, Estonia, France, Holland, Hungary, Ire-land, Italy, Latvia, Lithuania, Luxembourg, Finland, Sweden, Denmark, Norway, Poland, the United Kingdom, the Czech Republic, and Romania). The daily market (SDAC) aims to carry out electricity transactions by submitting bids for market players' sales and purchase of electricity. For instance, buying and selling agents located in Spain or Portugal will submit their bids to the daily market through OMIE, which is the sole designated NEMO in those countries (NEMO stands for a Nominated Electricity Market Operator, and they are the organizations mandated to run the day-ahead and intraday integrated electricity markets in the EU). Their buy

and sell bids are accepted based on their economic merit order and the available interconnection capacity between the price zones. Suppose at a particular hour of the day, the interconnection capacity between two zones is sufficient to allow the flow of electricity resulting from the negotiation; in this case the price of electricity at that hour will be the same in both zones if inverse, and at that hour the interconnection is fully occupied, at that time the pricing algorithm results in a different price in each zone. This described mechanism for electricity price formation is called market coupling.

The existence of the SDAC mechanism conditions the price dynamics of each national market, although the distances between countries and interconnection capacity restrictions, among other factors, cause the evolution of prices in many areas to vary independently.

Parameters and variables:	
$p_{h,t}$	price of electricity for hour h of day t
$y_{h,t}$	response variable, computed as the logarithm of $p_{h,t}$
$u_{h,t}$	non-biased Gaussian-distributed random error
σ_h^2	variance of $u_{h,t}$
θ_h	parameter of the Moving Average model
u_t	innovation process

6.2.3. Dataset

Hourly prices have been collected for six countries (Denmark, Germany, France, Italy, Spain, and the UK), starting 1 January 2013 and lasting until 31 December 2019. To see how the European daily market (SDAC) affects the prices of the different markets analyzed, provide the percentage of hours (corresponding to weekdays) in which there has been price coincidence in two countries in the sample. For example, during the

study period, prices in France and Spain coincided in 17.9% of the hours. Moreover, the highest percentage is for Denmark and Germany with 29.8%.

Another important feature of the dynamics of the hourly electricity price series is the strong seasonality. In many applications, the seasonal behavior can be perfectly described with stationary time series models. However, in this case, the strong seasonality is associated with a loss of stationarity, leading to periodic changes in the mean and correlation structure of the process. These types of process are known as periodically correlated processes [2, 75]. In their analysis of daily average prices, Koopman et al. [75] mention the lack of stationarity of the series and recommend using different ARIMA models for each day of the week. Tiao and Grupe [76] explored the properties of periodic models to characterize seasonal time series. In [76], the authors showed that the use of stationary ARMA models when processes are periodic leads to a loss of predictive accuracy. As a result of this, several authors prefer to predict hourly electricity prices with different models for weekdays and weekends [77, 78]. All these considerations led us to limit our analysis to working days (Monday to Friday), eliminating Saturdays and Sundays from the series.

This is a very critical aspect because it creates a discontinuity in the series. However, this decision greatly simplifies the analysis of the series and focuses on the most relevant days in the price series. The left plot in Figure 6-2 shows the median prices for each of the 24-hourly series for each country; whereas the right plot shows the robust estimate of the standard deviation (median of the absolute deviations from the median, adjusted by a factor for asymptotically normal consistency) of the same series. Prices show a clear bimodal curve with two different hours in the day, which are markedly higher than neighboring values: these are hours between 8 and 10 a.m. and 6 and 10 p.m. In a comparative perspective across different European markets, the data clearly show that Italy has values structurally higher if compared to the other markets. Based on Figure 6-2, Spain has the second highest median prices, followed by France and

Germany. The median price curves for Denmark and the UK are similar for the first half of the day and higher in the UK for the second half. Denmark and the UK have lower average prices in most hours than the other countries. The price differences among countries are very considerable, e.g., Italy has average values 50 to 80% higher than Denmark.

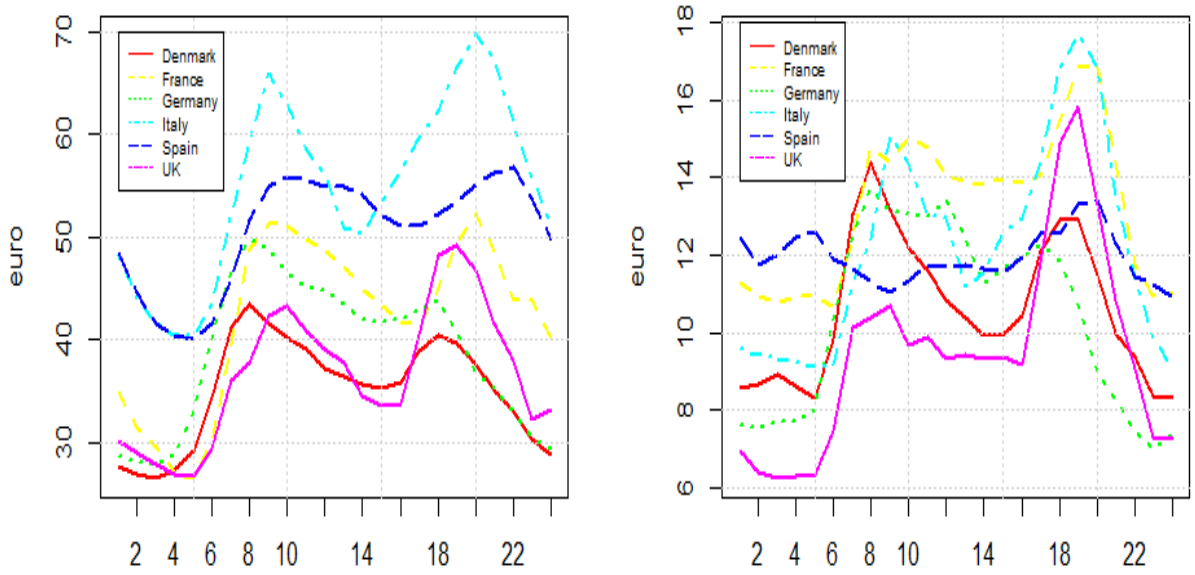

Figure 6-2: The median prices for each of the 24-hourly series for each country (left plot) and the robust estimate of the standard deviation (right plot).

Concerning the variability changes according to the hours in the different countries (right plot of Figure 6-2): The differences are very pronounced in general for all countries except Spain. The fact that the variability is not constant is very relevant when choosing the model. This case indicates that the hourly price series does not have constant variance and is not stationary. Following the recommendation of Tiao and Grupe [76], the use of an ARIMA model for the hourly series is not appropriate.

Figure 6-3 shows the daily average price series (black-colored line) with the mean values and the standard deviation. The difference in level between the Italian series and the Danish or British series is observed. The existence of jumps and spikes, the lack of trend, and the reversion effect to the mean can be seen in all the graphs. The red-colored line depicts the smoothed series using Lowes. The value in parentheses

below the standard deviation is the measure of the dispersion of the data against the smoothed curve (red). With respect to this indicator, the difference in behavior between the UK series and the others is very striking.

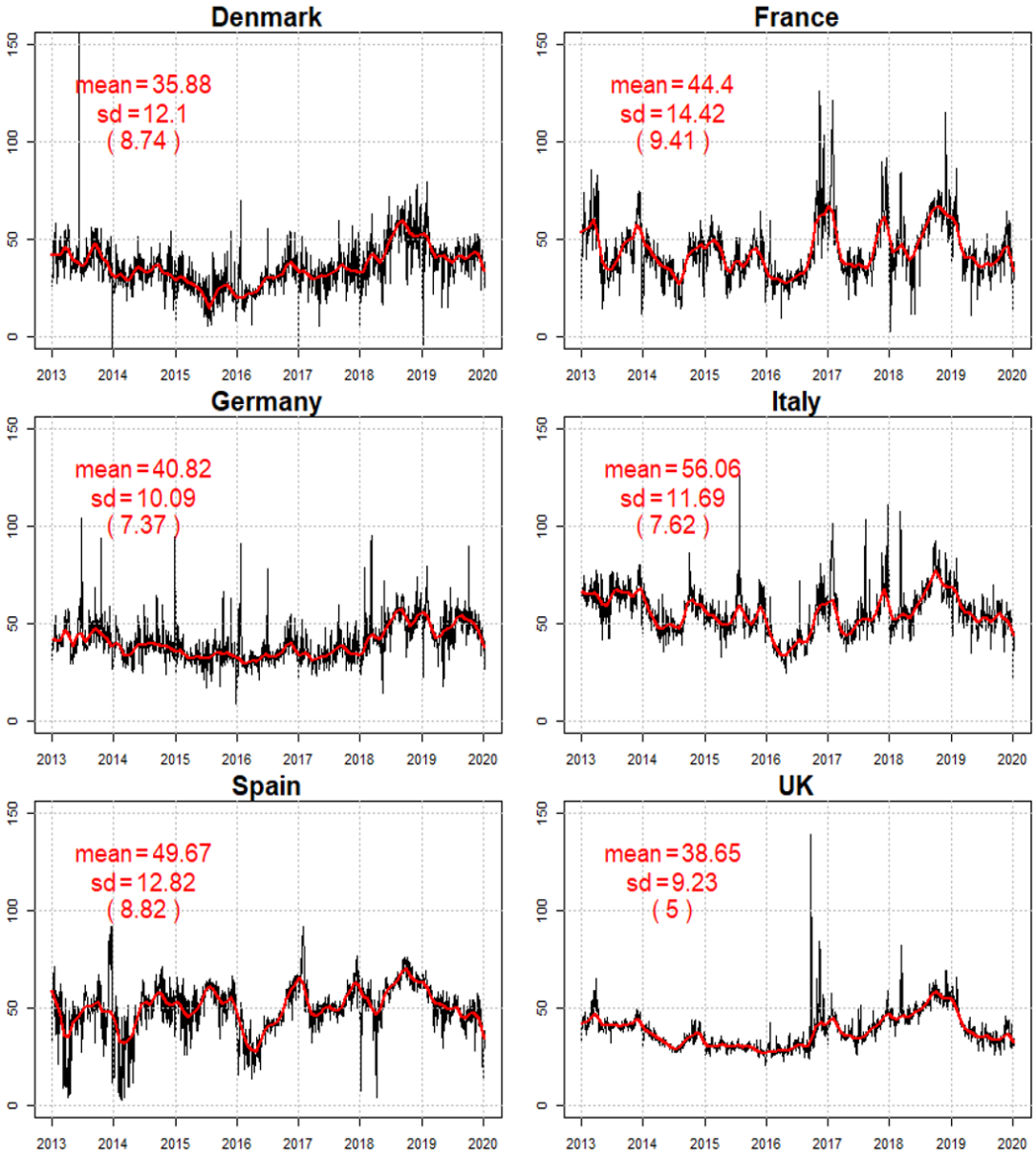

Figure 6-3: The daily average price (€) series with the mean values and the standard deviation.

The evolution of average prices over seven years shows there is no trend in any of the series. The graphs for some countries show strong similarities, e.g., Denmark and Germany. Furthermore, Italy and France, especially from 2016 onwards. The degree of similarity can be measured by the correlation matrix or by the correlation matrix of

the differenced series (Table 6-1). The correlation between Denmark and Germany is high for both average and incremental data. It is also high for the pairs (Denmark, UK), (France, Italy) and (France, UK).

Table 6-1: The correlation matrix of the differenced series

	Den	Fra	Ger	Ita	Spa
Den	1	0.360651	0.781651	0.034087	−0.05867
Fra	0.360651	1	0.175669	0.712271	0.361348
Ger	0.781651	0.17567	1	0.078789	−0.08945
Ita	0.034087	0.712271	0.078789	1	0.525755
Spa	−0.05867	0.361348	−0.08945	0.525755	1
UK	0.388412	0.61889	0.276344	0.457873	0.100781

6.3. ARIMA models and outliers

The best way to model the evolution of electricity prices is through 24 univariate models, one for each hour of the day. Working with 24 models introduces some complexity to the problem, but a great advantage arises; each of the 24 models is very simple. Following the usual procedure in analyzing other commodity prices, we will use the logarithm of the price as the variable to be modeled. Standard analysis of each series using the Box-Jenkins methodology suggests the ARIMA (0,1,1) model as an acceptable model to capture the price dynamics. Thus, calling $y_{h,t} = \log(p_{h,t})$ with $p_{h,t}$ being the price of electricity for hour h of day t, the model can be written as:

$$y_{h,t} = y_{h,t-1} + \theta_h u_{h,t-1} + u_{h,t}, \quad h = 1,2,\ldots,24 \tag{6-1}$$

where $u_{h,t}$ (with h fixed) is a white noise process with variance σ_h^2 and θ_h is the model parameter to be estimated from the data.

6.3.1. Detection of outliers

As previously mentioned, electricity prices often undergo sudden changes that affect the dynamics of the data on a transient basis. It is difficult in many cases to know the causes of these changes. Detecting and correcting for the effect of outliers is important

because they impact model selection, parameter estimation and, consequently, forecasts. There are several well-known computer programs specialized in the automatic detection of outliers in time series, such as X-12-ARIMA (developed by the U.S. Census Bureau) and TRAMO (developed by the Bank of Spain) [79]. A procedure used to detect outliers in time series is available in the R package tsoutliers [80]. The following types of outliers are considered: AO, additive outliers; LS, level shifts; TC, temporary changes and SLS, seasonal level shifts. The tsoutliers package [80] implements the procedure developed by [81]. The outlier detection procedure has been applied to each of the 24-time series for each country.

The bar chart in Figure 6-4 shows the total number of outliers in each country (total in gray, downward in blue, upward in red). During the analyzed period, 7 years, the market with the least outliers is the German market (1.02%), and the market with the highest proportion of outliers is the Spanish market (4%). It is important to highlight the high proportion of days affected with outliers, 4 of the six countries analyzed have over 10% of the days with at least one outlier observation. Most outlier observations in Denmark, Germany, France, and Spain correspond to sharp price declines. In Italy and Great Britain, the proportion of outliers in both directions is similar. The number of outliers detected logically depends on the criteria used to declare an observation as an outlier. The number of outliers changes with different criteria, but the structure observed by country and time is very similar.

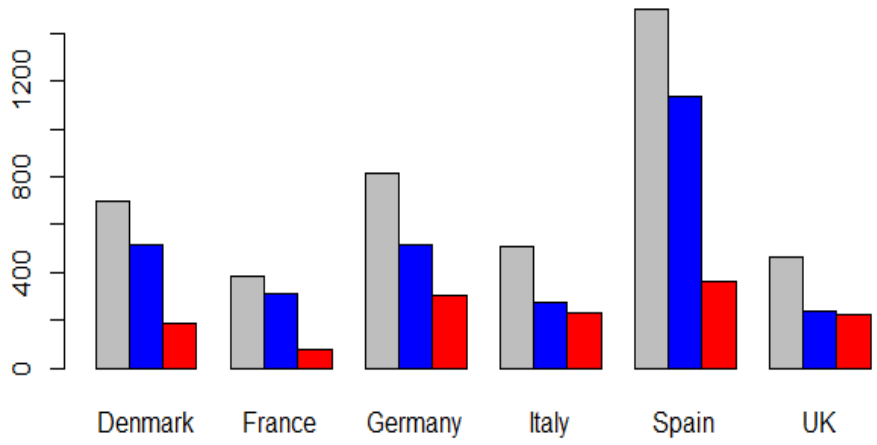

Figure 6-4: Total number of outliers in each country (total in gray, downward in blue, upward in red).

The complexity of predicting electricity prices can be deduced from the outlier analysis performed. The existence of outlier observations seriously affects the estimation of the model. Moreover, by their very definition, outliers are very difficult to predict. However, it is the critical issue of price-prediction models in many cases (especially in the Spanish case). Many papers [82-85] use explanatory variables, such as weather conditions, daily demand structure, and other factors to model and predict jumps in the price series. Although there have been attempts to predict the jumps, the results achieved so far are rather limited.

6.3.2. ARIMA model estimation

Once the outliers have been eliminated, the autocorrelation function and the partial autocorrelation function corresponding to the differentiated pricing log series of each hour in the markets studied show that univariate IMA(1,1) is a suitable model for all the hours. For a given hour, the optimal model (chosen following the usual model selection criteria) has a more complex structure but is only slightly better than the IMA (1,1) model.

As a summary of the analysis performed using the ARIMA time series models, the graphs in Figure 6-5 are presented. A figure with four graphs (3 colors) is shown for each of the six countries studied. The top line shows the standard deviation of prices

(in logarithms). This is the initial variability of each of the 24-time series. The series has been corrected by eliminating extreme values by analyzing and identifying outliers. The variability is logically reduced. The reduction in the standard deviation of the series due to the elimination of outliers is the blue band. The standard deviation for each hour of the corrected series is shown in the second line.

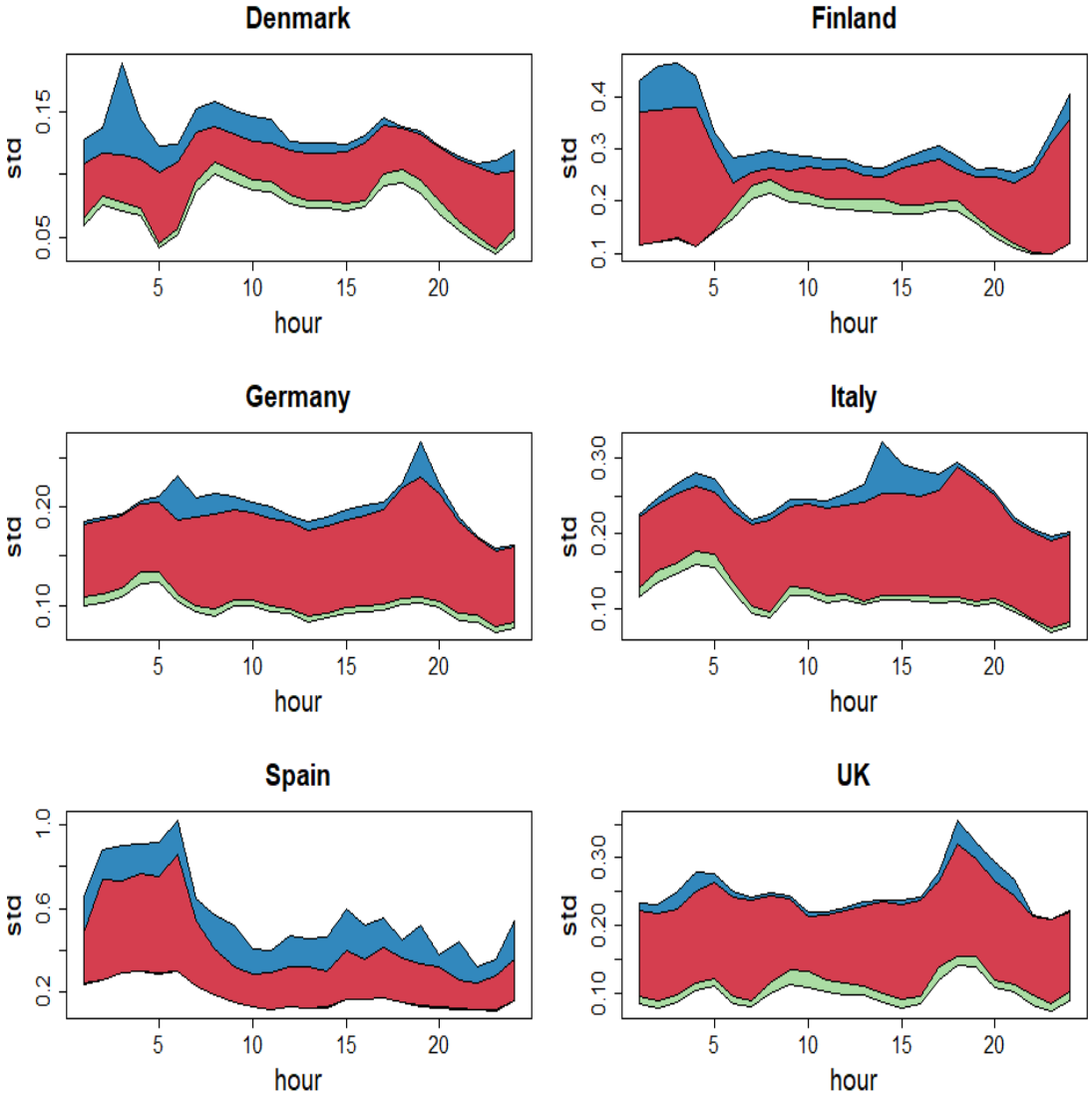

Figure 6-5: Summary of the analysis performed using the ARIMA time series models.

The corrected series is not stationary. Statistical analysis indicates that the main dynamics of prices largely correspond to the standard evolution of prices in other financial markets: the random walk. According to this model, the best prediction of the price of electricity for hour h of day $t + 1$ is to take the price observed for that hour

on day *t*. If this prediction rule is used, the standard deviations of the prediction errors are shown in the third line (starting from the top). The reduction in standard deviation obtained after differentiation corresponds to the red band in Figure 6-5. The variability with respect to the second graph is very significantly reduced in all countries.

Finally, the lower graph shows the standard deviation of the ARIMA (0,1,1) model errors for each hour (exponential smoothing). The addition of the moving average parameter slightly improves the price predictions except for the Spanish case, where there is hardly any change concerning the random walk. The improvement in the models by including the moving average parameter is the light green band and is barely noticeable in Figure 6-5.

The graph can be interpreted as an analysis of the variance of the series. The most important component explaining the variability is the random walk (red band), outliers' existence (blue band), and finally, the moving average parameter (green band).

Figure 5-6a shows the estimated standard deviations of the 24 models for each country. The standard deviations are quite stable at around 0.1 for Denmark, France, UK, and Italy. Germany has a higher variability of residuals than the previous four countries. The standard deviation of the first 6 h for Spain is much higher than the rest.

Figure 6-6b represents the estimations of the theta parameter of the IMA (1,1) model for each hour in the six markets. Denmark, UK, Italy, and France present highly significant theta estimates for all hours with values between 0.4 and 0.7. Germany shows theta values around 0.6 between 6 and 20 o'clock; outside this interval, the values are lower and unstable. The values of the theta parameter for Spain are very unstable, between -0.2 and 0.2, in many cases not significantly different from zero. The results observed in this graph are consistent with the sigma values represented in Figure 6-6a.

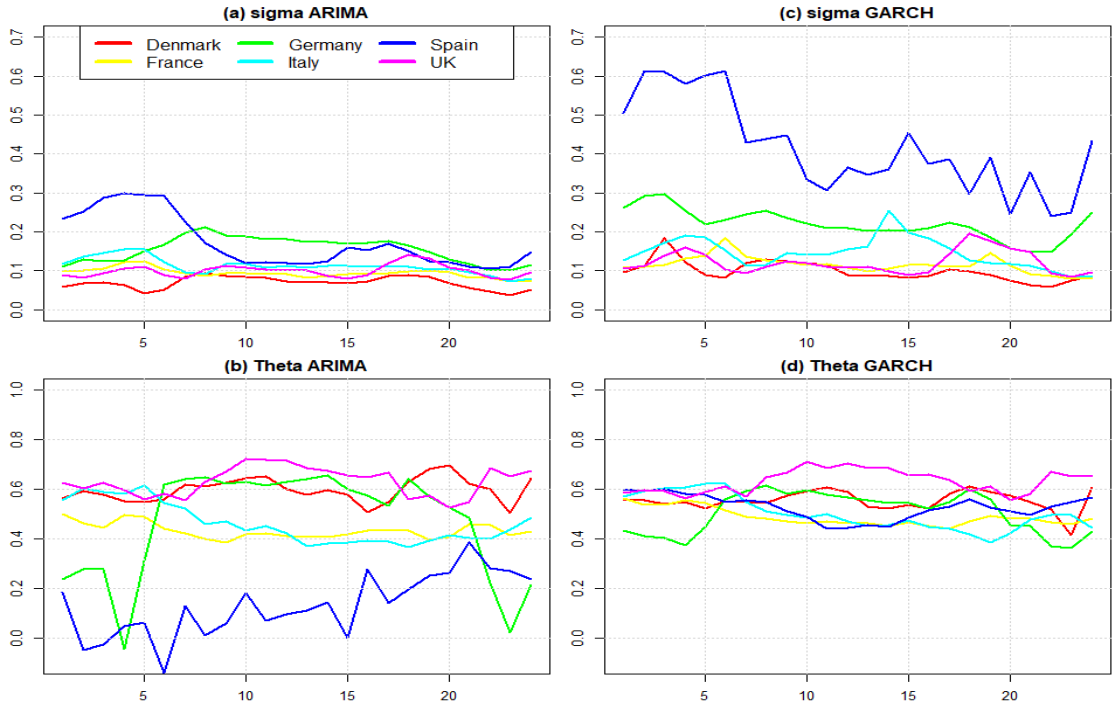

Figure 6-6: σ and θ estimates for ARIMA and GARCH models.

6.4. GARCH models

6.4.1. Introduction GARCH models

ARIMA models assume that the variance is constant over time. The evolution of $y_t = \Delta\log(p_{h,t})$ for the analyzed countries shows for all series there are periods with significant increases in variability. The variability or volatility of electricity prices is comparable to that of other financial markets (stock, bonds) or other commodities [56]. The deregulation has introduced new elements of uncertainty in the sector and therefore usual financial aspects such as financial risk management, derivative contracts, or hedging have been introduced in the industry. The variability bursts can be predicted with autoregressive models with conditional heteroscedasticity or ARCH models, initially introduced by [86] and extended by [87] to generalized ARCH or GARCH models.

There is no consensus in the literature on the most appropriate volatility model. According to [88], the optimal model depends on the forecasting horizon, and the

country analyzed. As explained above, most studies differ from our approach in two aspects: they use daily average price data, and when they use hourly data, they do so with a single model for the 24 h of the day. Our interest in this work is in day-ahead price predictions. This part has studied the performance of six classes of ARMAX-GARCH volatility models (GARCH, eGARCH, gjrGARCH, apARCH, iGARCH, and cGARCH), and we have analyzed their behavior from the point of view of estimation and prediction.

The GARCH models combine two equations to explain the evolution of the variable of interest y_t, representing the logarithm of electricity price for an hour h of the day t. Equation (6-2) represents the ARIMA model of the variable y_t. In this case, we will use the ARIMA (0,1,1) or IMA (1,1) model, also known as exponential smoothing.

$$y_t = y_{t-1} + \theta u_{t-1} + u_t, \quad t = 1,2,\ldots \tag{6-2}$$

where u_t is an unbiased Gaussian-distributed random error and parameter θ is the IMA parameter to be estimated.

The innovations u_t in equation (6-2) is a sequence of random variables whose variance σ_t^2 is not constant. The second equation of the model, the GARCH equations, aims to explicitly model the time varying variance process. To simplify the explanation, we begin with the following GARCH (1,1) model:

$$\sigma_t^2 = \omega + \alpha u_{t-1}^2 + \beta \sigma_{t-1}^2 \tag{6-3}$$

where ω, α and β are the model parameters to be estimated from the data.

Here, the term sGARCH refers to the previous model in Equation (6-3), standard GARCH. The three parameters of the model ω, α and β have to verify the following conditions: $\alpha \geq 0$, $\beta \geq 0$, $\alpha + \beta < 1$ and $\omega > 0$. The parameter α (the ARCH parameter) represents how volatility reacts to new information u_{t-1}, and β (the GARCH effect) capture the degree of volatility persistence. The specification in Equation (6-2) is GARCH(1,1), but this can easily be extended to GARCH(p, q). The

persistence is defined by $\hat{P} = \alpha + \beta$ and $\hat{\sigma}^2 = \omega/(1 - \hat{P})$ is unconditional variance. A particular case of this model is the integrated GARCH or iGARCH when $\alpha + \beta = 1$.

When positive or negative shocks (u_{t-1}) have different impacts on volatility, the exponential GARCH (eGARCH) of [89] may be preferred:

$$\log(\sigma_t^2) = \omega + \alpha + \gamma\left(\left|\frac{u_{t-1}}{\sigma_{t-1}}\right| - E\left|\frac{u_{t-1}}{\sigma_{t-1}}\right|\right) + \beta\log(\sigma_{t-1}^2) \qquad (6\text{-}4)$$

where ω, α, γ and β are the model eGARCH parameters to be estimated from the data. In addition to asymmetry, the eGARCH model in equation (6-4) can also accommodate leverage, which is the negative correlation between returns shocks and subsequent shocks to volatility.

The gjrGARCH [90] models positive and negative shocks on the conditional variance asymmetrically using dummy variable I_t that takes value 1 for $u_t < 0$ and 0 otherwise:

$$\sigma_t^2 = \omega + \alpha u_{t-1}^2 + \gamma I_{t-1} u_{t-1}^2 + \beta\sigma_{t-1}^2 \qquad (6\text{-}5)$$

where ω, α, γ and β are the model gjrGARCH parameters to be estimated from the data.

The variance exponent in equation (6-5) is 2, some authors prefer to replace it by δ a new parameter that is estimated from the data, giving rise to the asymmetric power ARCH model (hereinafter referred as apARCH) of [91]:

$$\sigma_t^\delta = \omega + \alpha(|u_{t-1}| - \gamma u_{t-1})^\delta + \beta\sigma_{t-1}^\delta \qquad (6\text{-}6)$$

where $\delta > 0$, and ω, α, γ, δ, and β are the model parameters to be estimated.

The Component GARCH model of [92] decomposes the conditional variance into a permanent and transitory component. Letting q_t represent the permanent component of the conditional variance, the model can be written as:

$$\sigma_t^2 = q_t + \alpha(u_{t-1}^2 - q_{t-1}) + \beta(\sigma_{t-1}^2 - q_{t-1}) \qquad (6\text{-}7)$$

$$q_t = \omega + \rho\, q_{t-1} + \phi(u_{t-1}^2 - \sigma_{t-1}^2) \qquad (6\text{-}8)$$

where ω, α, β, ρ, and ϕ are the model cGARCH parameters to be estimated from the data.

The parameters of all GARCH-type models are estimated using maximum likelihood since it is generally consistent and efficient and provides asymptotic standard errors that are valid under non-normality. The conditional log-likelihood is given by:

$$\log\left(L(\theta_1,\theta_2,\ldots,\theta_k)\right) = \sum_{t=1}^{T}\left(\log\left(f\left(\frac{u_t}{\sigma_t}\right)\right) - \log(\sigma_t)\right) \qquad (6\text{-}9)$$

where $f(\cdot)$ is the conditional probability density function and $\theta_i,\ i = 1,\ldots,k$ are the model parameters. For each model, the innovation process u_t is allowed to follow one of the following three distributions: the normal distribution, the student's t distribution, and the generalized error distribution. In our analysis, we used student's t-distribution as the most appropriate; the results do not change significantly when using one of the other two.

6.4.2. sGARCH models

In the GARCH-type models, the variance of the residuals is not constant; however, we believe it is useful for calculating the mean squared error (MSE) of the residuals as a measure of goodness of fit and compare the result with that obtained in the homoscedastic IMA (1,1) model. In the latter case, the MSE is an estimator of the constant variance of the model. Figure 6-6c show the curves for each country. For all countries and hours, the MSE of the GARCH model is higher than that of the ARIMA model. This is logical and expected because in the first model (ARIMA) the estimation was performed after a previous cleaning of outliers while in the second model (GARCH) the original data were used.

The estimates of parameter θ for the two models are plotted in Figure 6-6d. As can be seen, the θ estimates for the GARCH model are more stable, taking a value close to 0.6 for all hours in all regions. From a conceptual point of view, the second model (GARCH) is more appropriate because the ARIMA model has been inadequately

estimated to a series that is not homoscedastic. We will see later which of the two options is better from a predictive point of view.

Figure 6-7 shows the values of the estimates of the two parameters of the sGARCH equation. The α parameter represents the effect on volatility of new information (innovation). It measures changes in variance in the short run. In general, the estimated values are high compared to those corresponding to other financial markets, according to [93], one of the basic references in risk analysis, values of α above 0.1 correspond to very nervous or jumpy markets. The opposite happens with the β parameter, in financial markets it is usually in the range of 0.85 and 0.98 [93], in the case of electricity prices it is clearly lower.

Considering the restrictions of the parameters in (3), high values of α are associated to low values of β, and in this case volatility is very "volatile" and the observed series presents many spikes. The sum $\alpha + \beta$ measures the rate at which the shock of volatility dies over time. Persistence of volatility occurs when $\alpha + \beta = 1$ (iGARCH), thus σ_t^2 is non-stationary process and the unconditional variance become infinite.

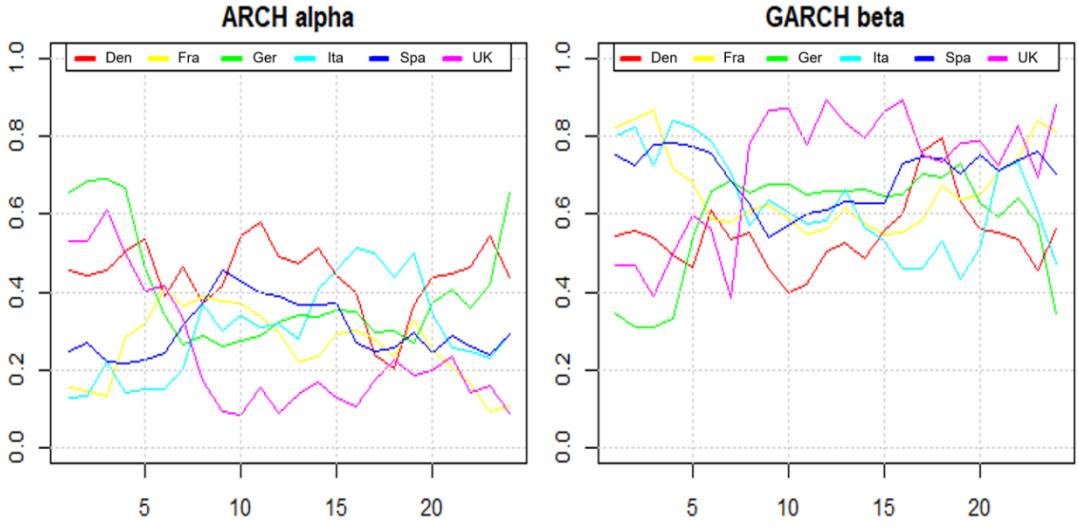

Figure 6-7: The values of the estimates of the two parameters of the sGARCH equation.

The left plot in Figure 6-8 plots $\hat{\omega}$, the ordinate at the origin of the eGARCH equation. For all markets, these are low values and therefore their contribution to the total volatility is insignificant. The right plot in Figure 6-8 depicts $\hat{\alpha} + \hat{\beta}$, the estimated

persistence. The values for Spain add up to 1 for 24 h, and those for Denmark at all hours except 8, 9 and 10 am. Germany is similar to Denmark. Countries France, UK, and Italy have values less than 1 for most hours. When the sum $\hat{\alpha} + \hat{\beta}$ is 1 the GARCH model becomes iGARCH. This explains the higher variance of the Spanish and German prices.

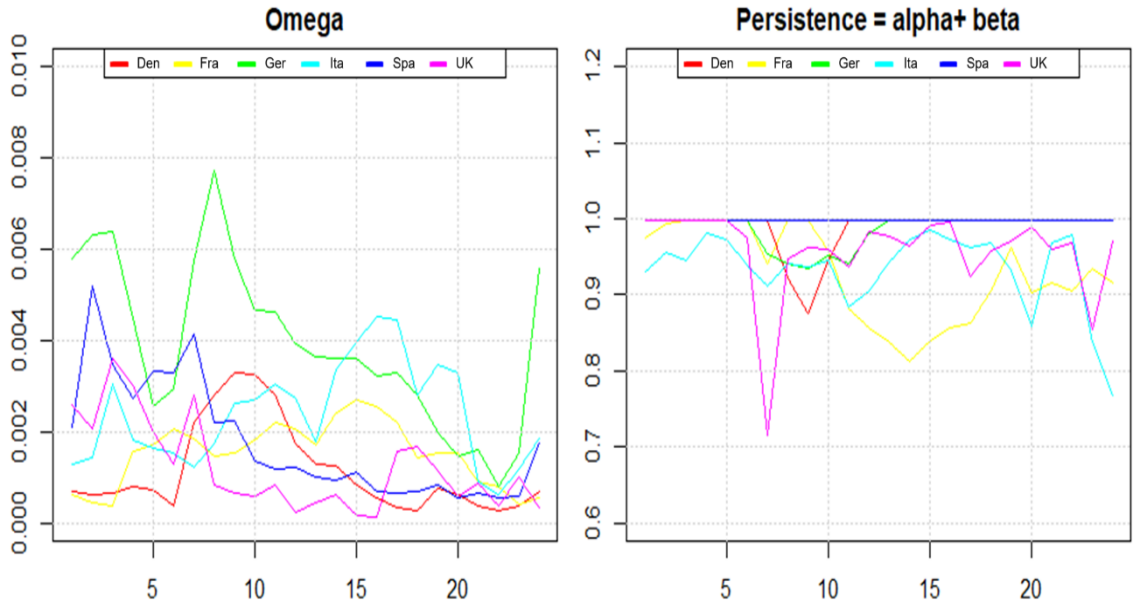

Figure 6-8: The ordinate at the origin of the eGARCH equation (left plot), and the estimate persistence (right plot).

6.4.3. Comparison of GARCH models

A significant result in comparing the GARCH models is that the estimated residuals in all of them are very similar. Table 6-2 shows the MSEs of the six models for all countries. Each MSE has been obtained as the average of the MSEs corresponding to the 24-hourly models. As can be seen in the table for each country, the six models have very similar MSE values. As indicated with the ARIMA models, the country with the highest MSE is Spain, followed by Germany.

Table 6-2: The MSEs of the six models for all countries.

	Den	Fra	Ger	Ita	Spa	UK
sGARCH	0.098841	0.11529	0.219578	0.145505	0.41604	0.121573
iGARCH	0.098849	0.115289	0.219584	0.145509	0.41604	0.121577

eGARCH	0.099824	0.115337	0.220317	0.145483	0.417037	0.121597
gjrGARCH	0.099503	0.115376	0.220105	0.145519	0.416976	0.121591
apARCH	0.100431	0.11536	0.220421	0.145456	0.417835	0.121576
csGARCH	0.098862	0.115299	0.219374	0.145589	0.41561	0.121573

Figure 6-9 shows the changes in the parameter estimate according to the different models for each country. The largest differences appear in Spain and the first hours in Denmark and to a lesser extent in France. In all three cases, the differences appear between the three models eGARCH, gjrGARCH, and apARCH that consider the asymmetric effect of innovations on volatility and the other three models (sGARCH, iGARCH, and cGARCH) that do not include this effect. We will see the differences below when dealing with the asymmetry effect in volatility modeling.

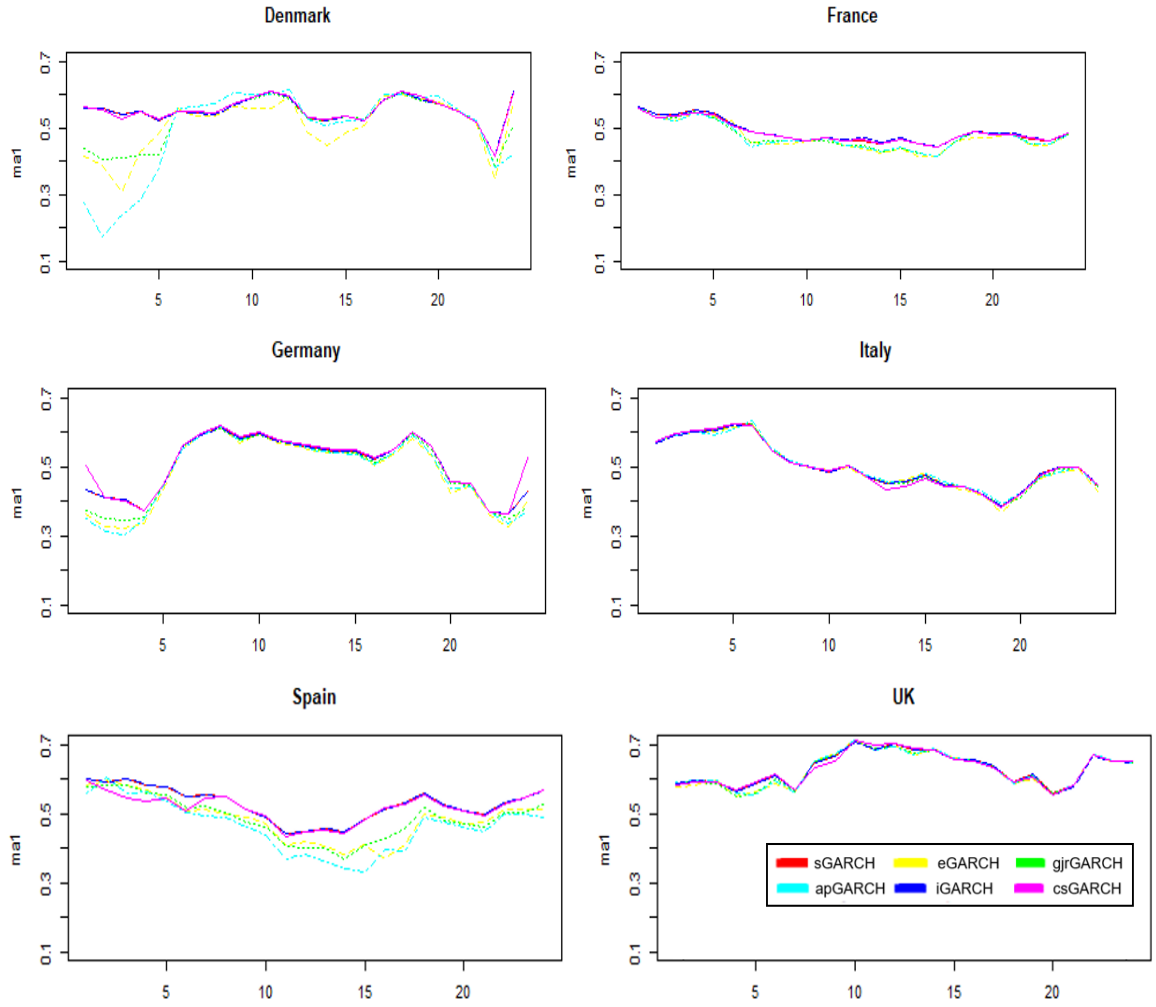

Figure 6-9: The changes in the parameter estimate according to the different models for each country.

6.5. Asymmetry

The eGARCH, gjrGARCH and apARCH models are important in capturing asymmetry, which is the different effects on conditional volatility of positive and negative shocks of equal magnitude. The parameter associated with asymmetry in the gjrGARCH and apARCH models is γ and the symmetry contrast with these models is $\gamma = 0$.

In the gjrGARCH model in equation (6-5), positive shocks, $u_{t-1} > 0$ has an impact on volatility of α while negative shocks have an impact of $\alpha + \gamma$. In this case, γ is positive, so negative shocks $u_t - 1 < 0$ increases volatility. In Denmark and Germany

this happens at night, while in Spain it occurs at practically all hours and with greater intensity in the central hours of the day.

In the eGARCH model in equation (6-4), positive shocks $u_{t-1} > 0$ have an impact on (log) volatility equal to $\alpha + \gamma$, while negative shocks $u_{t-1} < 0$ have an impact equal to $-\alpha + \gamma$. Symmetry occurs (equal impact) if $\alpha = 0$. Therefore, the symmetry contrast in the eGARCH model is $\alpha = 0$. According to [17], the condition given in the literature for asymmetry in eGARCH focuses on the incorrect parameter, γ, rather than α the correct parameter. Significant α values are negative, implying that negative shocks increase volatility. This result is consistent with the effect detected with the gjrGARCH model.

The apARCH model, as the gjrGARCH model, captures asymmetry in return volatility when $\gamma \neq 0$. Considering that $-1 < \gamma < 1$, when $\gamma > 0$ volatility tends to increase more when shocks are negative, as compared to positive shocks of the same magnitude. The opposite happens with negative γ. The interpretation of the values in this case is more complex due to the presence of the $\boldsymbol{\Delta}$ exponent.

Figure 6-10 shows the plots of the γ estimates for the gjrGARCH and apARCH models, and the α parameter (with sign changed) for the eGARCH model. It is interesting to see in Figure 6-10 that the asymmetric effects have the same sign in all three models. The asymmetry effect identified by the apARCH model is more pronounced, however, the comparison of the specific values is difficult because each model treats volatility with a different transformation.

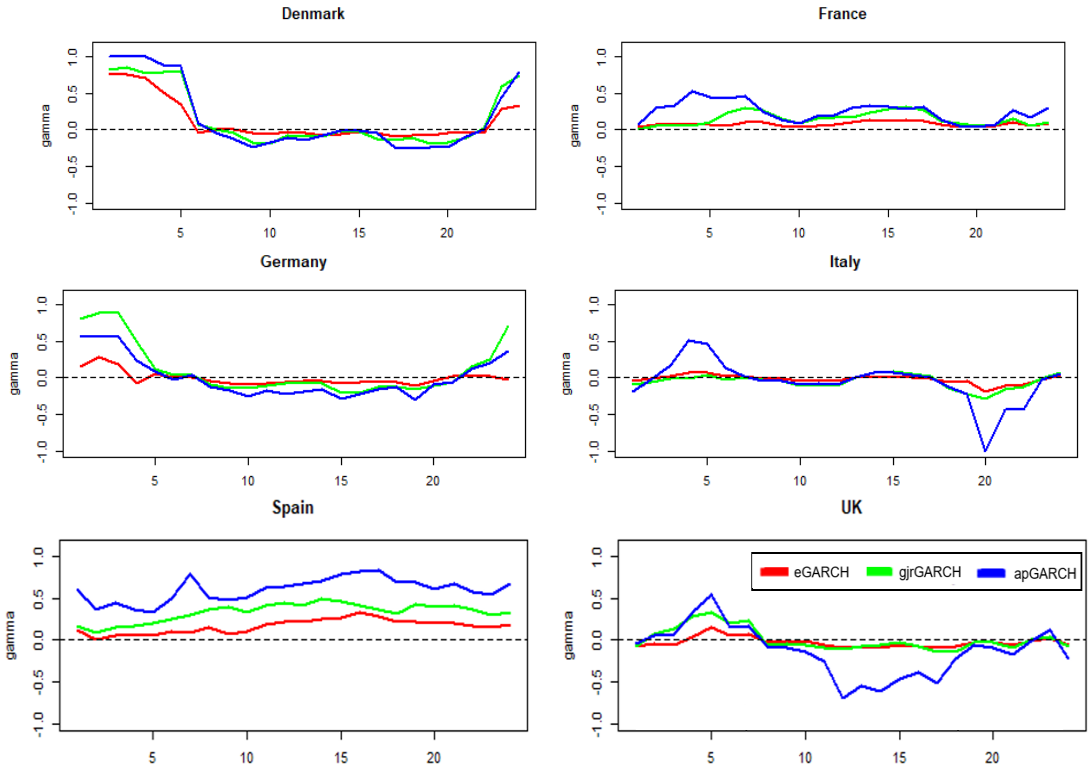

Figure 6-10: The γ estimates for the gjrGARCH and apARCH models and the α parameter (with sign changed) for the eGARCH model.

To conclude our review of the GARCH models studied, we will add some comments on the results of the component GARCH model (cGARCH) by [92]. The cGARCH model decomposes the total conditional variance into permanent and transitory variance components. This component GARCH model is widely used in finance. The approach is relatively different from the others. The inclusion of the permanent component of volatility adds flexibility to the model. Our interest is to test whether this flexibility improved the model's predictive ability versus the standard GARCH model (a particular case). The results of the two models are similar, so we can say that the cGARCH model does not add any advantage to the standard model.

6.6. Out-of-sample forecasts

In this section we are going to analyze the out of sample price forecasts. The out-of-sample forecasts involve predictions of observations that have not been used when estimating the model.

In this section, data from 2013 to 2018 has been selected to estimate the models and 2019 hourly prices have been reserved to assess the accuracy of the predictions. In this exercise, an attempt has been made to recreate the real situation faced by market participants every day, the need to predict the 24 next day's prices. Eight models have been used: the homoscedastic IMA (1,1) model, the best ARIMA model selected using the Auto-ARIMA function of the *forecast* package in R, and the six GARCH models described in the previous sections. The comparison is performed in two different situations: (A) with the real data including atypical observations and (B) with the outlier-free data identified with the *tso* function employed in Section 3 of this article.

There is no standard measure of forecasting accuracy. Some commonly used measures based on relative errors are misleading when applied to electricity prices. In particular, when electricity prices drop to zero, relative errors become very large regardless of the true absolute error. Alternative normalizations have been proposed in the literature. For instance, let $y_{i,t}$ and $\hat{y}_{i,t}$ be the observed and predicted hourly price for the hour h of the day t; and $\bar{y}$ the mean price for the week, the Mean Week Error MWE is defined as:

$$MWE_s = \frac{1}{120}\frac{\sum_{t=s+1}^{5+s}\sum_{i=1}^{24}\left|y_{i,t}-\hat{y}_{i,t}\right|}{\bar{y}}, \quad s = 1,\ldots,30$$

The mean weekly error (MWE) is a simple and "easy to interpret measure" to compare the accuracy of different models.

Table 6-3 provides the mean weekly mean errors for 2019 applied to the original observations (without removing outliers).

Table 6-3: MWE for original observations of 2019, without removing outliers.

	Den	**Fra**	**Ger**	**Ita**	**Spa**	**UK**
IMA (1,1)	0.171182	0.134041	0.133242	0.095868	0.101474	0.098577
ARIMA	0.178434	0.131107	0.132771	0.09362	0.097712	0.097419
sGARCH	0.060877	0.070303	0.130408	0.093386	0.09662	0.091322
eGARCH	0.060949	0.070297	0.130378	0.09337	0.096513	0.091365

	Den	Fra	Ger	Ita	Spa	UK
gjrGARCH	0.061093	0.070315	0.130327	0.093391	0.096529	0.091358
apARCH	0.061252	0.070314	0.130307	0.093374	0.09662	0.091348
iGARCH	0.060875	0.07032	0.130419	0.093383	0.096619	0.091318
csGARCH	0.060789	0.070293	0.130433	0.093375	0.096431	0.091324

The following conclusions can be drawn from this table:

- Robustly estimated ARIMA models have much higher prediction errors than GARCH models.
- The error level of all GARCH models (for the same country) is very similar. The same happens when comparing the IMA (1,1) model and the best ARIMA model. (Figure 6-11).
- The markets with the highest errors are Denmark, Germany and France when using the ARIMA models. Denmark and France improve a lot with GARCH models. Denmark and Germany are the two markets with the highest percentage of outliers in 2019 (Table 6-3).
- In view of the table, the standard GARCH model (sGARCH) is the simplest and most recommended alternative.

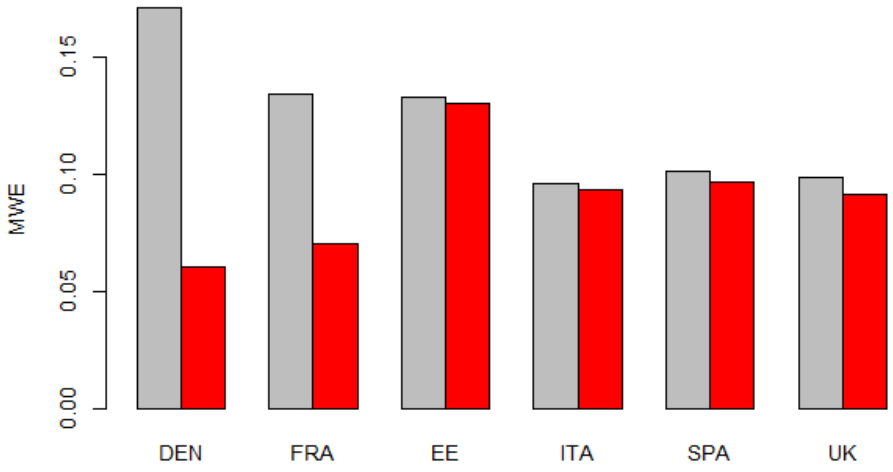

Figure 6-11: MWE of IMA(1,1) and sGARCH for each country (grey and red, respectively).

Table 6-4 makes the same comparison if the models were to predict prices without anomalous data (a situation that is unrealistic but provides information on the sensitivity of the models). In this case the ARIMA and GARCH models provide very

similar results. The simplest and most recommended model would be the IMA (1,1) model.

Table 6-4: MWE for a situation that is unrealistic but provides information on the sensitivity of the models (2019).

	Den	**Fra**	**Ger**	**Ita**	**Spa**	**UK**
IMA (1,1)	0.046258	0.063966	0.102891	0.083734	0.089806	0.086515
ARIMA	0.046461	0.062678	0.103183	0.082782	0.089062	0.085659
sGARCH	0.046364	0.063173	0.102148	0.083211	0.087178	0.085626
eGARCH	0.046482	0.063166	0.102140	0.083234	0.087261	0.085673
gjrGARCH	0.046500	0.063162	0.102144	0.083225	0.087222	0.085659
apARCH	0.046591	0.063163	0.102122	0.083238	0.087327	0.085675
iGARCH	0.046359	0.063179	0.102139	0.083213	0.087178	0.085622
csGARCH	0.046392	0.063161	0.102164	0.083213	0.087117	0.085651

A comparison between countries provides very different results. Denmark and France are the countries with the lowest prediction errors. Germany remains the most difficult to predict.

The analysis provides very interesting and useful results: when choosing a time series model to predict the hourly prices of the daily electricity market, GARCH models are very useful and recommended over the classic ARIMA models.

Figure 6-11 illustrates the behavior of the method using 24 IMA (1,1) x GARCH (1,1) models to predict two-week (Monday through Friday) of March 2019 prices in the six markets. Observed prices are shown in black and predictions in red. In the header of each graph the MWE for the period is provided. It can be seen that the procedure is able to adapt to daily seasonality.

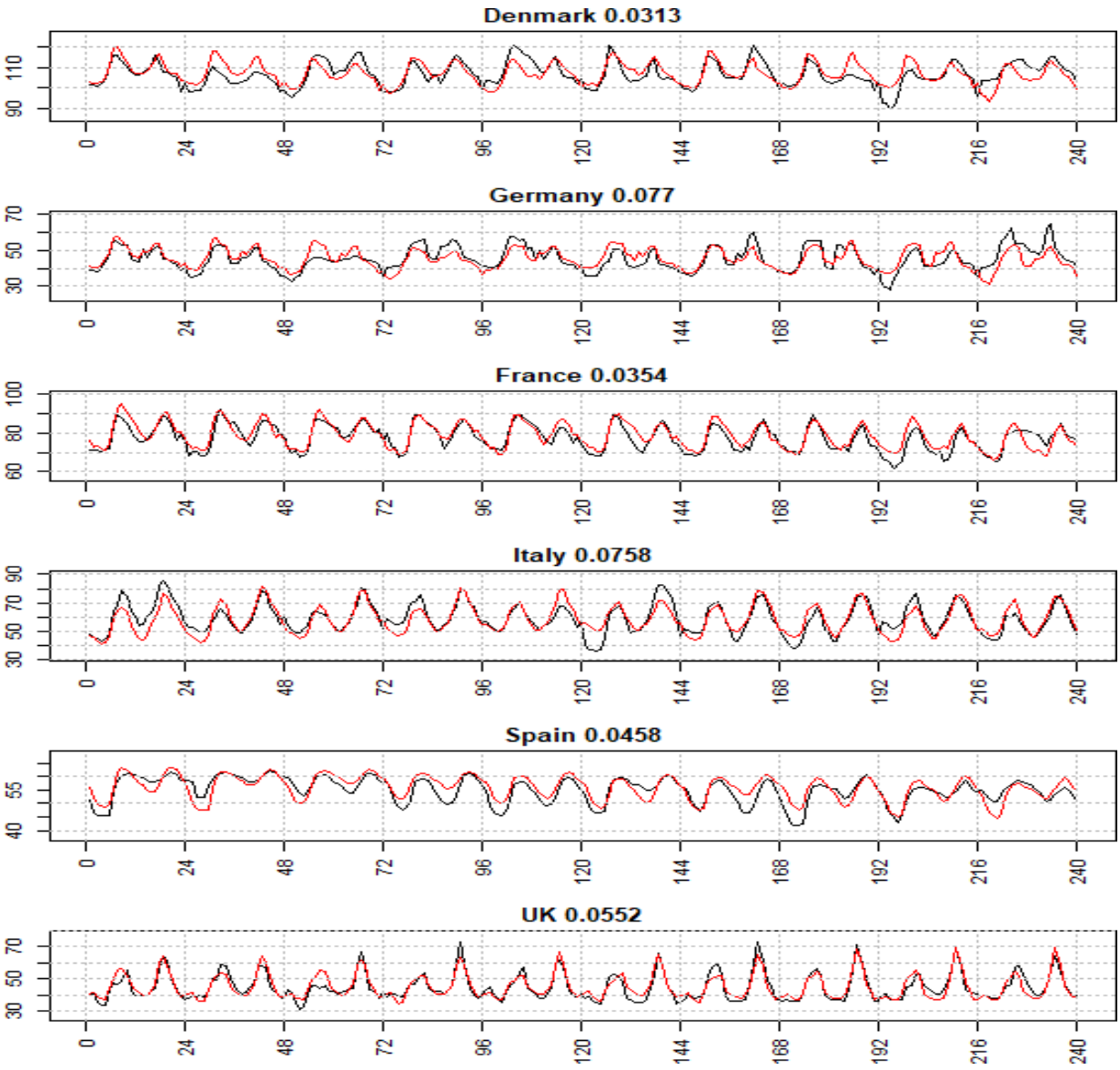

Figure 6-12: Behavior of the method to predict two-week (Monday through Friday) of March 2019 prices in the six markets.

6.7. Discussion

We have analyzed the evolution of hourly electricity prices in six European countries. All countries use the same pricing rule (uniform price auctions) and are part of SDAC which coordinates pricing and energy allocation simultaneously in most European countries. The existence of the SDAC mechanism conditions and tends to equalize prices in each national market, although the distances between countries, interconnection capacity restrictions, differences in energy demand and in the structure

of the power generation system in each country cause the evolution of prices in many areas to vary independently.

The study has several objectives. The first is to see how the pricing mechanism affects the temporal evolution of prices in each country. The answer to this question is evident: all the countries present series with a similar behavior (in general terms), with daily periodicity, high volatility and abrupt changes in the price level with reversion to the mean. The global comparative analysis among the six countries shows similarities and differences that will be detailed below. The dynamics are very well reflected in all cases by a random walk with a high presence of outlier observations. There is no evidence to conclude that any country behaves radically different from the rest, which was one of the key questions of the study.

In summary, we can highlight the following characteristics of the evolution of prices:

In all countries it is graphically verified that the price profile reproduces the demand profile (see Figure 6-3 and Figure 6-12).

Electricity prices usually undergo sudden changes that affect the dynamics of the data in a transitory way. In many cases it is difficult to know the causes of these changes. Detecting and correcting for the effect of outliers is important because they affect model selection, parameter estimation and, consequently, forecasts. There are several well-known computer programs specialized in the automatic detection of outliers in time series in this work the R *tsoutliers* package has been used [80]. All countries have a high percentage of outliers (see Figure 6-4). Spain and Germany stand out with a much higher proportion, in the case of Spain the outliers correspond mostly to sudden price decreases.

The ARIMA model that best fits the evolution of prices in the six countries is an IMA(1,1). The inclusion of more parameters hardly shows any improvement. The moving average parameter of the IMA(1,1) model explains a very low percentage of

variability in all hours and for all countries. The most important component in the predictive model is the random walk (see Figure 6-5).

GARCH models significantly improve the ARIMA models in all countries. The estimates of ϑ (moving average) for the GARCH model are more stable, taking a value close to 0.6 for all hours in all countries. From a conceptual point of view, this result shows that the series are not homoscedastic. The GARCH model obtained after the analysis coincides with those recommended by other authors in the analysis of daily average prices [62].

The values of the estimates of the two parameters of the sGARCH equation (see Figure 6-6) correspond in all cases to markets with large fluctuations (values of α greater than 0.1) and frequent changes in volatility. The estimated values are high compared to those corresponding to other financial markets. The opposite occurs with the β parameter, in financial markets it is usually in the range of 0.85 and 0.98 [2], in the case of electricity prices it is clearly lower. All this is consistent with time series with sudden jumps.

The sGARCH model is the simplest of all the models used to consider the heteroscedasticity of the series. The other models hardly improve on the standard sGARCH model, which leads us to conclude that it is not important to include the parameter that measures the asymmetry. This can be affirmed with specific details for the six countries.

An analysis of the prediction errors of the estimated models using out-of-sample observations has been performed. ARIMA models have much higher prediction errors than GARCH models. The level of error of all GARCH models (for the same country) is very similar. The same occurs when comparing the IMA (1,1) model and the best ARIMA model (Figure 6-10). The markets with the largest errors are Denmark, Germany and France when using the ARIMA models. Denmark and France perform a lot better with the GARCH models (Importantly, Denmark and Germany are the two

markets with the highest percentage of outliers in the evaluation window, 2019). In view of the results (see Table 6-3), the standard GARCH model (sGARCH) is the simplest and most recommended alternative for all countries to make hourly forecasts in the daily electricity market.

This study describes the main characteristics of hourly electricity prices in six European markets. It can be concluded that globally the behavior of the six markets is similar. Deciding whether the current system used by European countries (uniform price auctions) is the most appropriate is a very difficult question to answer empirically with current information. We hope that the results of this article will be useful to complement the theoretical studies on the different types of auctions in the financial and electricity markets.

6.8. Conclusions

In this chapter, the dynamics of hourly electricity prices in the six most-representative European countries have been described from a time series point of view. The analysis performed can help electric energy market agents select the model for making hourly predictions in the daily market.

As a first conclusion, an important recommendation is to independently analyze each of the 24-hourly time series. There are many motives in favor of this strategy. The first is that it is the method which provides better predictions. From the statistical point of view, the reason for the decomposition into hourly models versus the analysis of the global hourly series is the strong daily seasonality of the hourly process that causes periodic changes in the mean and the correlation structure of the process and makes the series non-stationary. Several references supporting this recommendation are provided in this study. The seasonality of electricity prices is fundamental because the driving force that determines their evolution is the demand, and this is conditioned by the social and economic activities of the users that generate daily, weekly, and annual

cycles. Supply characteristics also play an important role in price dynamics and explain their high volatility. For low levels of demand, generators supply electricity using plants with low marginal costs; as greater amounts of energy are needed, new generators with higher marginal costs enter the system. The relative insensitivity of demand to price fluctuations, and supply constraints at peak hours, make electricity prices in the day-ahead market extremely volatile.

Electricity prices often undergo sudden abrupt changes that affect the dynamics of the data on a transient basis. The evolution of electricity prices in six European Union countries, Denmark, France, Germany, Italy, Spain, and the United Kingdom, has been analyzed and compared. There are strong similarities with most of the daily electricity markets in Western countries. Further analysis reveals important differences among them. For example, the level of outlier prices is very different, especially their distribution over 24h of the day. Spain has a high percentage of outliers evenly distributed among the 24h of the day. Denmark and Germany have them concentrated in the evening hours. France and Italy have a much lower percentage of outliers, and they tend to be concentrated in the middle hours of the day. The United Kingdom has a very particular distribution of outliers throughout the day. In the UK, sharp price drops appear in the early morning hours (from 2 to 6 a.m.) and high outliers from 9 a.m. to 10 p.m.

Statistical analysis of the time series indicates that the main price dynamics largely correspond to the standard evolution of prices in other financial markets: the random walk. According to this model, the best prediction of the price of electricity for hour h of day $t + 1$ is to take the observed price for that hour on day t. The predictions made using the random walk are slightly improved using the exponential smoothing model. This statement is common for all countries and hours.

ARIMA models assume that the variance is constant over time. However, there are periods with significant increases in variability in any price series. These changes in

variability have been analyzed with the six different GARCH models (sGARCH, iGARCH, eGARCH, gjrGARCH, apARCH, and cGARCH). These models reveal interesting and differential characteristics of the different countries, which reinforce the results obtained with the descriptive statistics of the series and the outlier analysis.

Finally, the prediction errors of all models have been analyzed using out-of-sample data. An attempt has been made to recreate the real situation faced by market participants every day, the need to predict the one-day-ahead prices. Data from 2013 to 2018 has been selected to estimate the models and 2019 hourly prices have been reserved to assess the accuracy of the predictions.

The results obtained indicate that the ARIMA models have much higher prediction errors than the GARCH models, that all GARCH models provide very similar predictions, and that, therefore, the standard model (sGARCH) is recommended as a simpler and more accurate alternative.

Future research will focus on: (i) modeling and analyzing the rest of the European countries; (ii) modeling and analyzing the dynamics of most-representative non-European electric power systems; (iii) analyzing the impact of COVID and their effects over the electricity prices; and (iv) analyzing the impact of the most-recent political and economic events. The findings of this chapter were published in [96].

7. CONCLUSIONS AND FURTHER RESEARCH

In this chapter, the conclusions obtained during the development of the Doctoral Thesis will be shown, the scientific contributions that have resulted will be listed, and finally a list of possible future research topics will be shown.

7.1. Conclusions

7.1.1. Contributions referred to forecasting electricity demand

In reference to the study carried out to improve the quality of electricity demand forecasts in Spain and detailed in Chapter 4, it should be noted that temperature is one of the most important drivers of electric load, and selecting the right station or combination of stations is crucial for reducing the forecast error.

During the development of this thesis, we have proposed an algorithm that determines the optimal selection of weather locations based on (i) an initial reduction in problem complexity which decreases drastically the computation effort using a simplified demand time series without the holiday effect, and (ii) a posterior incremental/decremental search algorithm. The developed methods determine not only the optimal number of temperatures regressors to be used, but also identify their optimal geographical location.

The proposed methodology has been exhaustively tested using three insightful case studies using real data from the Spanish mainland electric power network. Two different weather forecast databases have been used: the Spanish meteorological agency AEMET and the European weather forecast agency ECMWF. The global forecast

accuracy increased by approximately 2-3%, denoting a higher enhancement between 2 PM and 8 PM (average increment of accuracy between 5.0-5.5%).

7.1.2. Contributions referred to renewable energy forecasting

In Chapter 5, the problem of optimally combining probabilistic forecasts is revisited. In this thesis, a method for calculating prediction intervals from a predictor obtained through a linear combination of predictions is proposed.

The developed method is based on the application of three techniques. First, the Berstein Online Aggregation is applied to compute the optimal combination of point forecasts, denoting an outperformance compared with the individual predictions in terms of accuracy. Second, to appropriately estimate the prediction intervals, the variance matrix of the prediction errors is calculated using the exponentially weighted moving average method. Finally, the Johnson SU-distribution is applied to improve the statistical properties of the aggregated predictions. Analyzing both the coverage and interval width shows that the proposed technique is computationally efficient and numerically accurate.

An exhaustive analysis was performed using Spanish wind power generation data by testing the accuracy of the point-aggregated forecasts and the reliability of the prediction intervals and by checking the coverage and interval width. The obtained results indicate that the proposed probabilistic combination method is both accurate and reliable: the forecasting error is lower than that of the individual predictions, and the coverage is better than that of the separate forecasts.

The results of the wind production prediction study demonstrate that combining different predictors is highly advantageous and significantly enhances individual predictions. Concerning the punctual forecasting accuracy, the error level is reduced by 28% on average. Specifically, the BOA exhibits an MSE value 20% lower than that of the best individual forecast. The aggregated prediction intervals have appropriate

coverage and significantly narrower widths than any of the intervals constructed with individual predictors (an average reduction of 30%; a reduction of 16% compared with that of the experts with a lower interval width), thereby improving the quality of probabilistic forecasting.

7.1.3. Contributions referred to electricity price forecasting

In Chapter 6, the dynamics of hourly electricity prices in the six most representative European countries have been described from a time series point of view. The analysis performed can help electric energy market agents select the model for making hourly predictions in the daily market.

As a first conclusion, an important recommendation is to independently analyze each of the 24-hourly time series. There are many motives in favor of this strategy. The first is that it is the method which provides better predictions. From the statistical point of view, the reason for the decomposition into hourly models versus the analysis of the global hourly series is the strong daily seasonality of the hourly process that causes periodic changes in the mean and the correlation structure of the process and makes the series non-stationary. Several references supporting this recommendation are provided in this chapter. The seasonality of electricity prices is fundamental because the driving force that determines their evolution is demand, and this is conditioned by the social and economic activities of the users that generate daily, weekly, and annual cycles. Supply characteristics also play an important role in price dynamics and explain their high volatility. For low levels of demand, generators supply electricity using plants with low marginal costs; as greater amounts of energy are needed, new generators with higher marginal costs enter the system. The relative insensitivity of demand to price fluctuations, and supply constraints at peak hours, make electricity prices in the day-ahead market extremely volatile.

Electricity prices often undergo sudden abrupt changes that affect the dynamics of the data on a transient basis. The evolution of electricity prices in six European Union countries, Denmark, France, Germany, Italy, Spain, and the United Kingdom, has been analyzed and compared. There are strong similarities with most of the daily electricity markets in Western countries. Further analysis reveals important differences among them. For example, the level of outlier prices is very different, especially their distribution over 24 hours of the day. Spain has a high percentage of outliers evenly distributed among the 24 hours of the day. Denmark and Germany have them concentrated in the evening hours. France and Italy have a much lower percentage of outliers, and they tend to be concentrated in the middle hours of the day. The United Kingdom has a very particular distribution of outliers throughout the day. In the UK, sharp price drops appear in the early morning hours (from 2 to 6 a.m.) and high outliers from 9 a.m. to 10 p.m.

Statistical analysis of the time series indicates that the main price dynamics largely corresponds to the standard evolution of prices in other financial markets, the random walk. According to this model, the best prediction of the price electricity for hour h of day $t + 1$ is to take the observed price for that hour on day t. The predictions made using the random walk are slightly improved using the exponential smoothing model. This statement is common for all countries and hours.

The ARIMA models assume that the variance is constant over time. However, there are periods with significant increases in variability in any price series. These changes in variability have been analyzed with the six different GARCH models (sGARCH, iGARCH, eGARCH, gjrGARCH, apARCH, and cGARCH). These models reveal interesting and differential characteristics of the different countries, which reinforce the results obtained with the descriptive statistics of the series and the outlier analysis.

Finally, the prediction errors of all models have been analyzed using out-of-sample data. An attempt has been made to recreate the real situation faced by market

participants every day, the need to predict the one-day-ahead prices. Data from 2013 to 2018 has been selected to estimate the models and 2019 hourly prices have been reserved to assess the accuracy of the predictions.

The results obtained indicate that the ARIMA models have much higher prediction errors than the GARCH models, that all GARCH models provide very similar predictions and, therefore, that the standard model (sGARCH) is recommended as a simpler and more accurate alternative.

7.2. Contributions to the technical literature

The methods developed and the results obtained in this Doctoral Thesis have been published in several JCR journals (one Q1, one Q2 and one Q3 publication), and in four papers in international congresses of recognized prestige in the field.

7.2.1. Journal articles published

In reference to Chapter 4, which develops a method for optimal location of meteorological stations, an article has been published in the IEEE Access magazine.

Authors:	E. Caro, J. Juan and **S. Nouhitehrani**
Title*:*	*Optimal Selection of Weather Stations for Electric Load Forecasting.*
Magazine:	IEEE Access, 11
Pages:	42981-42990
Date*:*	2023
[Journal Q2 (105/276). Impact factor: 3.5 (1 year), 3.7 (5 years)] [94]	

Regarding Chapter 5, the methodology developed to combine probabilistic predictions of renewable energies has been published in the journal Sustainable Energy Technologies and Assessments, which is positioned in the first quartile of the "Energy and Fuels" area.

Authors:	**S. Nouhitehrani**, E. Caro and J. Juan
Title*:*	*Computation of Prediction Intervals of Wind Energy based on the EWMA and BOA Techniques.*
Journal:	Sustainable Energy Technologies and Assessments, 66
Pages:	103806
Date*:*	2024
[Journal Q1 Energy and Fuels (28/119). Impact factor: 8 (1 year), 7.5 (5 years)] [Journal Q2 Green & Sustainable Science & Technology (16/46). Impact factor: 8 (1 year), 7.5 (5 years)] [95]	

Finally, in reference to Chapter 6, the study carried out to analyze and forecast the electricity spot price for the main European markets has been published in the journal Energies.

Authors:	**S. Tehrani**; J. Juan, and E. Caro.
Title*:*	*Electricity Spot Price Modeling and Forecasting in European Markets.*
Magazine:	Energies
Pages:	1-26
Date*:*	2022
[Journal Q3 (80/119) Impact factor: 2.6 (1 year), 3.3 (5 years)] [96]	

7.2.2. International Conferences

International Symposium of Forecasting:

Two presentations have been made at the renowned *International Symposium of Forecasting*, publishing partial results in reference to Chapter 4 [97, 98].

Authors:	E. Caro, J. Juan, **S. Nouhitehrani**
Title:	Effect of meteorological variables in electric load forecasting: Spanish insular systems
Congress:	ISF 2021 - International Symposium of Forecasting
Date:	June 27-30, 2021

Authors:	**S. Nouhitehrani**, E. Caro, J. Juan
Title:	Impact of Temperature Modeling over The Electric Load Forecasting Accuracy
Congress:	ISF 2021 - International Symposium of Forecasting
Date:	June 27-30, 2021

International conference on Time Series and Forecasting:

Two presentations have been made at the *International conference on Time Series and Forecasting*, publishing partial results in reference to Chapter 5 and 6 [99, 100].

Authors:	**S. Nouhitehrani**, J. Juan, E. Caro
Title:	Combination of Probabilistic Predictions for Wind Energy Production
Congress:	ITISE 2023 - International Work-Conference on Time Series
Place:	Gran Canaria, España
Date:	July 12-14, 2023

Authors:	E. Caro, J. Juan, **S. Nouhitehrani**
Title:	Impact of Temperature Modelling over the Spanish Electric Consumption Forecasts
Congress:	ITISE 2021 - International Work-Conference on Time Series
Place:	Gran Canaria, España
Date:	July 19-21, 2021

7.3. Future work

Concerning the advances in electricity demand forecasting (Chapter 4), future work will focus on analyzing the effect of optimizing the location of additional weather variables such as solar irradiance and/or humidity.

With respect to the improvements concerning the optimal combination of probabilistic forecasts (Chapter 5), future work will focus on the following: (i) analyzing the precision of the proposed method using other energy market variables such as photovoltaic generation or hydropower production in Spain; (ii) expanding the implemented procedure to electricity market variables in other countries; and (iii) comparing both the performance and accuracy of the proposed method against those of mathematical models proposed in the state-of-the-art technical literature.

Finally, concerning the analysis and forecasting of electricity prices for European countries (Chapter 6), future research will focus on: (i) modeling and analyzing the rest of the European countries; (ii) modeling and analyzing the dynamics of most-

representative non-European electric power systems; (iii) analyzing the impact of COVID and their effects over the electricity prices; and (iv) analyzing the impact of the most recent political and economic events.

References

[1] Cancelo J, Espasa A. Forecasting daily demand for electricity with multiple-input nonlinear transfer function models: a case study. Techrep, Carlos III University. 1991.

[2] Caro E, Juan J, Cara J. Periodically correlated models for short-term electricity load forecasting. Appl Math Comput. 2020;364, pp. 124642.

[3] Dordonnat V, Koopman S, Ooms M, Dessertaine A, Collet J. An hourly periodic state space model for modelling French national electricity load. Int J Forecast. 2008;24(4), pp. 566-87.

[4] A Brief History of the Electricity Market in Europe. European Parliament, 2019, <europarl.europa.eu/news/en/headlines/economy/20190911STO05420/brief-history-electricity-market-europe/>.

[5] The Evolution of Electric Power Markets. Edison Electric Institute, 2019, <www.eei.org/issues-policies/market-regulation/evolution-of-electric-power-markets/>.

[6] Sources of electricity generation in Spain and its contribution, Electrification of the Economy - Energia y Sociedad. 2024, Energia y Sociedad, accessed 20 March 2024, <https://www.energiaysociedad.es/fuentes-de-generacion-electrica-en-espana-y-su-aportacion/>.

[7] Curvas agregadas de oferta y demanda OMIE, OMIE. 2024, OMIE , accessed 20 March 2024, <https://www.omie.es/en/market-results/daily/daily-market/aggragate-suply-curves?scope=daily&date=2024-01-10&hour=1/>.

[8] Informe_anual_omie_2017_espanol_1.pdf. Accedido: 17 de agosto de 2022. [En línea] Disponible en: <https://www.omie.es/sites/default/files/2020-03/informe_anual_omie_2017_espanol_1.pdf/>.

[9] Cancelo JR, Espasa A, Grafe R. Forecasting the electricity load from one day to one week ahead for the Spanish system operator. Int J Forecast. 2008;24(4), pp. 588-602.

[10] Cottet R, Smith M. Bayesian modeling and forecasting of intraday electricity load. J Am Stat Assoc. 2003;98(464), pp. 839-49.

[11] Predicción por municipios, The Spanish meteorological agency (AEMET). 2024, <http://www.aemet.es/es/eltiempo/prediccion/municipios/>.

[12] Modelos de predicción numérica, ECMWF, 2024. ECMWF: European Centre for Medium-Range Weather Forecasts ,< https://www.tiempo.com/modelos/>. pp.

[13] The Spanish meteorological agency (AEMET). 2023, AEMET, accessed 4 April 2023, <http://www.aemet.es/es/eltiempo/observacion/>.

[14] Península-Seguimiento de la demanda de energía eléctrica, RED ELÉCTRICA DE ESPAÑA (REE). 2024 , RED ELÉCTRICA DE ESPAÑA, accessed 4 April 2023, <https://demanda.ree.es/visiona/peninsula/demandaqh/total/>.

[15] Box G, Jenkins G. Time Series Analysis: Forecasting and Control. San Francisco, CA, USA: Holden-Day; 1970.

[16] Engle RF, Granger CWJ, Rice J, Weiss A. Semiparametric estimates of the relation between weather and electricity sales. J Am Stat Assoc. 1986;81, pp. 310-20.

[17] Chang CL, McAleer M. The correct regularity condition and interpretation of asymmetry in EGARCH. Econ Lett 2017;161, pp. 52-5.

[18] Hong T. Energy forecasting: Past, present, and future. Foresight: The International Journal of Applied Forecasting. 2014(32), pp. 43-8.

[19] Hong T, Pinson P, Wang Y, Weron R, Yang D, Zareipour H. Energy Forecasting: A Review and Outlook. IEEE Journal of Power and Energy. 2020;7, pp. 376-88.

[20] Sobhani M, Hong T, Martin C. Temperature anomaly detection for electric load forecasting. International Journal of Forecasting. 2020;36, pp. 324-33.

[21] Fan S, Methaprayoon K, Lee W. Multiregion Load Forecasting for System with Large Geographical Area. IEEE Transactions on Industry Applications. 2009;45, pp. 1452-9.

[22] Lai SH, Hong T. When one size no longer fits all: electric load forecasting with a geographic hierarchy. SAS White pap. 2013, pp. 1-14.

[23] Hong T, Wang P, White L. Weather station selection for electric load forecasting. International Journal of Forecasting. 2015;31(2), pp. 286-95.

[24] Sobhani M, Campbell A, Sangamwar S, Li C, Hong T. Combining Weather Stations for Electric Load Forecasting. Energies. 2019;12(8), pp. 1-11.

[25] Moreno-Carbonell S, Sánchez-Úbeda EF, Muñoz A. Rethinking weather station selection for electric load forecasting using genetic algorithms. International Journal of Forecasting. 2020;36(2), pp. 395-712.

[26] Boya C, Ardila-Rey J. A Method for Weather Station Selection Based on Wavelet Squared Coherence for Electric Load Forecasting. IEEE Access. 2020;8, pp. 197431-8.

[27] Ziel F, Liu B. Lasso estimation for GEFCom2014 probabilistic electric load forecasting. International Journal of Forecasting. 2016;32(3), pp. 1029-37.

[28] Charlton N, Singleton C. A refined parametric model for short term load forecasting. International Journal of Forecasting. 2014;30(2), pp. 364-8.

[29] Nedellec R, Cugliari J, Goude Y. GEFCom2012: Electric load forecasting and backcasting with semi-parametric models. International Journal of forecasting. 2014;30(2), pp. 375-81.

[30] Vilmarest J, Goude Y. State-Space Models for Online Post-Covid Electricity Load Forecasting Competition. IEEE Open Access Journal of Power and Energy. 2022;9, pp. 192-201.

[31] Owens R, Hewson T. ECMWF Forecast User Guide. ECMWF. 2018;https://doi.org/10.21957/m1cs7h

[32] Roga S, Bardhan S, Kumar Y, Dubey SK. Recent technology and challenges of wind energy generation: A review. Sustainable Energy Technologies and Assessments, 52(Part C). 2022, pp. 102239. ISSN 2213-1388. https://doi.org/10.1016/j.seta.2022.

[33] Giebel G, Kariniotakis G. Wind power forecasting - a review of the state of the art. In Renewable Energy Forecasting: From Models to Applications (pp 59-109) Woodhead Publishing. 2017. https://doi.org/10.1016/B978-0-08-100504-0.00003-2.

[34] Lai Z, Ling Q. A dual spatio-temporal network for short-term wind power forecasting. Sustainable Energy Technologies and Assessments. 2023;60, pp. 103486. ISSN 2213-1388. https://doi.org/10.1016/j.seta.2023.

[35] Wang X, Guo P, Huang X. A review of wind power forecasting models. Energy Procedia. 2011;12, pp. 770-8. https://doi.org/10.1016/j.egypro.2011.10.103.

[36] Bates JM, Granger CW. The combination of forecasts. Journal of the Operational Research Society. 1969;20(4), pp. 451-68. https://doi.org/10.1057/jors.969.103.

[37] Yan H, Wu Z. A hybrid short-term wind power prediction model combining data processing, multiple parameters optimization, and multi-intelligent models apportion strategy. IEEE Access. 2020;8, pp. 227126-40. https://doi.org/10.1109/ACCESS.2020.3046001.

[38] He B, Ye L, Pei M, Lu P, Dai B, Li Z, Wang K. A combined model for short-term wind power forecasting based on the analysis of numerical weather prediction data. Energy Reports. 2022;8, pp. 929-39. https://doi.org/10.1016/j.egyr.2021.10.102.

[39] Hanifi S, Liu X, Lin Z, Lotfian S. A critical review of wind power forecasting methods—past, present, and future. Energies. 2020;13(15), pp. 3764. https://doi.org/10.390/en13153764.

[40] Lin Y, Yang M, Wan C, Wang J, Song Y. A multi-model combination approach for probabilistic wind power forecasting. IEEE Transactions on Sustainable Energy. 2018;10(1), pp. 226-37. https://doi.org/10.1109/TSTE.2018.2831238

[41] Jiandong D, Peng W, Wentao M, Shuai F, Zequan H. A novel hybrid model based on nonlinear weighted combination for short-term wind power forecasting. International Journal of Electrical Power & Energy Systems. 2022;134, pp. 107452. https://doi.org/10.1016/j.ijepes.2021.

[42] Tascikaraoglu A, Uzunoglu M. A review of combined approaches for prediction of short-term wind speed and power. Renewable and Sustainable Energy Reviews. 2014;34, pp. 243-54. https://doi.org/10.1016/j.rser.2014.03.033.

[43] Chen Y, Hu X, Zhang L. A review of ultra-short-term forecasting of wind power based on data decomposition-forecasting technology combination model. Energy Reports. 2022;8, pp. 14200-19. https://doi.org/10.1016/j.egyr.2022.10.342

[44] Li Y, Janik P, Schwarz H. Prediction and aggregation of regional PV and wind generation based on neural computation and real measurements. Sustainable Energy Technologies and Assessments. 2023;57, pp. 103314. ISSN 2213-1388. https://doi.org/10.1016/j.seta.2023..

[45] Sun Z, Zhao S, Zhang J. Short-term wind power forecasting on multiple scales using VMD decomposition, K-means clustering, and LSTM principal computing. IEEE Access. 2019;7, pp. 166917-29. https://doi.org/10.1109/ACCESS.2019.2942040.

[46] Yagang Z., Ruixuan L. Short term wind energy prediction model based on data decomposition and optimized LSSVM. Sustainable Energy Technologies and Assessments. 2022;52, pp. 102025. htpps://doi.org/10.1016/j.seta.2022..

[47] He Y, Liu R, Li H, Wang S, Lu X. Short-term power load probability density forecasting method using kernel-based support vector quantile regression and

Copula theory. Applied Energy. 2017;185, pp. 254-66. https://doi.org/10.1016/j.apenergy.2016.10.079.

[48] Dokur E, Erdogan N, Salari ME, Karakuzu C, Murphy J. Offshore wind speed short-term forecasting based on a hybrid method: Swarm decomposition and meta-extreme learning machine. Energy. 2022;248, pp. 123595. https://doi.org/10.1016/j.energy.2022.

[49] Clemen RT. Combining forecasts: A review and annotated bibliography. International Journal of Forecasting. 1989;5(4), pp. 559-83. https://doi.org/10.1016/0169-2070(89)90012-5.

[50] Palm FC, Zellner A. To combine or not to combine? Issues of combining forecasts. Journal of Forecasting. 1992;11(8), pp. 687-701. https://doi.org/10.1002/for.3980110806.

[51] Timmermann A. Forecast combinations. Handbook of Economic Forecasting. 2006;1, pp. 135-96. https://doi.org/10.1016/S574-0706(05)01004-9.

[52] Wang H, Zhang Y-M, Mao J-X. Sparse Gaussian process regression for multi-step ahead forecasting of wind gusts combining numerical weather predictions and on-site measurements. Journal of Wind Engineering and Industrial Aerodynamics. 2022;220, pp. 104873. https://doi.org/10.1016/j.jweia.2021.

[53] Wintenberger O. Optimal learning with Bernstein online aggregation. Machine Learning. 2017;106, pp. 119-41. https://doi.org/10.48550/arXiv.1404.1356.

[54] ohnson NL, Kotz S, Balakrishnan N. Continuous univariate distributions: John Wiley & Sons; 1995.

[55] Gaillard P, Goude Y. Opera: Online prediction by expert aggregation. URL: https://CRANR-projectorg/package=operar package version. 2016.

[56] Akbari-Dibavar A, Mohammadi-Ivatloo B, Zare K. Electricity market pricing: uniform pricing vs. pay-as-bid pricing. Electricity Markets: New Players Pricing Uncertainties. 2020, pp. 19-35.

[57] Fabra N-H, Von Der Fehr D, editors. Harbord Designing Electricity Auctions: Uniform, Discriminatory and Vickrey. In Proceedings of the First Conference on Wholesale Markets for Electricity, Toulouse, France; 2002.

[58] Pezzutto S, Grilli G, Zambotti S, Dunjic S. Forecasting electricity market price for end users in EU28 until 2020—Main factors of influence. Energies. 2018;11(6), pp. 1460.

[59] Kastl J. Auctions in financial markets. International Journal of Industrial Organization. 2020;70, pp. 102559.

[60] Agurto R, Fuentes F, García CJ, Skoknic E. The macroeconomic impact of the electricity price: Lessons from Chile. Empir Econ. 2021;60(5), pp. 2407-28.

[61] Aggarwal SK, Saini LM, Kumar A. Electricity price forecasting in deregulated markets: A review and evaluation. Int J Electr Power Energy Syst. 2009;31(1), pp. 13-22.

[62] Weron R. Electricity price forecasting: A review of the state-of-the-art with a look into the future. Int J Forecast. 2014;30(4), pp. 1030-81.

[63] McHugh C, Coleman S, Kerr D. Hourly electricity price forecasting with NARMAX. Mach Learn Appl. 2022;9, pp. 100383.

[64] González JP, San Roque AMSM, Perez EA. Forecasting functional time series with a new Hilbertian ARMAX model: Application to electricity price forecasting. IEEE Trans Power Syst. 2017;33(1), pp. 545-56.

[65] Pórtoles J, González C, Moguerza JM. Electricity price forecasting with dynamic trees: A benchmark against the random forest approach. Energies 2018;11(6), pp. 1588.

[66] Zhang R, Li G, Ma Z. A deep learning based hybrid framework for day-ahead electricity price forecasting. IEEE Access. 2020;8, pp. 143423-36.

[67] Bibi N, Shah I, Alsubie A, Ali S, Lone SA. Electricity spot prices forecasting based on ensemble learning. IEEE Access. 2021;9, pp. 150984-92.

[68] Shah I, Bibi H, Ali S, Wang L, Yue Z. Forecasting one-day-ahead electricity prices for italian electricity market using parametric and nonparametric approaches. IEEE Access. 2020;8, pp. 123104-13.

[69] Pourdaryaei A, Mokhlis H, Illias HA, Kaboli SHA, Ahmad S, Ang SP. Hybrid ANN and artificial cooperative search algorithm to forecast short-term electricity price in de-regulated electricity market. IEEE Access. 2019;7, pp. 125369-86.

[70] Elattar EE, Elsayed SK, Farrag TA. Hybrid local general regression neural network and harmony search algorithm for electricity price forecasting. IEEE Access. 2020;9, pp. 2044-54.

[71] Pourdaryaei A, Mokhlis H, Illias HA, Kaboli SHA, Ahmad S. Short-term electricity price forecasting via hybrid backtracking search algorithm and ANFIS approach. IEEE Access. 2019;7, pp. 77674-91.

[72] Tschora L, Pierre E, Plantevit M, Robardet C. Electricity price forecasting on the day-ahead market using machine learning. Appl Energy. 2022;313, pp. 118752.

[73] Escribano A, Ignacio Peña J, Villaplana P. Modelling electricity prices: International evidence. Oxford bulletin of economics statistics. 2011;73(5), pp. 622-50.

[74] Derek WB, Nektaria V, Karakatsani. Forecasting the Energy Markets the Oxford Handbook of Economic Forecasting. New York: Oxford University Press; 2003.

[75] Koopman SJ, Ooms M, Carnero MA. Periodic seasonal Reg-ARFIMA–GARCH models for daily electricity spot prices. J Am Stat Assoc. 2007;102(477), pp. 16-27.

[76] Tiao GC, Grupe MR. Hidden Periodic Autoregressive-Moving Average Models in Time Series Data. Biometrika 1980;67, pp. 365.

[77] Carpio J, Juan J, López D. Multivariate Exponential Smoothing and Dynamic Factor Model Applied to Hourly Electricity Price Analysis. Technometrics 2014;56, pp. 494-503.

[78] García-Martos K, Rodríguez J, Sánchez MJ. Mixed Models for Short-Run Forecasting of Electricity Prices: Application for the Spanish Market. IEEE Trans Power Syst. 2007;22, pp. 2.

[79] Gómez V, Maravall A. Programs TRAMO and SEATS. Instructions for the User; Banco de España, Eds.; 1996; Working paper number 9628. Madrid, Spain.

[80] López-de-Lacalle J. Tsoutliers: detection of outliers in time series. R package version 06-8. 2019.

[81] Chen C, Liu LM. Joint Estimation of Model Parameters and Outlier Effects in Time Series. J Am Stat Assoc. 1993;88, pp. 284-97.

[82] Kostrzewski M, Kostrzewska J. The Impact of Forecasting Jumps on Forecasting Electricity Prices. Energies 2021;14, pp. 336.

[83] Diewald L, Prokopczuk M, Simen CW. Time-variations in Commodity Price Jumps. J Empir Financ. 2015;31, pp. 72-84.

[84] Kostrzewski M, Kostrzewska J. Probabilistic Electricity Price Forecasting with Bayesian Stochastic Volatility Models. Energy Econ. 2019;80, pp. 610-20.

[85] Seifert J, Uhrig-Homburg M. Modelling Jumps in Electricity Prices: Theory and Empirical Evidence. Rev Deriv Res. 2007;10, pp. 59-85.

[86] Engle RF. Autoregressive conditional heteroscedasticity with estimates of the variance of United Kingdom inflation. Econometrica 1982;50, pp. 987-1007.

[87] Bollerslev T. Generalized autoregressive conditional heteroskedasticity. J Econom. 1986;31(307-327), pp.

[88] Hickey E, Loomis DG, Mohammadi HF. Forecasting hourly electricity prices using ARMAX–GARCH models: An application to MISO hubs. Energy Econ.34, pp. 307-15.

[89] Nelson DB. Conditional heteroskedasticity in asset returns: A new approach. Econometrica 1991;59, pp. 347-70.

[90] Glosten LR, Jagannathan R, Runkle DE. On the relation between the expected value and the volatility of the nominal excess return on stocks. J Financ. 1993;48, pp. 1779-801.

[91] Ding Z, Granger CW, Engle RF. A long memory property of stock market returns and a new model. J Empir Financ. 1993;1, pp. 83-106.

[92] Lee GJ, Engle RF. A permanent and transitory component model of stock return volatility. In Cointegration Causality and Forecasting A Festschrift in Honor of Clive WJ Granger; Oxford University Press Oxford, UK. 1999, pp. 475-97.

[93] Alexander C. Market Risk Analysis, Pricing. Hedging and Trading Financial Instruments. West Sussex, England: John Wiley & Sons; 2009.

[94] Caro E, Juan J, Nouhitehrani S. Optimal Selection of Weather Stations for Electric Load Forecasting. IEEE Access. 2023. https://doi.org/10.1109/ACCESS.2023.3270933

[95] Nouhitehrani S, Caro E, Juan J. Computation of prediction intervals of wind energy based on the EWMA and BOA techniques. Sustainable Energy Technologies and Assessments. 2024;66, pp. 103806. https://doi.org/10.1016/j.seta.2024.103806.

[96] Tehrani S, Juan J, Caro E. Electricity spot price modeling and forecasting in European markets. Energies. 2022;15(6), pp. 5980. https://doi.org/10.3390/en15165980

[97] Caro E, Juan J, Nouhitehrani S. Effect of meteorological variables in electric load forecasting: Spanish insular systems. In International Symposium of Forecasting (ISF). 2021.

[98] Nouhitehrani S, Caro E, Juan J. Impact of Temperature Modeling over The Electric Load Forecasting Accuracy. In International Symposium of Forecasting (ISF). 2021.

[99] Nouhitehrani S, Caro E, Juan J. Combination of Probabilistic Predictions for Wind Energy Production. In International Work-Conference on Time Series (ITISE). 2023.

[100] Caro E, Juan J, Nouhitehrani S. Impact of Temperature Modelling over the Spanish Electric Consumption Forecasts. In International Work-Conference on Time Series (ITISE). 2021.